ISTANBUL TECHNICAL UNIVERSITY ★ GRADUATE SCHOOL OF SCIENCE ENGINEERING AND TECHNOLOGY

MODELING AND TESTING THE FLEXURAL BEHAVIOUR OF A CFRP PRE-IMPREGNATED COMPOSITE IN ITS MOLTEN CONFIGURATION

M.Sc. THESIS

Kaveh DARGAHI NOUBARY

Department of Mechanical Engineering

Solid Mechanics Programme

JANUARY 2015

ISTANBUL TECHNICAL UNIVERSITY ★ GRADUATE SCHOOL OF SCIENCE ENGINEERING AND TECHNOLOGY

MODELING AND TESTING THE FLEXURAL BEHAVIOUR OF A CFRP PRE-IMPREGNATED COMPOSITE IN ITS MOLTEN CONFIGURATION

M.Sc. THESIS

Kaveh DARGAHI NOUBARY
(503111521)

Department of Mechanical Engineering

Solid Mechanics Programme

Thesis Advisor: Prof. Dr. Ata MUĞAN

JANUARY 2015

<u>İSTANBUL TEKNİK ÜNİVERSİTESİ ★ FEN BİLİMLERİ ENSTİTÜSÜ</u>

CFRP PREPREG KOMPOZİTLERİN ERGİMİŞ DURUMDAKİ KONFİGURASYONLARININ EİĞLME DAVRANIŞLARININ MODELLENMESİ VE TESTİ

YÜKSEK LİSANS TEZİ

Kaveh DARGAHI NOUBARY
(503111521)

Makine Mühendisliği Anabilim Dalı

Katı Cisimlerin Mekaniği

Tez Danışmanı: Prof. Dr. Ata MUĞAN

OCAK 2015

Kaveh Dargahi Noubary, a **M.Sc.** student of ITU **Graduate School of Science and Technology** student ID 503111521, successfully defended the **thesis** entitled "**Modeling and Testing the Flexural Behaviour of a CFRP Pre-impregnated composite in its molten configuration**", which he prepared after fulfilling the requirements specified in the associated legislations, before the jury whose signatures are below.

Thesis Advisor :	**Prof. Dr. Ata MUGAN** İstanbul Technical University	....
Jury Members :	**Doç. Dr. Mahmut Cüneyt FETVACI** Istanbul University	....
	Yrd. Doç. Dr. Mesut KIRCA İstanbul Technical University	....

Date of Submission : 15 December 2014
Date of Defense : 19 January 2015

To my parents,

FOREWORD

This thesis study is undertaken through a grant of Erasmus student exchange program. The thesis is also defended at Technical University of Munich, Germany.

I would like to express my very great appreciation to professor Drechsler and my supervisors professor Ata Mugan, Mr. Roland Lichtinger, Mr. Thorsten Hans and Mr. Alexane Margossian. Without their helpful and constructive advices, this thesis would not have been possible. I would also like to thank Mr. Philipp Hormann for his help on making me familiar with my supervisors.
Finally, I wish to thank my nice parents and sister who have always supported and encouraged me.

December 2014 Kaveh DARGAHI NOUBARY

TABLE OF CONTENTS

Page

ABBREVIATIONS

App	**:** Appendix
ASTM	**:** American Society for Testing and Materials
CFRP	**:** Carbon Fiber Reinforced Plastic
CM	**:** Centerline Marked
CTL	**:** Composite Testing Laboratory
DMA	**:** Dynamic Mechanical Analysis
DMTA	**:** Dynamic Mechanical Thermal Analysis
FEM	**:** Finite Elemente Method
FPR	**:** Four Pulse Ramp
FRP	**:** Fiber Reinforced Polymer
IAR	**:** Incremental Amplitude Ramp
ITU	**:** Istanbul Technical University
LCC	**:** Lehrstuhl für Carbon Composites
MMC	**:** Metal Matrix Composites
NIR	**:** Near Infrared spectroscopy
PMMA	**:** Polymethyl Methacrylate
PP-LGF	**:** Long Glass Fiber reinforced Polypropylene
S-N	**:** Stress-Number of cycles
SMA	**:** Shape Memory Alloys
TUM	**:** Technische Universität München
CM	**:** Centerline Marked
UM	**:** Centerline Unmarked

LIST OF TABLES

Page

LIST OF FIGURES

Page

MODELING AND TESTING THE FLEXURAL BEHAVIOUR OF A CFRP PRE-IMPREGNATED COMPOSITE IN ITS MOLTEN CONFIGURATION

SUMMARY

The goal of this thesis is to develop a material model for prepreg materials, which is a combination of viscoelastic and elastic properties. For validation of developed model, quasi-static tensile test of Celstran®CFR-TP PA6 CF60-01 thermoplastic prepreg has been investigated. This test is developed at Institute for Carbon Composites (LCC), Technical University of Munich, in a separate study parallel to current thesis. As a first step, outputs of tensile test which are deformation, force, stress and strain have been considered to determine viscoelastic parameters. In literature, viscoelastic materials are defined by a Prony series expansion of the dimensionless relaxation modulus [4, 22]. In this definition, Prony series coefficients are determined by fitting series to stress-strain curve of tensile, creep or relaxation tests. This curve is considered as proportion of stresses to strains with respect to time. In order to make this proportion dimensionless, it is divided by its initial value (i.e. time = 0). After determination of viscoelastic model, elastic properties of final model (modulus of elasticity and Poisson’s ratio) have been adapted from other experimental tests done at LCC. Final material model of this thesis is created as a combination of elastic and viscoelastic material properties. Afterwards, developed model has been used to simulate quasi-static tensile test with commercial finite element software, ABAQUS. In this simulation, virtual specimen in same dimensions as real one has been modeled and its upper part has been defined as cantilever boundary condition and lower part has been exposed to tensile force as real sample. This simulation procedure is carried out with consideration and comparison of effects and influences of different parameters such as element type, displacement or force ramp, etc. Eventually stress-strain diagrams for both cases have been drawn and a comparison between experimental and simulation outputs is obtained, and their correlation has been discussed.

CFRP PREPREG KOMPOZİTLERİN ERGİMİŞ DURUMDAKİ KONFİGURASYONLARININ EĞİLME DAVRANIŞLARININ MODELLENMESİ VE TESTİ

ÖZET

Gelişen teknolojiyle birlikte mevcut olan malzemeler yetersiz kalmış ve birçok özelliği aynı anda barındıran malzemelere ihtiyaç duyulmuştur. Aslında çok eski zamanlardan beri kullanılmakta olmasına rağmen, günümüzde bilinen anlamıyla kompozit malzemeler bu ihtiyacı karşılamak amacıyla ortaya çıkmış ve yaygın olarak kullanılan malzemeler gruplarından olmuşlardır. İki ya da daha fazla sayıda birbirinden farklı malzemenin makroskobik boyutta bir araya gelmesiyle elde edilen kompozit malzemeler, birbiri içerisinde çözünmemekte ve herbir malzemeden gelen özellikleri bir arada barındırmaktadır. Temel olarak matris adı verilen, malzemeyi bir arada tutmaya ve desteklemeye yarayan malzeme ile takviye malzemesi olarak adlandırılan ve taşıma görevini üstlenen malzemeden oluşan kompozit malzemeler üstün özellikleri sayesinde günümüzde hemen hemen her alanda kullanılmaktadır. Bu tez kapsamında hem elastik hem de viskoelastik özellikleri bir arada barındıran prepreg malzeme için bir malzeme modeli geliştirilmiş ve geliştirilen modeli gerçeklemek amacıyla da teze paralel olarak Münih Teknik Üniversitesi Karbon Kompozit Enstitüsü (TUM, LCC) laboratuvarında çekme testi yapılmıştır.

Prepreg malzemeler sahip olduğu üstün özellikleri sayesinde başta havacılık, uzay, askeri, denizcilik, spor alanları olmak üzere, gelişmiş malzemelere ihtiyaç duyulan birçok alanda kullanılmaktadır. Tez kapsamında öncelikli olarak malzeme belirlenmesi kararlaştırılmış ve prepreg malzeme olarak Celstran® CFR-TP PA6 CF60-01 seçilmiş olup bu malzeme ile ilgili detaylı bilgiler Ek-A da verilmiştir. Piyasadan satın alınan malzeme istenilen numune boyutuna ulaşabilmek için öncelikli olarak tigersawing makinası kullanılarak dikey kesitlere bölünmüştür. Elde edilen kesitler testere yardımıyla yatay parçalara ayrılmıştır. El yordamıyla yapılan kesimde insandan kaynaklı hata olasılığı çok yüksek olduğunda numune için istenilen boyut, disc sander makinasıyla verilmiş ve tüm bu işlemler Münih Teknik Üniversitesi Karbon Kompozit Enstitüsü Kompozit Test Laboratuarında gerçekleştirilmiştir. Hazırlanan numune 10.3177x6.355x0.985 mm boyutlarındadır.

Malzemenin belirlenmesinin ardından ikinci aşama olarak çekme testi yapılmış ve elde edilen sonuçlara göre viskoelastik malzeme tanımlanmıştır. Prepreg malzemelerin özelliklerinin belirlenmesinde çok çeşitli mekanik testler kullanılmakta olup Dinamik Mekanik Analiz (DMA) testi polimer ve polimer esaslı kompozit malzemelerin termo – mekanik özeliklerinin belirlenmesinde yaygın olarak uygulanmaktadır. DMA testinde, daha önceden belirlenmiş bir birim uzama miktarı numuneye uygulanır ve sonucunda oluşan kuvvet ve yer değiştirmeler algılayıcılar yardımıyla ölçülür. Sonrasında uygun denklemler kullanılarak gerilme değeri elde edilir. Tez kapsamında yapılan çekme testinde prepreg malzeme önce 280^{o}C sıcaklığa dek ısıtılmış ve aynı sıcaklıkta 10 dk bekletilmiştir. Malzemenin ısıtıldığı sıcaklık, erime noktasının üzerinde olduğundan malzeme yumuşaktır. Sonrasında

genliği 0.05 N/dk olan kuasi-statik kuvvet 1N değerine ulaşana dek liflere dik doğrultuda uygulanmış ve elde edilen veriler yardımıyla gerilme – birim uzama grafiği elde edilmiştir. Deney sonuçlarına bakılacak olursa grafiklerin ilk 3.49s lik bölümü farklılık göstermektedir. Bunun sebebi makina hatası olup deneyin ilk saniyelerinde makina sağlıklı sonuçlar verememekte ya da gerekli kuvveti uygulayamamaktadır. Bu sebepten dolayı deney sonuçları 3.4902 saniye geçikmeli olarak yeniden çizdirilmiş ve bu grafikler esas alınmıştır. Çekme testi sonucunda elde edilen ve viskoelastik malzemelerin tanımlanmasında kullanılan deformasyon, kuvvet, gerilme ve birim uzama gibi parametrelerin belirlenmesinin ardından viskoelastisitenin tanımlanmasında yaygın olarak kullanılan Prony birimsiz gevşeme modülü serisinin kullanılması daha önce yapılan literatür araştırmaları sonucunda uygun görülmüştür. Prony serisi katsayıları çekme testi, sürünme ya da gevşeme testi sonucunda elde edilen gerilme - birim uzama grafiği ile belirlenmektedir. Bu eğri gerilmenin birim uzamaya zamana göre oranı olarak düşünülmektedir. Gevşeme modülünü birimsiz hale getirmek için, elde edilen değer başlangıç anında aldığı değere (örneğin t=0 anındaki) bölünür.

Kullanılacak olan viskoelastik model tanımlanmasının ardından, üretilen modelin elastik özellikleri (Elastiklik Modülü ve Poisson Oranı) Münih Teknik Üniversitesi Karbon Kompozit Enstitüsünde (TUM LCC) yapılan deneyler sonucunda elde edilen verilerden elde edilmiştir. Bu tez kapsamında üretilen son modelin elastik ve viskoelastik malzeme özellikleri yapılan deneyler sonucunda elde edilen veriler ile belirlenmiştir.

Deney sonuçlarının elde edilmesinin ardından tezin üçüncü aşaması olan modelleme kısmına geçilmiş ve bilgisayar ortamında malzeme modeli oluşturulmuştur. Yapılan testlere ek olarak bilgisayar ortamında modelleme de pek çok araştırmacının ilgisini çekmiş ve dünyanın çeşitli yerlerinde birçok araştırmacı tarafından geliştirilmeye çalışılmaktadır. Simülasyon ya da diğer adıyla bilgisayar ortamında modelleme, gerçek hayatta olan sistemlerin bilgisayar ortamında modelinin oluşturulması olup günümüzde yaygın bir şekilde kullanılmakta ve gelişen teknoloji ile de her geçen gün yaygınlaşmaktadır. Gerçek hayatta yapılması çok uzun zaman alan ve çok pahalıya mal olan deneyler, bilgisayar ortamında modellenerek yapılmakta ve böylece hem zamandan hem de maliyetten tasarruf sağlanmaktadır. Bu amaçla ticari bir sonlu elemanlar analizi yazılımı olan ABAQUS (Dassult Systems) kullanılmış ve kuasi - statik çekme testi modeli bu programda geliştirilmiştir. Malzemenin doğrusal viskoelastik özelliklerinin kullanılmasında Paralel Reolojik Sistem ya da diğer ismiyle Genelleştirilmiş Maxwell Modelinin kullanılması uygun görülmüştür. Genelleştirimi Maxwell modeli ile polimer ve elastomer malzemelerin büyük deformasyonları ile doğrusal olmayan viskoz davranışları açıklanabilir. Bu modelde malzeme çok sayıda ağın paralel olarak birleştirilmesiyle oluşturulmaktadır. ABAQUS modelinde kullanılan numune, gerçek numune ile birebir aynı boyutlarda modellenmiş ve üst yüzeyi ankastre sınır koşulları, alt yüzeyi ise tıpkı gerçek deneyde olduğu gibi çekme kuvvetlerine maruz bırakılmıştır. Numune 6 farklı şekilde modellenmiştir. Model1 de numune 3 boyutlu şekil değiştirebilen plaka olarak modellenmiş, standart, doğrusal elemanlar kullanılmış ve kuvvet uygulanarak yer değiştirme ölçülerek gerilme hesaplanmıştır. Model2 de kuadratik eleman tipi kullanılmış, numuneye kuvvet uyulanmış ve yer değiştirme sonucu elde edilmiştir. Doğrusal eleman tipi kullanılan Model3 e yer değiştirme uygulanmış ve analiz sonucunda elde edilen kuvvet değerlerinden gerime hesabı yapılmıştır. Model4 tıpkı Model3 gibi modellenmiş olup farklı olarak kuadratik eleman kullanılmış ve aynı yöntem izlenmiştir. Model5, Model1 in doğrusal elastik malzeme modeli ile modellenmiş versiyonu olup detaylı bilgi tez içerisinde verilmiştir. Son model olan Model6 ise Model1 deki gibi modellenmiş olup elastistiklik modülü farklıdır. Bu modelde de sisteme kuvvet uygulanmış ve oluşan yer değiştirme miktarları kullanılarak gerilme değerine ulaşılmıştır. Her bir model için gerilme - birim uzama grafikleri elde edilmiş ve gerçek deney sonuçları, simülasyon sonuçları karşılaştırılmıştır. Tezin sonuç bölümünde deney sonuçları ile simülasyon sonuçları tartışılmıştır. Modellerin bu grafikleri kullanılarak deney sonuçlarıyla yakınsamasına bakılmış ve en uygun modelin Model6 olduğu görülmüştür. En uygun modelin nasıl seçildiğine, hangi ölçütlerin göz önünde bulundurulduğuna dair detaylı bilgiler tezin sonular bölümünde verilmiştir. Özetle tüm modeller göz önünde bulundurulduğunda doğrusal eleman kullanılan modellerin kuadratik eleman kullanılanlara göre daha iyi sonuçlar verdiği, analizde giriş değeri olarak kuvvet değeri vermenin daha uygun olduğu kararına varılmıştır.

Bu tez toplamda 5 bölümden oluşmakta olup, 1. bölümde tezin amacı anlatılmış, ve viskoelastisite, Dinamik Mekanik Analiz (DMA) ve prepreg malzemeler hakkında bilgiler verilmiştir. Tezin 2. Bölümünde numune hazırlanması ve yapılan çekme testi anlatılmış, deney sonucunda elde edilen veriler verilmiştir. 3. Bölümde çekme testi simülasyonu ve modellenmesi anlatılmıştır. Tezin 4. Bölümünde elde edilen deneysel verilerle modelleme sonucunda elde edilen sonuçlar karşılaştırılmış ve son bölümde de tezde yapılan işlemler özetlenmiş ve gelecekte yapılabilmesi muhtemel işlemler hakkında bilgi verilmiştir.

1. INTRODUCTION

Composites are defined as materials, which contain two or more combined parts at a macroscopic level, which are insoluble in each other. One part of these structures is called the reinforcing phase and the one in which it is embedded is called the matrix. Reinforcing parts can be fibers flakes or particles [18]. Fiber reinforced composites are the topic of current thesis. Pre-impregnated composites (pre-pregs) consist of reinforcement fibers pre-impregnated with a resin matrix and have been in use for many years. These types of composites have been used in aerospace, military, general aviation, satellite, marine, sporting equipment, automotive, wind energy [1]. Because of this wide use, there is an essential need for characterizing their properties. Different types of mechanical tests have made these characterizations. Dynamic mechanical analysis (DMA) is widely used to achieve this goal. Moreover, simulation of these composites has always been a matter of interest for research groups. Simulation models can prepare visually impressive tools that can easily process many complex mechanical members with less time and energy consume. For this reason, they are widely used in engineering designs. As it is clear only if we ensure that the simulation provides correct results, it can be used for real parts.

1.1 Purpose of Thesis

The goal of this thesis is to develop a suitable material model for simulation of CFRP-prepregs with ABAQUS. In the course of this endeavor, a literature study on static and dynamic DMA tests and their involved parameters has been done. In addition, usage of these tests in determination of material properties has been discussed. Then a material model based on Celstran®CFR-TP PA6 CF60-01 thermoplastic prepreg (for material properties see App. A) has been developed and DMA quasi-static tensile test has been used to validate resultant material model. This test has been performed at a temperature higher than melting point of sample and due to its thermoplasticity, sample has become soft and formable within testing. Finally, the correlation between simulation results and empirical data has been discussed to ensure validity of created model for using in real members.

1.2 Literature Review

1.2.1 Viscoelasticity

1.2.1.1 Definition

Elasticity is the science of studying elastic stresses and strains, their governing equations, and the effects of external forces that cause them. An elastic strain is defined as a strain that disappears instantaneously once the forces are removed. In other hand for polymers, viscoelastic effects are very important. Description of the deformation behavior of polymeric materials is more complicated than that of metals or ceramics, which have homogenous molecular structure. Because it is strongly dependent on both temperature and time [2].

Viscoelasticity is the characteristic of materials that display both viscous and elastic. In viscoelastic materials, resistance to shear force and strain with time is observed when stress is applied. In other words, they have time dependent properties, which are viscous part; furthermore, they have a tendency to return to their original state once the stress is removed, which is elastic part. Loss and Storage moduli are defined to deal with viscoelastic behavior of materials (see section 1.2.2.3).

By loading and unloading a sample, its viscoelastic behavior can be studied with the formation of a hysteresis loop. The energy lost per unit volume in the entire deformation cycle is indicated by the area of the hysteresis loop. Viscoelasticity is attributed to time-dependent molecular interactions with deformation of material. As it is mentioned, stress-strain behavior of viscoelastic materials is dependent on time. A suitable analogy that applies well is the attachment of a spring and dashpot. The spring models the elastic portion of the material, and the dashpot viscoelastic portion [2].

1.2.1.2 Parallel rheological framework

The parallel rheological framework or generalized Maxwell model is considered as most generalized model of defining linear viscoelastic properties. Large deformations of polymers and elastomeric materials that show permanent set and nonlinear viscous behavior can be explained by this model. It consists of multiple viscoelastic networks and an elastoplastic network in parallel.

This framework makes it possible to define a nonlinear viscoelastic-elastoplastic model made of various networks parallelly connected, as shown in Figure 1.1 [3].

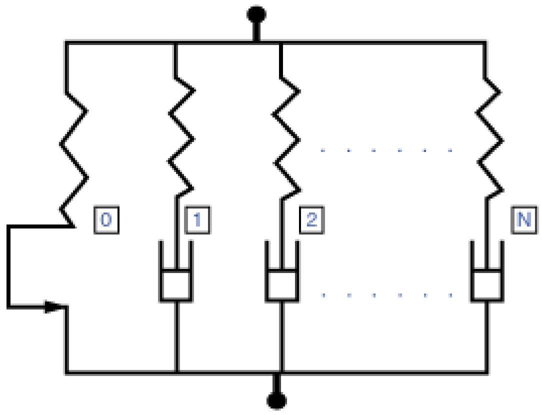

Figure 1.1 : Nonlinear viscoelastic-elastoplastic model with multiple parallel networks [3].

In ABAQUS, this framework is used to model material behavior, which is case of our study. The elastic part of the response for all the networks is specified using the elastic material model. Any of the elastic models available in ABAQUS can be used. diam nonumy eirmod tempor invidunt ut lab ore sit et dolore magna.

By specifying the identifier, stiffness ratio, and creep law for each viscoelastic network, viscous behavior can be defined (see [3]).

1.2.1.3 Prony series approximation of viscoelastic behavior

Consider a small time varying shear strain $\gamma(t)$, is applied to a small rectangular element. Viscoelastic material model defines the response shear stress $\tau(t)$ as:

$$\tau(t) = \int_0^t G_R(t-s)\dot{\gamma}(s)\, ds \tag{1.1}$$

Where $G_R(t)$ represents the time-dependent shear relaxation modulus and characterizes the material's response. A relaxation test in which a strain γ is suddenly applied to a specimen and then held constant for a long time can illustrate this behavior. Zero time is defined at the beginning of the experiment, when the strain is suddenly applied, so that:

$$\tau(t) = G_R(t)\gamma \quad \textbf{(1.2)}$$

Viscoelastic material model is long-term elastic in the condition that, after having been subjected to a constant strain for a long time, the response settles down to a constant stress; i.e.

$$G_R(t) \rightarrow G_\infty \; as \; t \rightarrow \infty \quad \textbf{(1.3)}$$

Dimensionless form of the shear relaxation modulus can be defined as:

$$g_R(t) = G_R(t)/G_0 \quad \textbf{(1.4)}$$

Where $G_0 = G_R(0)$ is the instantaneous shear modulus at time zero.

The limiting values of the dimensionless relaxation function are $g_R(0) = 1$ and $g_R(\infty) = G_\infty/G_0$.

In ABAQUS, the viscoelastic material is defined by a Prony series expansion of the dimensionless relaxation modulus:

$$g_R(t) = 1 - \sum_{i=1}^{N} \bar{g}_i^P \left(1 - e^{-t/\tau_i^G}\right) \quad \textbf{(1.5)}$$

Where $N, \bar{g}_i^P$ and τ_i^G, $i = 1,2, \dots, N$ indicate material constants [4].

1.2.2 Dynamic mechanical analysis

In order to determination of thermo-mechanical properties of polymers and polymer-based composites or materials, Dynamic mechanical analysis (DMA) or dynamic mechanical thermal analysis (DMTA), as a very useful and efficient testing technique, is introduced. It provides an accurate and sensitive testing method as a function of time, frequency, or temperature [8].

In DMA tests, a certain mechanical strain is applied to the sample and the resulting mechanical stress is measured by sensors. DMA can detect cure development and important transitions in the cure process such as gelation and vitrification (see section 1.2.2.4). Against chemical analysis, DMA arrange information on the mechanical behavior during the cure process [12,9], where thermosetting resin converts from a viscous liquid to a cross-linked solid; it is more sensitive to the transitions in the cure cycle, and more suitable for practical property study [9].

1.2.2.1 Tensile tests

DMA tests can be performed with different procedures and geometries (see section 1.2.2.3). In tensile tests a tensile load is applied to sample and its deformation is measured. This load can be quasi-static or dynamic. Loading procedure and heating rate varies in different tests. Temperature can be kept constant or changing with loading. Quasi-static loading, refers to loading where inertial effects are negligible. In other words, time and inertial mass are unrelated. This kind of loadings are applied so slowly that the structure deforms also very slowly (very low strain rate) and therefore the inertia force is very small and can be ignored. In contrast to static tests, dynamic tests refer to tests, which a dynamic time dependent load is applied to specimen. It is more common to use sinusoidal dynamic loads. Vibration frequency can be constant or varying with respect to time. As a simple procedure of tensile test, one end of sample can be kept cantilever and other end can be loaded quasi-statically or dynamically. In current thesis, quasi-static tensile loading of specimen has been studied.

As an example of tensile tests, non-linear viscoelastic tensile deformation of a long glass fiber reinforced polypropylene (PP-LGF) has been studied [5]. In this study a non-linear rheological material model has been developed. In this model, stress is decomposed into a time independent quasi-static and a time and strain dependent viscous portion. A series of stress relaxation experiments gives the viscous material behavior. Eyring’s equation is used to describe this behavior by means of strain dependent viscosity parameters. Figure 1.2 shows two types of tensile tests used in this study, in which the straining process is interrupted by a number of dwell times i.e. step-cycle tests and cyclic step-relaxation tests.

Figure 1.3 displays the experimental results of tensile tests, whereby the stress is plotted versus the true local strain, given by:

$$\varepsilon_H = ln\left(\frac{L_0 + \Delta L}{L_0}\right) \tag{1.6}$$

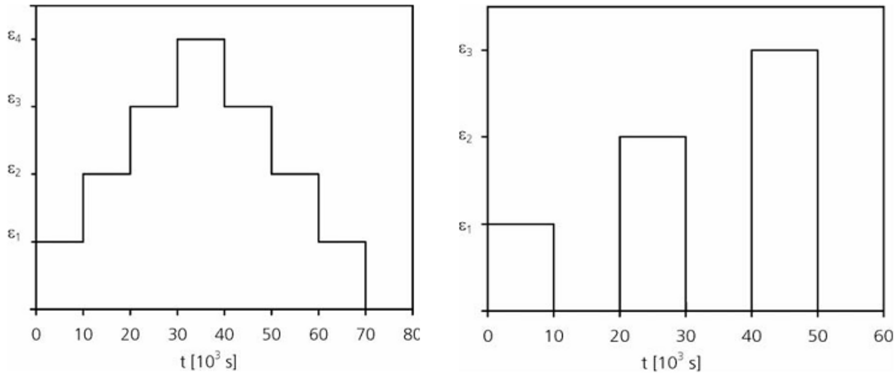

Figure 1.2 : Strain versus time of a cyclic step-relaxation test, Right: Strain versus time of a step-cycle test [5].

L_0 is the reference length before testing, and ΔL is the change in length. Tests were carried out for various strain rates, $\dot{\varepsilon}_H$.

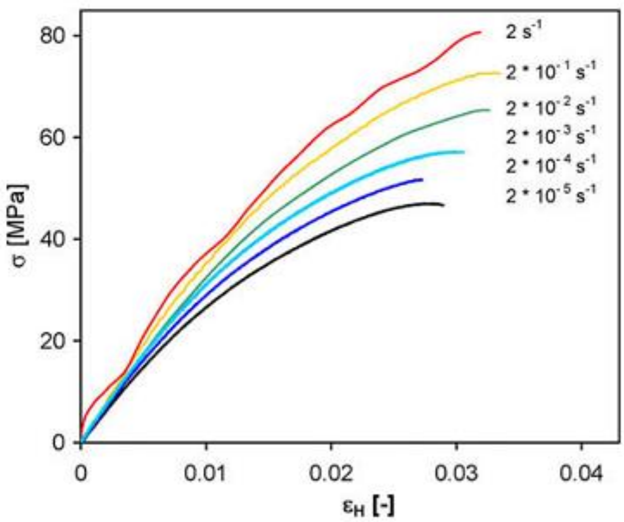

Figure 1.3 : Stress-strain dependence obtained for the PP-LGF for various strain rates. The stress is plotted against the true local strain [5].

For all investigated strain rates the stress–strain curves never follows a linear elastic relation, even for very small strains.

Results of a cyclic step-relaxation experiment are illustrated in Figure 1.4, in this process the loading and unloading procedure are interrupted by several dwell times of 10,000 s duration.

The total strain is composed of a permanent plastic part and a reversible elastic part $\varepsilon_H = \varepsilon_{H,pl} + \varepsilon_{H,el}$. In rheological model, by introducing two independent model branches this behavior can be expressed. One representing the quasi-static and other the dynamic viscous behavior of the material. Figure 1.7 shows such a model.

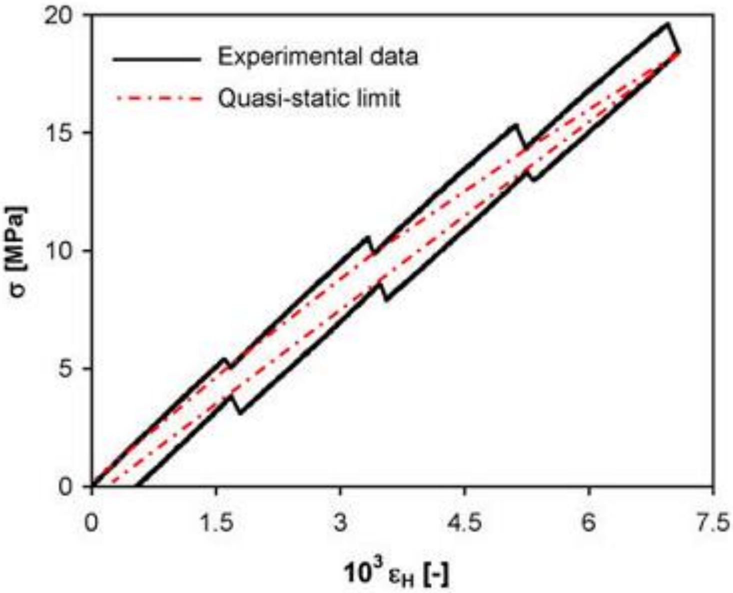

Figure 1.4 : Cyclic step - relaxation test. Strain rate is $\dot{\varepsilon}_H = 2 \times 10^{-5}$. Dash-dotted line is the extrapolated quasi-static material behavior in the limit of a vanishing strain rate [5].

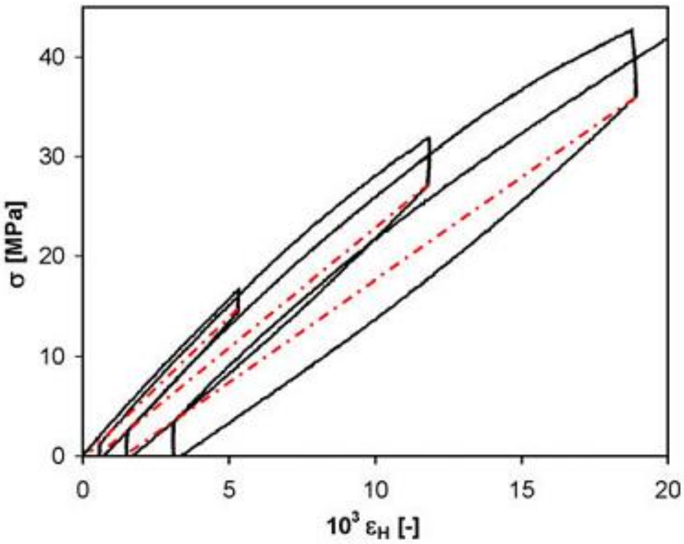

Figure 1.5 : Step - cycle test . The continuous l ine represents the measured data. The loading and unloading steps were performed at a strain rate of $\dot{\varepsilon}_H = 2 \times 10^{-5}$ and interrupted by dwell times of 10,000 s duration. The dash-dotted lines give for each deformation step the linear unloading path in the quasi-static limit [5].

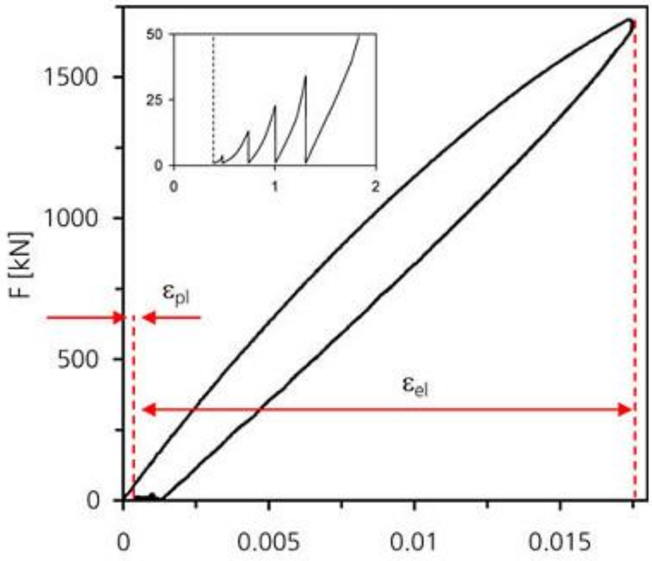

Figure 1.6 : To analyze the plastic deformation a tensile specimen was strained to a defined value and subsequently unloaded into the stress-free state where it was kept for 10,000 s.Persistent strain is interpreted as the irreversible plastic strain increment [5].

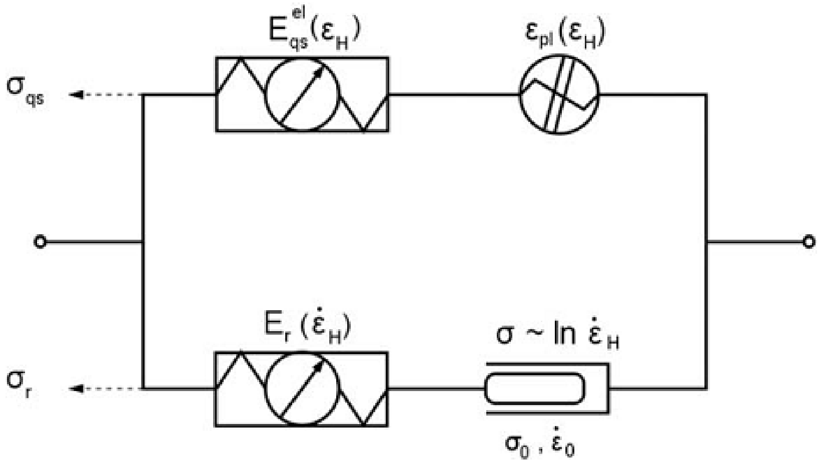

Figure 1.7 : A rheological material model composed of two branches representing the quasi-static stress σ_{qs} and the relaxing dynamic stress σ_r [5].

Because of the parallel connection of the two model branches, the total stress results from a summation of the single stresses. In this model, amounts of σ_{qs} and σ_r are introduced by:

$$\sigma_{qs}(\varepsilon_H) = \left(\varepsilon_H - \varepsilon_{H,pl}(\varepsilon_H^{max})\right).E_{el}(\varepsilon_H^{max}) \qquad \textbf{(1.7)}$$

and

$$\sigma_r = \sigma_0 \, asinh\left(\frac{\dot{\varepsilon}_H}{\dot{\varepsilon}_0}\right) \quad \textbf{(1.8)}$$

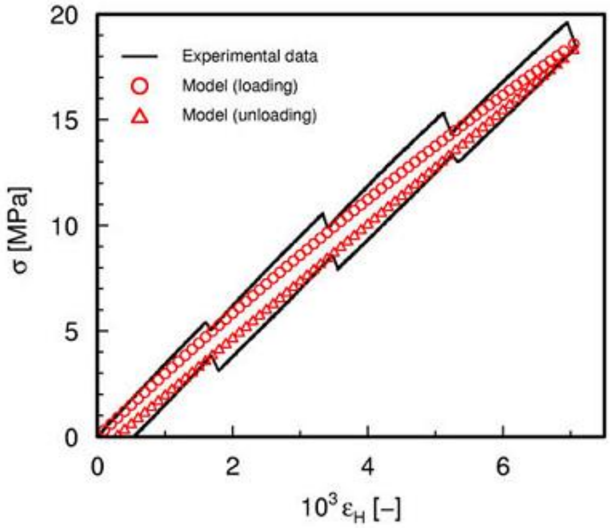

Figure 1.8 : Comparison of the experimental step-relaxation test with the model description for the quasi-static stress–strain relation for a loading and an unloading process [5].

As it is seen in Figure 1.8, the introduced model in this study is able to correctly reproduce the quasi-static and dynamic stress–strain behavior of the fiber-reinforced polypropylene.

1.2.2.2 DMA testing geometries

Each of the geometries discussed in this chapter has a different set of equations for calculating stress and strain from force and deformation. There are four types of bending which are commonly used in DMA tests. The simplest of these is the *three-point bending* shown in Figure 1.9a. Generally, size of sample should be about 10% longer on each end than the span [10].

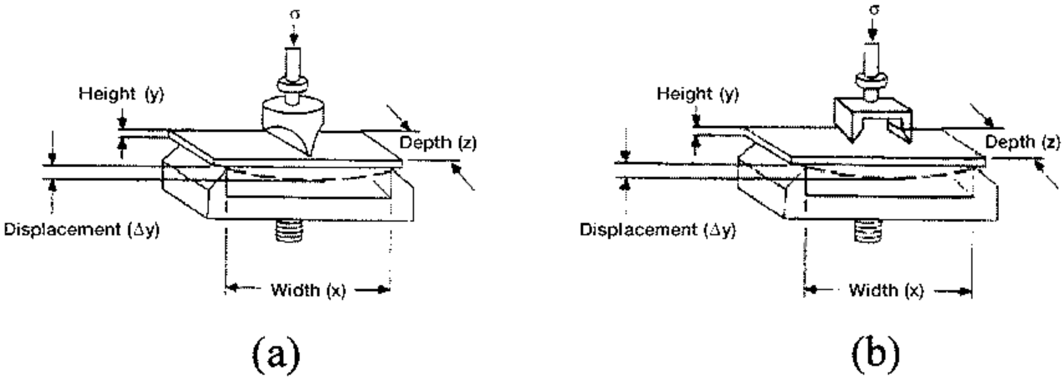

Figure 1.9 : (a) Three-point bending, (b) Four-point bending [10].

True four-sided span is called to a sample with edges parallel to the opposite side and perpendicular to the neighboring sides. *Four-point bending* replaces the single edge of three-point bending on top with a pair of edges, as shown in Figure 1.9b. In this geometry, the applied stress is distributed over a larger area than in three-point bending. And the load is applied on two points rather than one. Two types of cantilever fixtures are used: *dual cantilever*, shown in Figure 1.10a, and *single cantilever*, shown in Figure 1.10b. In both cantilever geometries, specimens should be true as described above and the load must be applied with the clamps perpendicular to the long axis of the sample [10].

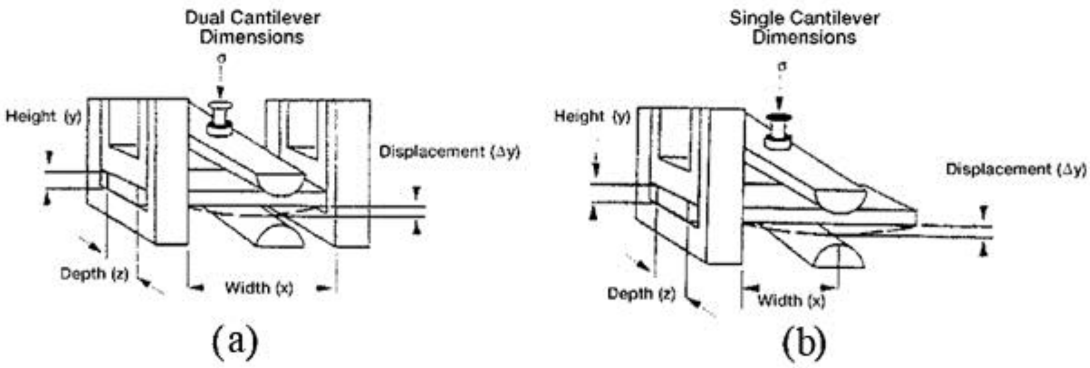

Figure 1.10 : (a) Dual cantilever, and (b) Single cantilever bending geometries [10].

It should be cared to clamp the specimen truly, with true forces, and not to exert a twisting or distortion in clamping. In most experiments moduli from dual cantilever tests tend to be 10–20% higher than the same material measured in three–point bending. This is as a result of shearing strain caused by fixing the specimen in place at the ends and middle in three-point bending test, which makes the deformation of sample harder [10].

1.2.2.3 Storage and Loss moduli

For characterization of the viscoelastic behavior of a material, it is deformed sinusoidally, and the resulting stress is reported. In the case of ideal elastic material, the stresses and strains can be considered in phase, and the phase shift δ=zero. Moreover for an ideal viscous material, the stresses and strains are 90° out of phase (i.e., δ=90°). A viscoelastic behavior, a combination of an ideal elastic response and an ideal viscous response, is more common. A viscoelastic response with a phase lag between the stress and the strain is shown in Figure 1.11. Dynamic (commonly sinusoidal) loadings are used to study the viscoelastic behavior of a material. The material is subjected to an oscillatory strain with frequency ω. From the Figure 1.11, the following expressions for strain and stress can be written [2]:

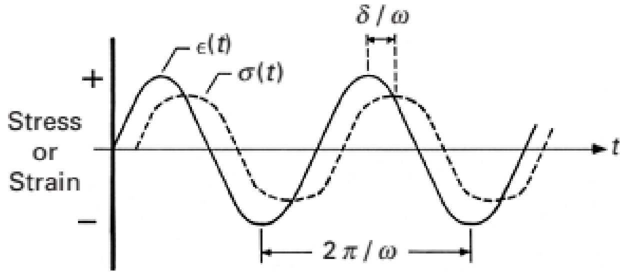

Figure 1.11 : Viscoelastic response of material with time lag between stress and strain [2].

$$\varepsilon = \varepsilon_0 \sin \omega t \tag{1.9}$$

And

$$\sigma = \sigma_0 \sin(\omega t + \delta) \tag{1.10}$$

δ represents the phase angle or phase lag between the stress and strain in eq. (10). From these expressions, two moduli can be defined:

$$E' = \left(\frac{\sigma_0}{\varepsilon_0}\right) \cos \delta \tag{1.11}$$

And

$$E'' = \left(\frac{\sigma_0}{\varepsilon_0}\right) \sin \delta \tag{1.12}$$

Where E' represents the tensile storage modulus and E" the tensile loss modulus.

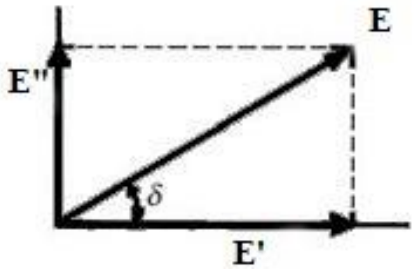

Figure 1.12 : Relationship between tensile storage and tensile loss modulus [2].

Moreover, by using complex variables following equations can be written:

$$\varepsilon = \varepsilon_0 \exp i(\omega t) \quad \textbf{(1.13)}$$

$$\sigma = \sigma_0 \exp i(\omega t + \delta) \quad \textbf{(1.14)}$$

And

$$E = \frac{\sigma}{\varepsilon} = \frac{\sigma_0}{\varepsilon_0} \exp i\delta = \frac{\sigma_0}{\varepsilon_0} (\cos\delta + i\sin\delta) = E' + iE" \quad \textbf{(1.15)}$$

Where i is the imaginary number $\sqrt{-1}$.

In a manner like tensile modulus, the shear modulus can be obtained. (Torsion pendulum is general experimental setup to obtain this) The complex modulus:

$$G = G' + iG" \quad \textbf{(1.16)}$$

Where G' represents the shear storage modulus and $G"$ the shear loss modulus. The storage modulus is a factor for measuring the stored energy, i.e., the elastic part. The loss modulus is a factor for measuring the energy lost as heat, i.e., the viscous part.

A term called the Loss tangent can be defined as follows [2]:

$$\text{Loss tangent} = \tan\delta = \frac{\text{energy loss}}{\text{energy stored}} = \frac{G"}{G'} = \frac{E"}{E'} \quad \textbf{(1.17)}$$

By means of three-point bending test an experimental study of the effects of oscillation amplitude on the elastic storage modulus, has been done [11]. Test material is LEXAN, an amorphous unoriented polycarbonate having 1.5, 3 and 4.5 mm nominal thicknesses. In this study dynamic and static loading have been performed with frequency of vibrations as 1 Hz. A centerline drawing has separated some of samples from pothers. These samples are called centerline marked (CM) samples. Other samples are noted as centerline unmarked (UM). In this study, the results of CMs and UMs have been compared. The effects of drive amplitude on the value of E' has been studied in two ways. In the first method, the amplitude is incrementally increased from zero to the maximum amplitude for each sample thickness. This method is referred as Incremental Amplitude Ramp (IAR). The second test is to cycle the sample through four rapid incremental pulses or Four Pulse Ramp (FPR). Study shows that the maximum obtainable amplitudes for 1.5, 3 and 4.5 mm thicknesses are 550, 250 and 100 mm, respectively.

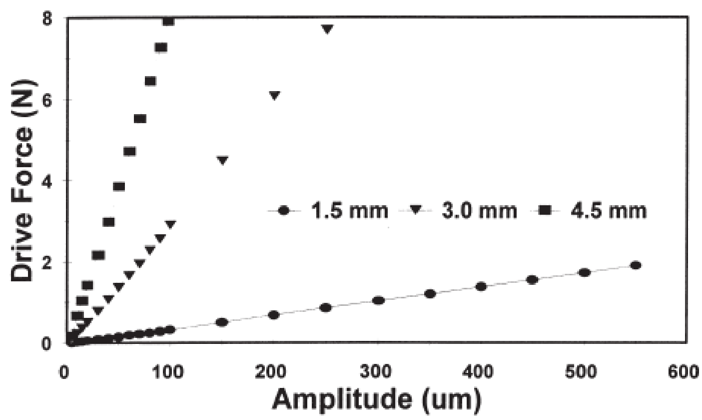

Figure 1.13 : Experimental results of Drive force with respect to Amplitude [11].

The diagrams of Loss modulus with respect to time for three different types of samples are drawn as fellow:

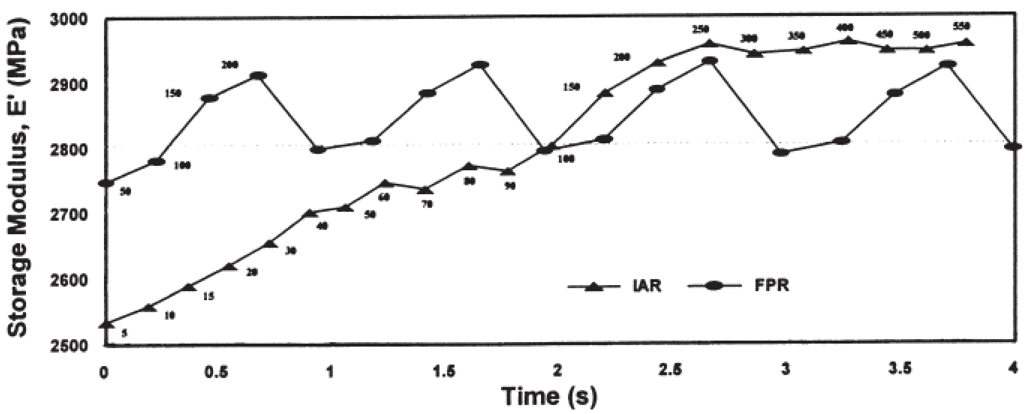

Figure 1.14 : Results for 1.5 mm thick samples [11].

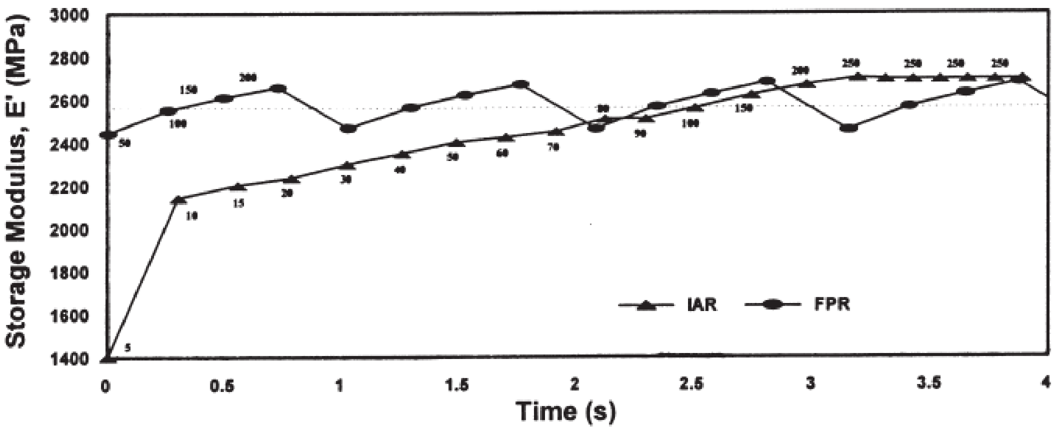

Figure 1.15 : Results for 3 mm thick samples [11].

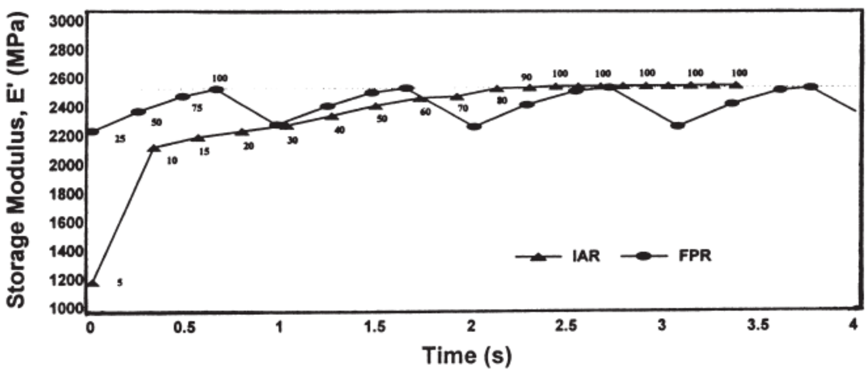

Figure 1.16 : Results for 4.5 mm thick samples [11].

This study shows there is a tendency for E' to increase non-linearly with amplitude irrespective of the sample span-to-thickness ratio used.

The influence of isothermal time interval on the internal friction of equiatomic TiNi shape memory alloys (SMAs) have been measured by DMA with the step cooling method [15]. In this study changes of $tan\,\delta$ and Storage modulus with respect to temperature have been obtained (Figure 1.17 and Figure 1.18).

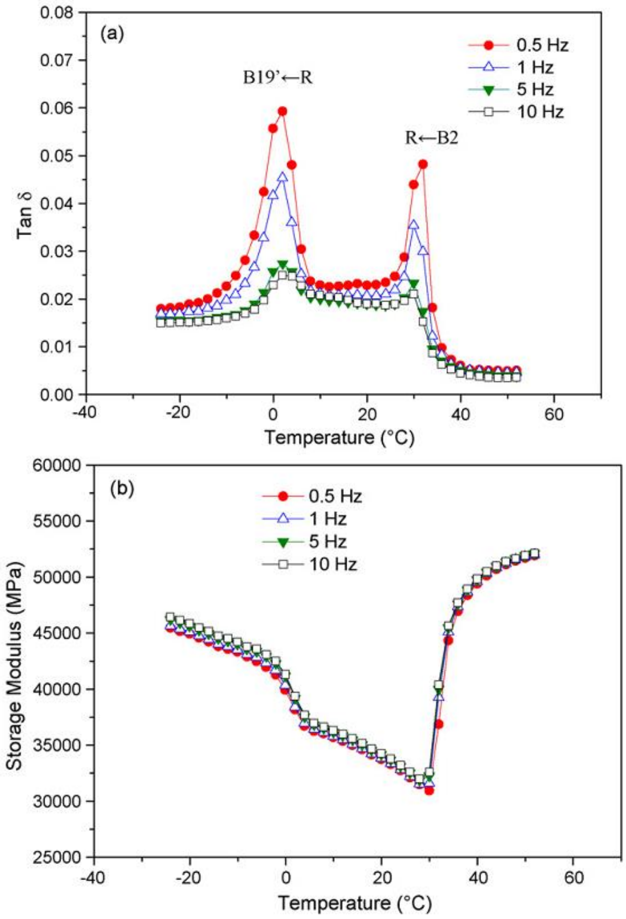

Figure 1.17 : (a) tanδ and (b) E' cooling curves measured by step cooling method with isothermal time intervalt= 1 min [15].

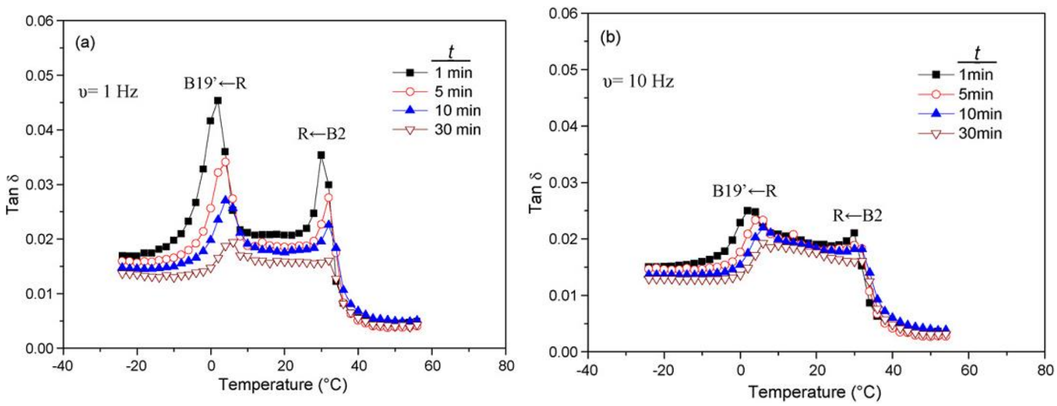

Figure 1.18 : tanδ cooling curves measured by step cooling method at (a) ν= 1 Hz and (b) ν=10Hz [15].

Temperature-dependent elastic moduli of two cured epoxy systems and two silica–epoxy nanocomposites have been studied by performing DMA test with different loading fixtures, and by mechanical tests at various temperatures [8]. The used epoxy systems are HexFlow RTM6 (Hexcel, USA) and Araldite-F (Ciba-Geigy, Australia). The support span is 17.39 mm for the single cantilever-loading mode, 34.78 mm for the double cantilever mode and 50 mm for the three-point bending mode. Temperature ramp from low to high is performed with a heating rate of 21˚C/min at an oscillation frequency of 1 Hz. The oscillation amplitude of displacement is kept at 40mm for most specimens. A loading rate of 5 mm/min is selected for all tensile tests. A loading rate of 2 mm/min is used for all the flexural tests.

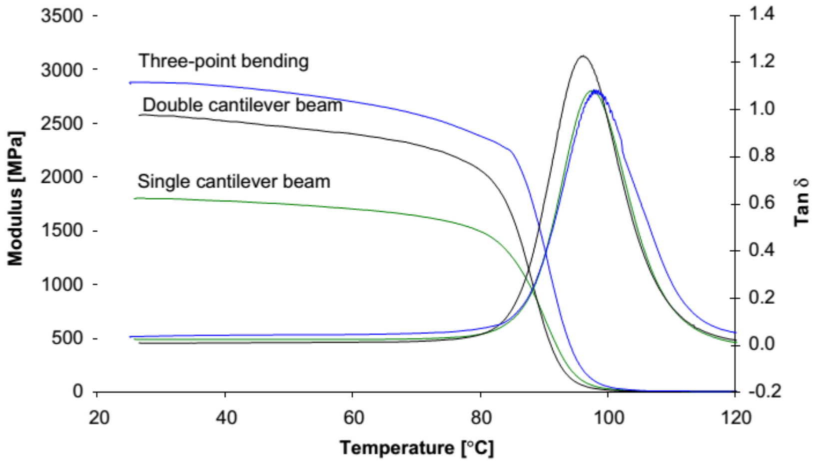

Figure 1.19 : Storage moduli of Araldite-F epoxy measured by DMA with three different modes [8].

The furnace temperature of DMA machine for all tests is increased continuously up to the designated temperature and then hold at that temperature for at least 20 min before start of testing.

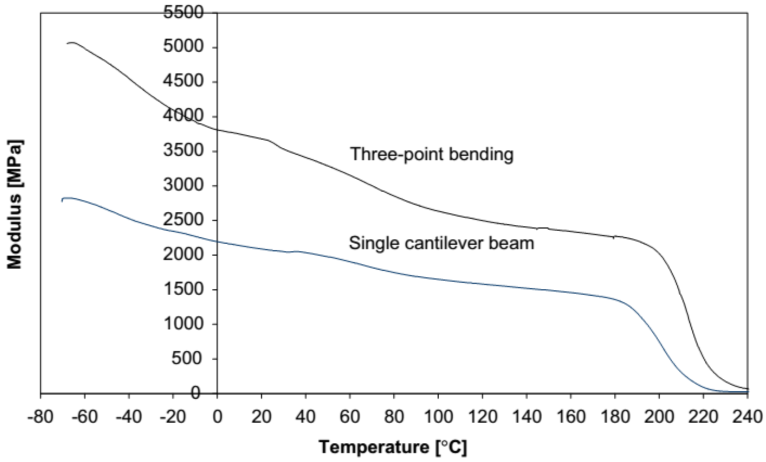

Figure 1.20 : Storage moduli of RTM6 epoxy measured by DMA with two loading modes [8].

The furnace temperature of DMA machine for all tests is increased continuously up to the designated temperature and then hold at that temperature for at least 20 min before start of testing.

Elastic moduli of RTM6 resin measured by DMA with tensile testing results measured at six temperatures have been compared.

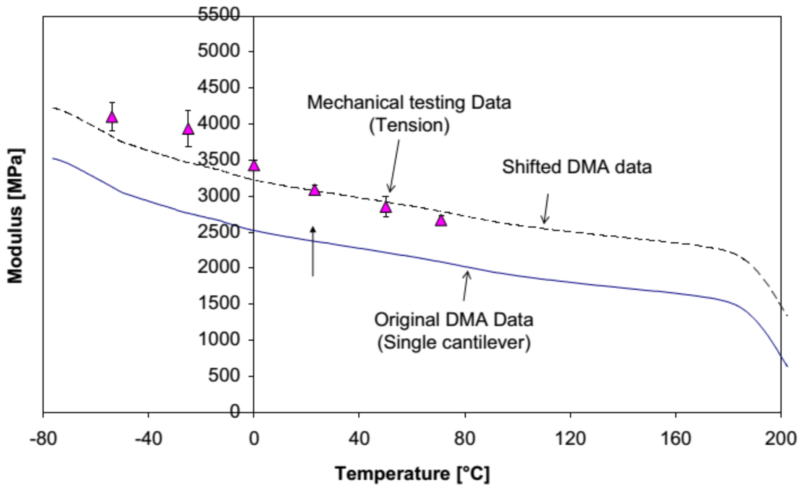

Figure 1.21 : Comparison of elastic moduli of RTM6 resin measured by DMA with tensile testing results measured at six temperatures [8].

As it can be seen in Figure 1.21, the original DMA test result does not correlate well with the elasticity moduli obtained from the tensile tests. Yet, by implementing a vertical shifting based on the elastic modulus at ambient temperature (231˚C) measured from tensile tests; good fit can be observed for the DMA data to the tensile testing results. Finally, it can be concluded that although there are disparities between the temperature-dependent elastic moduli measured by DMA, and those measured by normal mechanical tests, good agreement has been confirmed for two epoxy systems, and two nanocomposites after DMA data were corrected based on the static mechanical testing data. In addition, the three-point bending mode is found to be the most suitable for measuring temperature-dependent moduli by DMA.

1.2.2.4 Material characterization

Different mechanical properties of materials, effects of operating conditions and changes of material's characteristics with respect to time and temperature can be studied by DMA. As an example cure process of plymer materials can be studied. This procedure is the mechanism of toughening or hardening of polymer chains by heat or chemical supplements.

Cure development of wood-phenolic joints have been studied by DMA [12]. Three point bending tests on sandwich beams have been used in this study. Each sandwich specimens are composed of two wood strips, separated by an adhesive layer (PF resin). Sizes of specimens are 50×12×1 mm. Frequency of tests is 1 Hz, and amplitude of strain is 0.03 mm. Strains of 10^{-4} mm at 90, 100, 110, 115, 120 and 130˚C have been applied in this study.

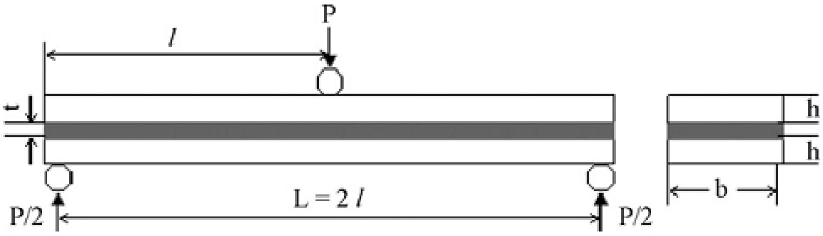

Figure 1.22 : Three-point bending sandwich beam with the grey adhesive layer between two wood adherends and ascillating load P [12].

Load P and mid-span deflection Δ of the beam are out of phase by some angle δ. The storage component of the sandwich beam stiffness is given as $C' = \frac{P'}{\Delta}$ where $P' = P\ cos\delta$.

Figure 1.23 shows changes of E', G'_a, C' with respect to temperature. Where index a represents adhesive.

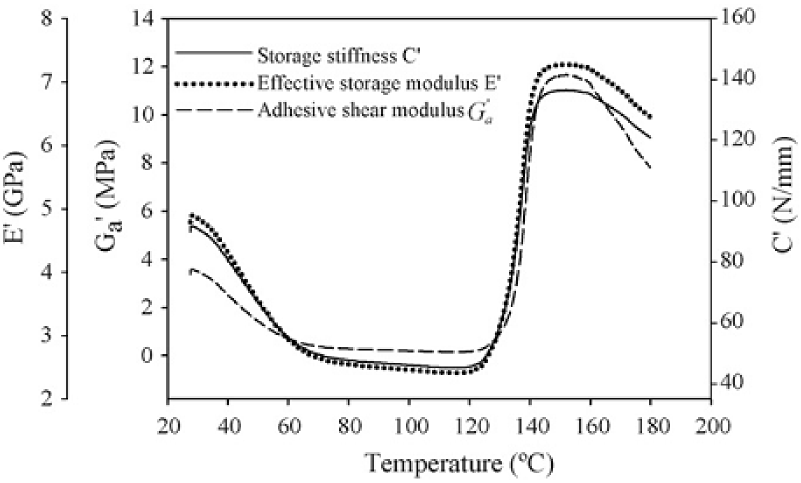

Figure 1.23 : Effective storage modulus (E′) and storage stiffness (C′) changes with temperature during curing at 3˚C/min for a foil-wrapped PF-high bonded wood joint. Shear modulus of the adhesive layer (G'_a) was calculated with an analytical solution from C′ [12].

In these experiments the ratio of the maximum to minimum E', R, approaches a value of 4 in two extreme cases when the shear modulus is negligible before curing and is comparable to the adherents after curing. Experimentally, a large portion of measured values for R is near four. This fact can be explained as the increase of modulus of wood adherent because of moisture lost during the test accounted for the large values of R in excess of four. Further, some dependency of R on resin loading is observed. This indicates that a consistent sample preparation is important for evaluating cure performance with DMA.

As another example of studying material behavior, dynamic viscoelastic properties of sweet potato has been studied by DMA [13]. Both compression tests, three-point bending tests, stress-relaxation analysis with constant strain of 1%, creep test, temperature sweep test and frequency sweep tests have been performed.

In stress-relaxation test, the sample is kept at a constant strain of 1% in a three-point bending clamp to make it relax for 5 min; while in a compression mode, the sample was kept at a constant strain of 5% for 10 min. The temperature inside the furnace is kept at about 23˚C.

In creep test, constant stress is set at 0.1 MPa, and the creep time and the recovery time are both made 5 min for the two clamps.

In temperature sweep tests, a dynamic deformation with amplitude of 30μm is applied on sample in the compression clamp at a frequency of 1 Hz, and then the viscoelastic properties of the samples, such as storage modulus, loss modulus and loss factor ($\tan\delta$), are measured when the temperature increased from 30˚C to 105˚C. In addition, two heating rates, 2˚C/min and 10˚C/min, are used to determine the effect of different heating rates on the viscoelastic properties.

The frequency sweep tests are conducted by holding temperature and deformation constantly and scanning across the frequency range of interest. The frequency range is set at 50–0.1 Hz; the dynamic deformation of 30 μm is applied in both the three-point bending and the compression mode.

Figure 1.24 and 1.25 show the results of analysis.

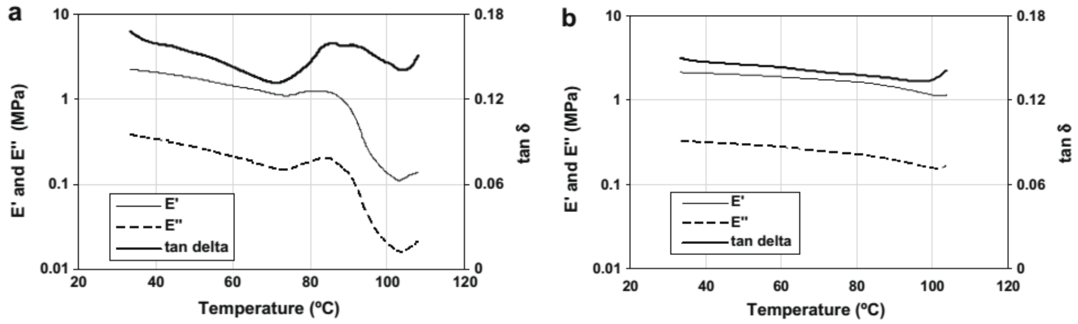

Figure 1.24 : Temperature scanning curves in different heating-up rates with a constant deformation of 30μm and loading frequency of 1 Hz in the compression clamp. (a): 2˚C/min, strain: 0.29%; (b): 10˚C/min, strain: 0.27% [13].

m

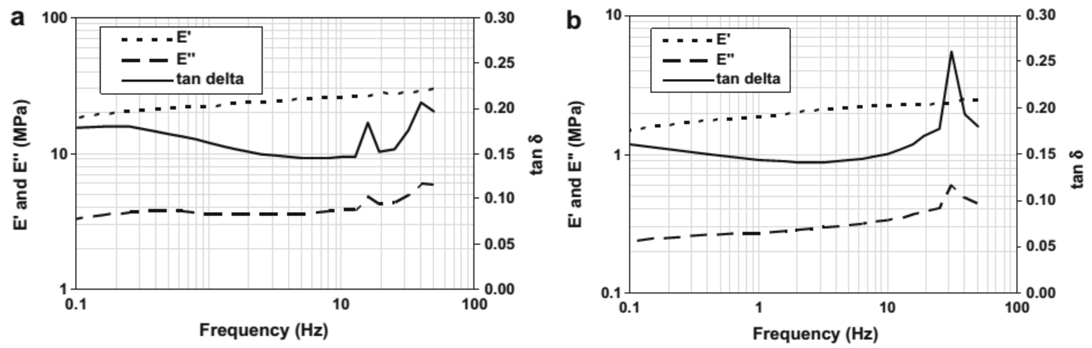

Figure 1.25 : Frequency scanning curves. (a): 3-point bending mode with a constant deformation of 30μm at ambient temperature; (b): compression mode with a constant strain of 0.27% at ambient temperature [13].

It is observed, according to the regression results of relaxation tests in three-point bending clamp, relaxation behavior of the sweet potato can be represented well using five element Maxwell model. The creep-recovery tests revealed that four element Burgers model fitted experimental data of both clamps well.

As an example of dynamic DMA, study of fatigue tensile behavior of carbon/epoxy composite has been done [6]. This study contains both warp and fill directional loading cases. The specimens consist of three warp yarn layers and four fill yarn layers with the warp and fill yarn insertion densities 4.72 ends/cm (12 ends/in.) and 3.91 picks/cm (10 picks/in.), respectively. Main properties of the composite are listed in table 2.1. The damage inception and advancement are controlled during the tests with acoustic AE registration; the AE signals were processed with AMSY-5 system (Vallen Systems Gmbh).

Table 1.1 : Quasi-static mechanical characteristics of the non-crimp 3D orthogonal woven carbon/epoxy composite [6].

Parameter		Test direction	
		Warp	Fill
Interval secant modulus *E*, GPa, strain range 0.1–0.2%		57.4	57.4
Average values for strain interval 0.3%,…, 0.9%		59.8	63.8
Strength, σ_{ult} (MPa)		953	901
Ultimate elongation, ε_{ult} (%)		1.59	1.49
Damage thresholds			
σ^d_{min} (MPa)	The first AE event; sporadic fiber–matrix debonds at the yarn edges	256	203
σ^d_1 (MPa)	AE events of low energy; transversal cracks inside impregnated yarns and on their boundaries	368	356
σ^d_2 (MPa)	AE events of high energy; well developed transversal cracks in the impregnated yarns and matrix pockets, local debonds parallel to the sample surface	414	419

The average fatigue life for the warp directional loading case is observed in this study about three times longer than that for the fill directional loading case. However, the range of the maximum cycle stress, corresponding to 3000,000 cycle life, is the same (between 412 and 450 MPa), for both loading directions.

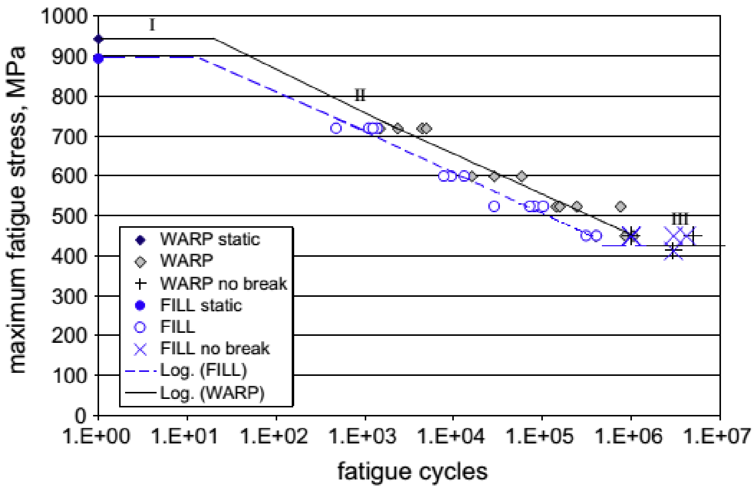

Figure 1.26 : Fatigue life diagrams for carbon/epoxy non-crimp 3D orthogonal woven composite, loaded in warp and fill directions. The symbols + and indicate tests in which the samples did not fail [6].

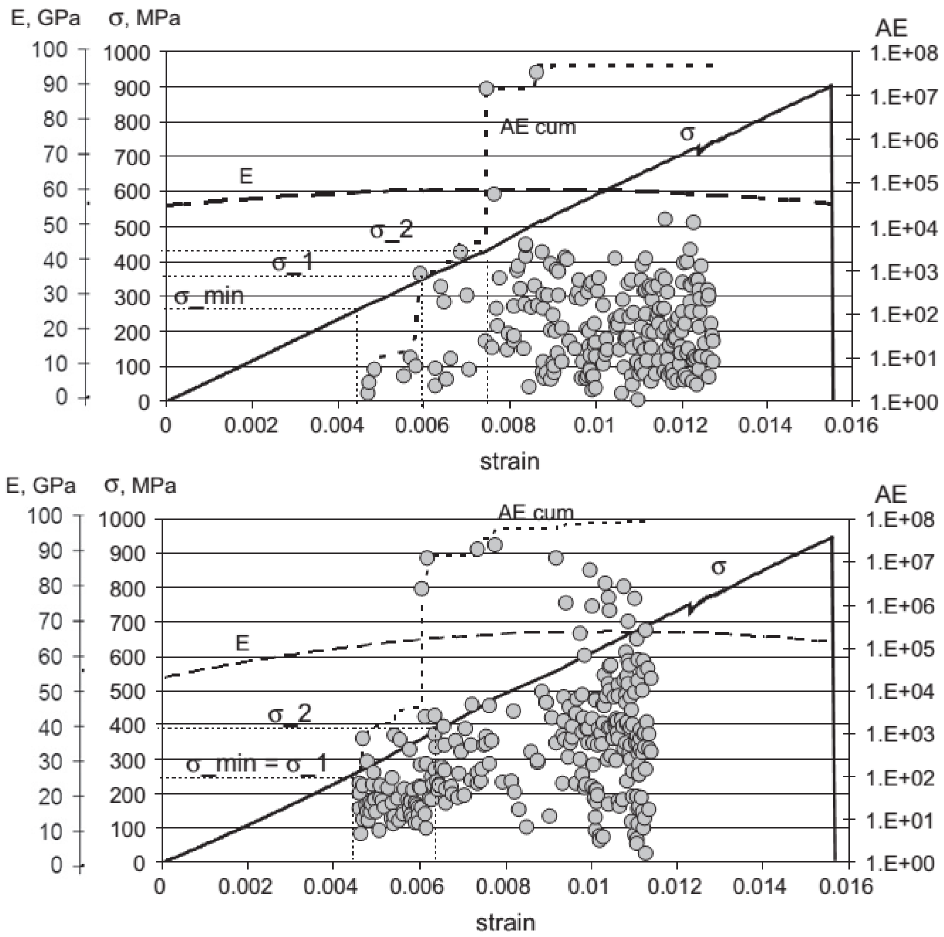

Figure 1.27 : Results of quasi-static tensile tests. Representative test for loading in warp (Up) and fill (Down) direction. The plot shows variations of stress (σ), tangent modulus (E), energy of individual AE events, and cumulative energy (in arbitrary units) with strain. Values of σ^d_{min}, σ^d_1 and σ^d_2 designate characteristic damage thresholds determined from the AE results, see Table 2.1 [6].

The obtained fatigue test data and, particularly, the S–N curves, when they are compared to the results of previous fatigue studies of some other types of 3-D reinforced composites, provide additional support to the previously made general conclusion that certain reduction of fatigue performance always takes place due to the presence of through thickness reinforcement of any kind.

Mechanical response of materials for quasi-static and dynamic loadings has been studied in literature. For example discontinuous ceramic fiber reinforced Al-2% Cu metal matrix composites (MMC) have been studied [7]. The effect of volume fraction on the mechanical behavior and dynamic impact response and failure mechanisms has been characterized. The matrix alloy used is Al–2% Cu (0.01 wt%

Si, 0.01 wt% Fe and 2.17 wt% Cu). The reinforcement phase is Saffil® short fiber Al_2O_3 in preforms of 4%, 7%, 15%, and 30% volume fraction. The Saffil® fiber has a chemical composition of 95–97% Al_2O_3 with 3–5% SiO_2, with a median diameter of 3.0–3.5μm, density of 3.4 g/cm^3, Young's modulus of 300 GPa, and ultimate tensile strength of 1.5 GPa. Quasi-static tensile testing is conducted on the Al–2% Cu matrix alloy and the four MMC materials containing 4%, 7%, 15%, and 30% Saffil® short fiber reinforcement. The MMC materials are tested parallel to the direction of dominant fiber loading to determine the in-plane tensile behavior. Flat rectangular tensile specimens of 0.5 mm thickness are tested according to ASTM D 3552. Figures 1.28 and 1.29 represent the results of experiments.

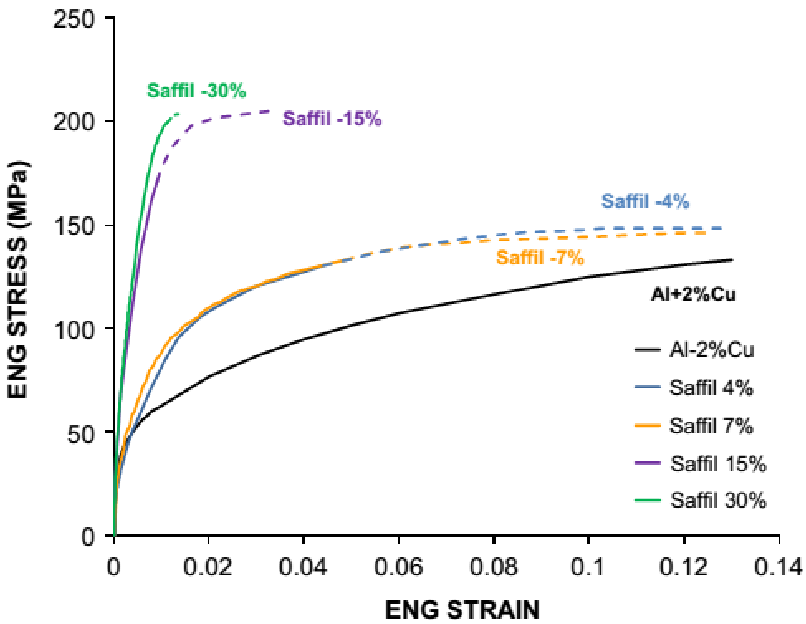

Figure 1.28 : Typical stress–strain curves from quasi-static tension tests (tested to failure) of Al–2% matrix and four MMC materials tested in-plane. Dashed lines indicate range of variability in strain to failure [7].

As it is seen in Figure 1.28, the unreinforced matrix alloy shows the lowest tensile strength and the highest strain to failure in tension (~13%) of all the materials. By increasing the volume fraction of fiber, the tensile strength increases and the strain to failure decreases, except for the 4% and 7% Saffil MMC had nearly identical response. The strength and failure of MMC materials are sensitive to the heterogeneous arrangement of the reinforcement phase.

In Figure 1.29, the strength of the materials uniformly increases as the volume fraction of Saffil fiber increases over the investigated range of 0–30%. Samples are not loaded to failure in compression, and unloading curves are used to determine the elastic modulus values, which are summarized in Table 2.2.

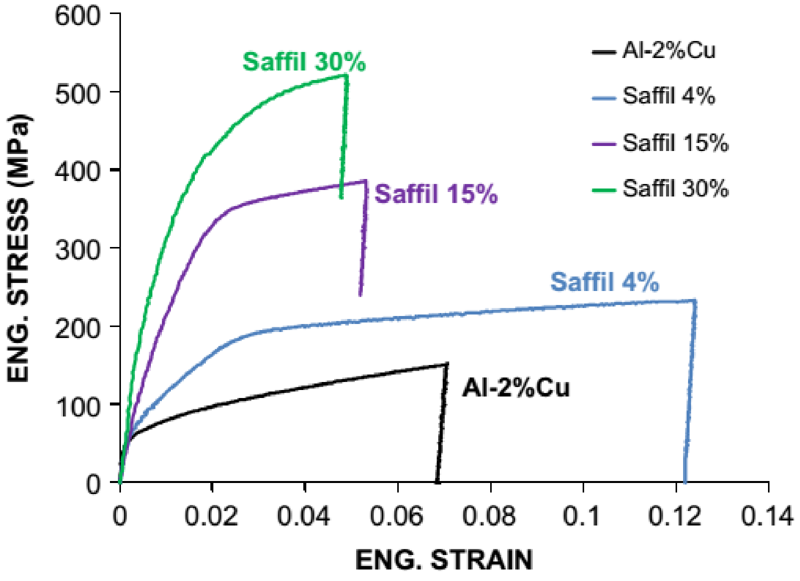

Figure 1.29 : Typical stress–strain curves, including unloading, from in-plane quasi-static compression tests of Al–2% Cu matrix and four MMC materials [7].

As final conclution of this research, These MMC materials exhibited a strong strength asymmetry in tension versus compression response. These MMC materials appear to be stronger in compression and increasment of volume fraction of fiber cause increase in the asymmetry in response. A fail in a ductile manner is observed in MMC materials with 7% and less volume fraction of fiber, while MMC with 15% and greater reinforcement display brittle failure in tension. Remarkable plasticity in compression is observed for all tested materials.

Table 1.2 : Elastic modulus values from compression testing [7].

Material	Modulus (GPa)
Al-2% Cu	70.6 ± 3.0
Saffil-4% MMC	95.0 ± 2.3
Saffil-15% MMC	98.5 ± 6.1
Saffil-30% MMC	106.1 ± 19.9

Mechanical propertes of coated pellets have been studied by DMA [14]. This study shows that, the mechanical properties of the pellets are affected by coating. Ordinary technique, which employs the diametral compression test suggest pellets with a soft core to increase strength. And suggests pellets with a rigid core to increase in elasticity and deformability. Dissipated energy can be determined by using DMA, however, the sinusoidal stress–relaxation cycles, in terms of loss modulus or phase angle.

1.2.3 Prepreg

Based on polymers behavior upon heating, they can be divided into two broad categories:

- Thermosetting polymers,
- Thermoplastics.

In a polymer with cross-linked molecules, softening with heating does not occur. These cross-linked polymers are called *thermosetting* polymers. Decomposition of thermosetting polymers upon heating is explained by cross-linking of their molecules. Cross-linking makes slippage of molecules on each other difficult; this property has a significant role in strength and rigidity of polymer. A typical example of this behavior can be rubber cross-linked with sulfur. The toughness of this type of rubber is 10 times of natural rubber. Familiar examples of thermosetting composites are epoxy, polyester, phenolic, polyurethane, and silicone. On the other hand, *thermoplastics* are called to polymers that soften or melt in high temperatures. They are mostly linear polymers. For example, low- and high-density polyethylene and polymethyl methacrylate (PMMA). Ductility is a general property of thermoplastics. They withstand plastic deformation [2].

Used material in present study (Celstran® CFR-TP PA6 CF60-01), is fiber reinforced thermoplastic composite.

Ease of use, consistent properties, and high quality surface finish make pre-impregnated composites (pre-pregs) increasingly common in the composite industry. A prepreg can be defined as FRP reinforcement, which is pre-impregnated with a resin. Although many types of resins can be used, but in most cases the resin is an epoxy. However, most of thermoset and thermoplastic resins can be used.

Cure state of prepregs have been studied in literature, and suitable methods to characterize cure state of epoxy prepregs have been introduced by DMA [9]. For example phenol novolac epoxy resin (EPN, F-46) have been selected without further treatment for DMA testing [9]. Rectangular specimen by 20.0mm×6.0mm×0.20mm have been made and longitudinal direction of the fiber in the prepreg have been selected parallel to the length of the samples. Cure parameter (α) in this research have been defined as follow:

$$\alpha = \frac{T_g - T_{g,0}}{T_{g,\infty} - T_{g,0}}, \alpha = \frac{\Delta \tan\delta - \Delta \tan\delta_0}{\Delta \tan\delta_\infty - \Delta \tan\delta_0} \quad \textbf{(1.18)}$$

Where $T_{g,\infty}$ is the glass temperature of the fully cured resin and $\Delta\, tan\, \delta$ indicates the area under *tanδ* curve. Immobility of molecules at low temperatures, do not let them to resonate with the oscillatory loads. Thus, they remain solid. Changing from glass state into the rubber like elastic state is known as glass transition. This temperature is often considered as the temperature of the maximum loss modulus (E''_{max} or G''_{max}) or the maximum loss factor ($\tan \delta_{max}$).

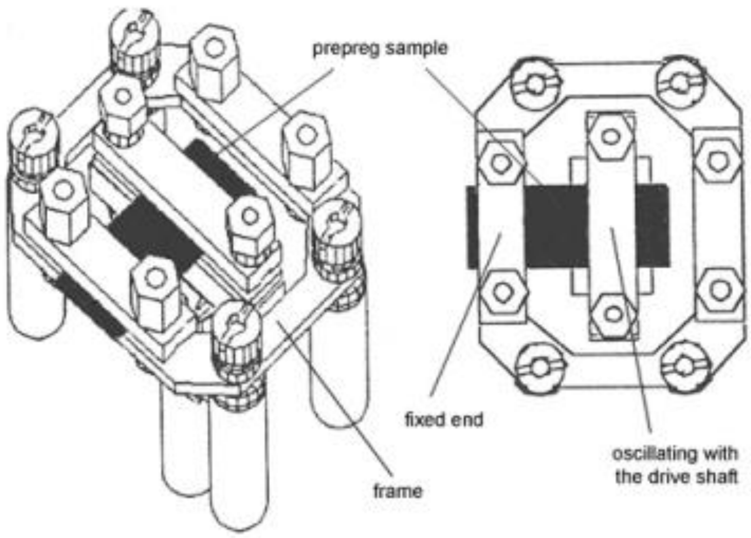

Figure 1.30 : Scheme of the measuring system in DMA [9].

Accuracy of sample geometries often plays a great role in accuracy of the DMA measurements. In this study storage and loss modulus are calculated from following equations:

$$E' = \frac{l^3}{wt^3}\frac{F}{D}\, g\, Sin\, \delta\, , E'' = \frac{l^3}{wt^3}\frac{F}{D}\, g\, Cos\, \delta \quad \textbf{(1.19)}$$

One end of the sample is oscillating up and down with frequency of 1 Hz. The strain amplitude is 0.01%, and temperature is rising from 110°C to 240°C . Heating rate is about $30°C/m$. The change of dynamic flexural modulus and storage modulus with respect to time is shown in Figure 1.31.

As it is seen in the Figure 1.31, at first area $tan\,\delta$ increases as the time passes, until it reaches to a peak. This point is called *Glass transition***.** This is the reversible conversion from a strong and almost brittle state into a molten or rubber-like state. In second area, a peak in loss modulus is observed. This peak is called *Gelation transition*. The small peak in E" or the shoulder in $tan\,\delta$ at third area illustrates the *vitrification transition*. Vitrification of a thermosetting resin happens once the glass transition temperature of the system exceeds the cure temperature. After vitrification, the cure reaction within the resin occurs at a slower rate.

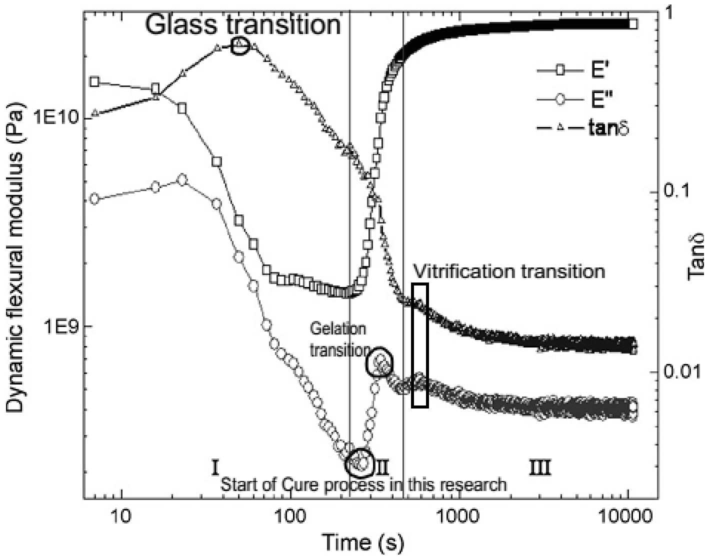

Figure 1.31 : Typical isothermal measurement of prepreg by means of DMA [9].

As an example of deformation behavior of multilayer prepregs under loading, in-plane deformation of two different unidirectional thermoset prepregs have been studied [17]. This work contains experimental study and FE modeling. ABAQUS subroutine has been used to model friction. The purpose of development of this method is to predict the reaction force and fiber reorientation during in-plane forming of thermoset prepreg and detecting effects of fiber angle in tensile deformation of prepreg. This study focuses on two aerospace graded thermoset epoxy/carbon prepreg materials: HexPly®T700/M21, 268 g/m^2 (referred to as T700/M21) from Hexel. Cycom®HTS/977-2, 134 g/m^2 (referred to as HTS/977-2) from Cytec. Desired cure temperature of systems is 180 °C, but they are always kept below 90˚C to avoid unwilling curing. Two layer settlements have been investigated in this study: $[45/-45/90]_s$ and $[45/90/-45]_s$. Layers transverse to the pulling direction are called 90˚ layers. Each specimen consisted of six equally sized prepreg layers. To have a homogeneous contact between the layers and remove air as much as possible, the layers were stabilized under vacuum for at least 30 min at pressure of 0.1 MPa. De-coupled shells are selected to model the plies in ABAQUS. In this case, continuum shell elements are used to define bending properties and continuum membrane elements are used to describe in-plane behavior.

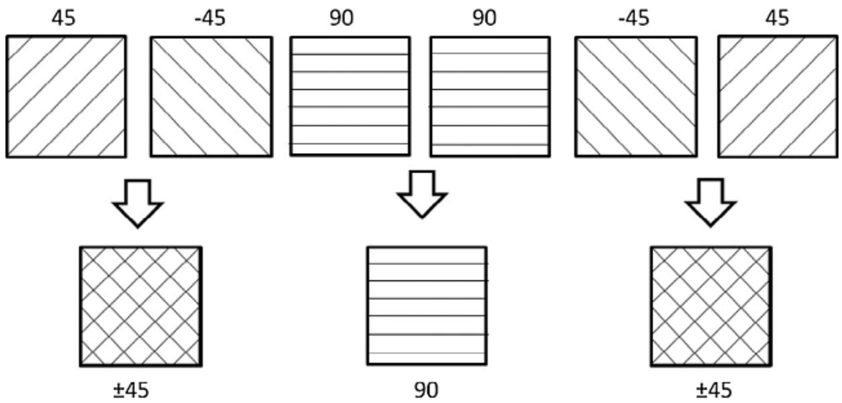

Figure 1.32 : Stacking sequence $[45/-45/90]_s$ (above) and expected, effective deformation behavior (below) [19].

To model the in-plane shear a reinforced Kelvin-Voigt model is used, composed of an isotropic elastic (spring) material model in combination with a Newtonian fluid (damper), (see section 1.2.1.2). FE simulation result is shown in Figure 1.33:

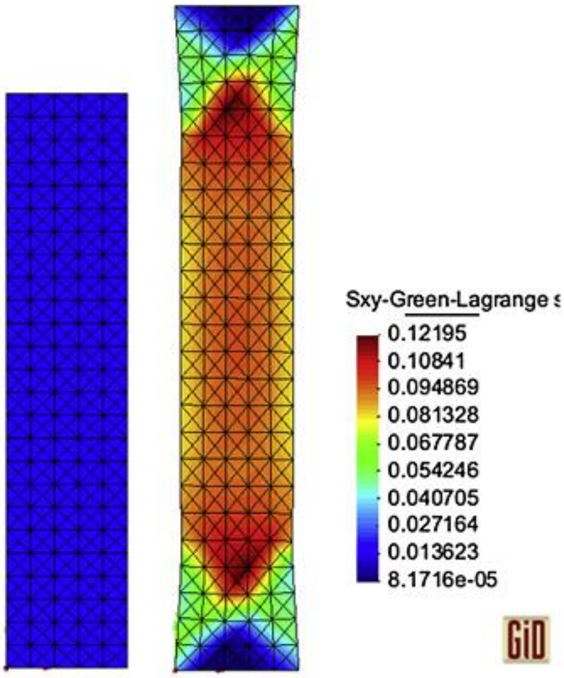

Figure 1.33 : Bias extension test simulated in AniForm [19].

Visual observations of the samples during in-plane deformation tests confirmed that the stack deforms together rather than as single plies.

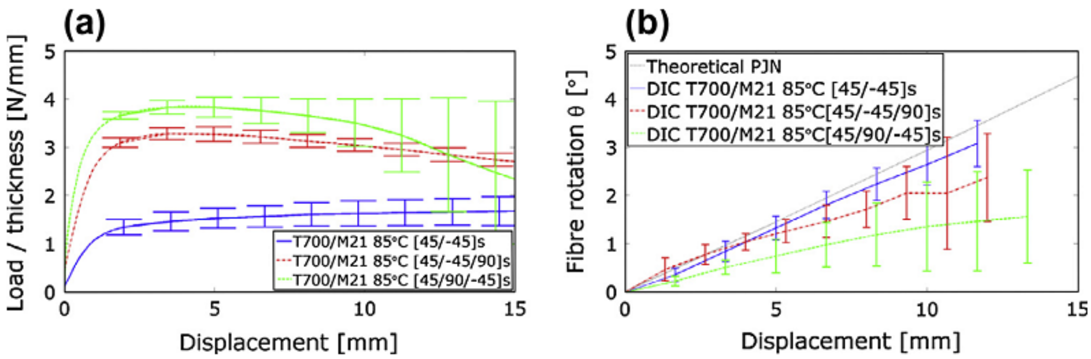

Figure 1.34 : Experimental results from in-plane forming tests for T700/M21 at 85 ˚C and 40 mm/min [19].

As can be seen in Figure 1.34, the lowest required stacking load to deformation is for $[45/-45]_s$. its rotation is approximately according to the PJN theory. Figure 1.34 further shows that adding 90˚ layers, can magnificently increase the load to deformation compared to the $[45/-45]_s$. To summarize the experimental findings; keeping the 90˚ layers only in the center, makes an increasement in the fiber rotation, meanwhile it makes a reduction in the load to deformation compared to when the 90˚ layers are assigned in between the ±45˚ layer pair. The former therefore needs less energy to deform.

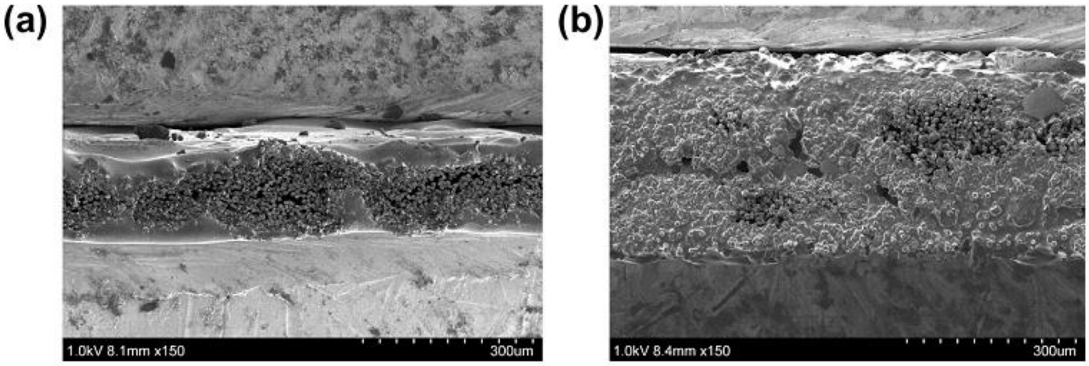

Figure 1.35 : SEM micrograph of virgin, uncured (a) HTS/977-2, (b) T700/M21, cuts are made transverse to fiber direction [19].

Impregnation degree is an important factor of prepreg characterization. Impregnation degree of the prepreg by near infrared (NIR) spectroscopy has been investigated [20]. That is the key factor to ensure the quality of prepreg. In this study, the light from the sources is focused on prepreg with 17 cm height and 25 mm diameter. The instrument equipment is shown in Figure 1.36.

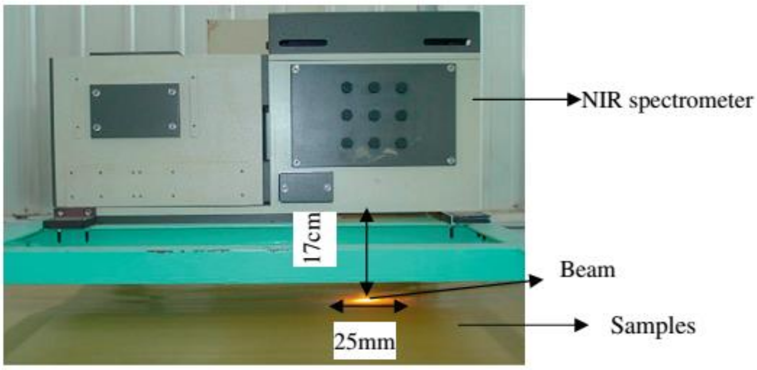

Figure 1.36 : Photograph of noncontact equipment of NIR spectrometer [20].

In experiment, the size of each prepreg is 50×50 mm. Each test specimen consisted of two parts superposition prepreg; it got the resin (*R*) of the same weight.

The impregnation degree of the prepreg is calculated by formula (20).

$$I = (R_1 - R_2) \times R^{-1} \times 100\% \qquad \textbf{(1.20)}$$

Where R_1 is the resin weight of the first prepreg; R_2 is the resin weight of the second prepreg; R is the sum of R_1 and R_2; and I is the degree of the non-impregnation prepreg.

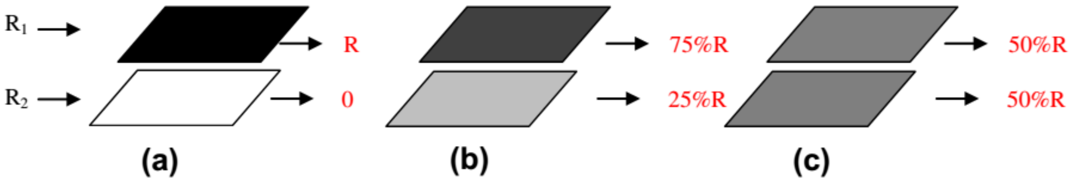

Figure 1.37 : The analysis of the impregnation degree [20].

Study of this method can give a new direction on the quality analysis and the manufacture of prepreg.

2. EXPERIMENT

The material selected for this study is Celstran® CFR-TP PA6 CF60-01 produced by Ticona GmbH, which has 48% carbon fiber volume fraction. It is composed of PA6 (polyamide 6, or nylon 6) and fibers are uni-directional. This material exhibits a high strength-to-weight ratio, excellent toughness and impact resistance. It is well suited for industrial, automotive and sporting goods applications where strength and toughness are critical as well as ease of processing. More information about this composite can be found in *Appendix A*.

2.1 Sample Preparation

Sample preparation took place in the Composite Testing Laboratory (CTL) of the Institute for Carbon Composites (LCC) at the Technical University of Munich (TUM). Prepreg sheets were available as Figure 2.1.

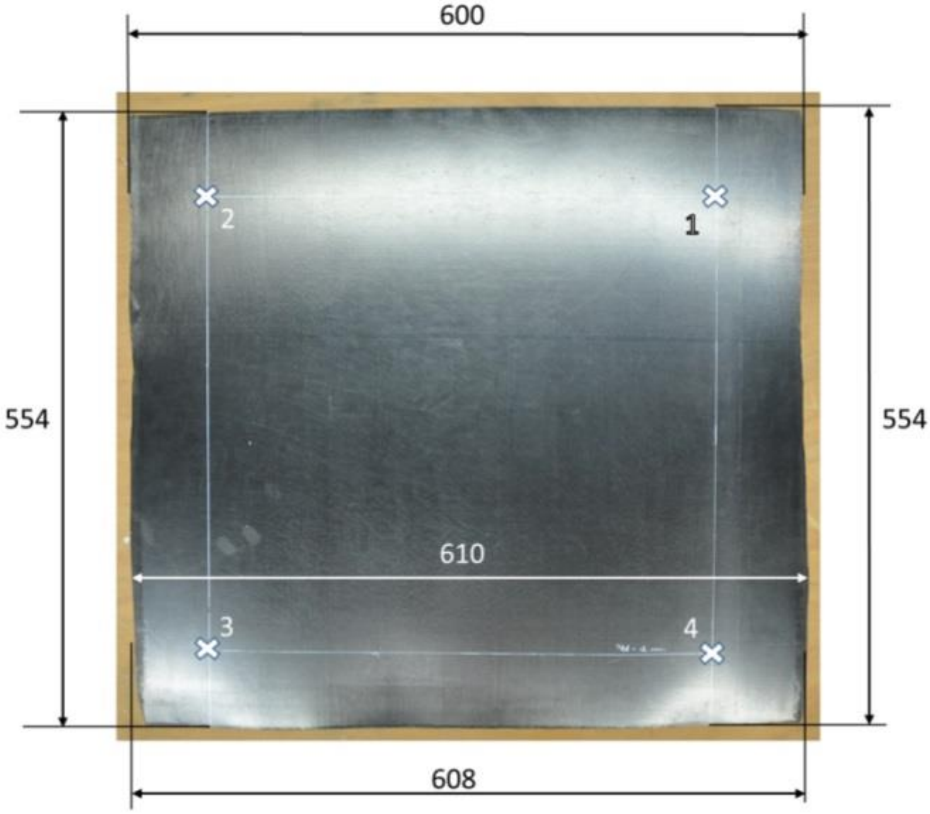

Figure 2.1 : Prepreg sheet.

Initially prepreg sheet is cut to strips by tiger sawing, and then strips are cut to rectangular pieces by hand sawing. For trimming disc sander (TSG 2501E) is used to make final accurate sample ready (Figure 2.2). Size of sample is 10.3177×6.355×0.985 mm. Tensile test is performed in direction perpendicular to fibers.

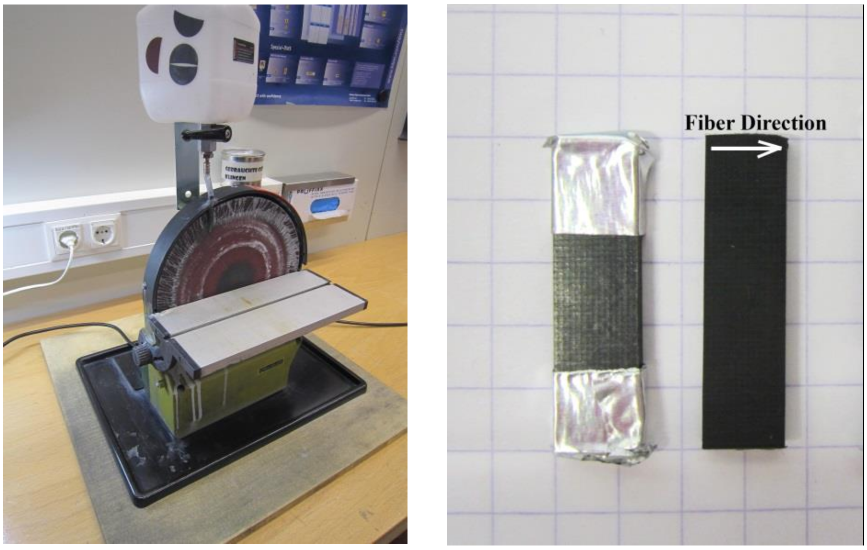

Figure 2.2 : Left: Disc sander, Right: Final samples.

2.2 DMA Machine

For tensile test, TA Instruments Q800 Dynamic Mechanical Analyzer (DMA) is used at Chemical Laboratory of the Institute for Carbon Composites (LCC) at the Technical University of Munich (TUM). Mechanical properties of many different materials can be investigated by this thermal analytical machine (Figure 2.3). It is the 3rd generation of DMA from TA Instruments, which consolidates new technologies in hardware and software. For testing, the sample is fixed in one of several clamps. In design of these clamps, Finite Element Analysis has been used to minimize mass and compliance. Intrinsic and extrinsic mechanical properties of the material are figured out by inflicting a deformation on the sample.

To set up a thermal analysis system, the DMA instrument works in affiliation with a controller and associated software [18]. This system manages all inputs and desired outputs of experiment.

Figure 2.3 : DMA machine-Chemical Lab, LCC.

2.3 Tensile Test

Tensile test procedure, which is used in this thesis has been developed in another research parallel to current study. In this procedure, initially sample is heated until reaching to 280 ℃ and it is kept at that temperature for 10 minutes. Then it is imposed to a quasi-static force ramp until reaching to 1 N. This procedure can be summarized as fellow:

- Motor drive: Off (i.e. the motor is switched off).
- Heating ramp of 10℃/min to 280℃.
- Isothermal for 10 min at 280℃.
- Motor drive: On.
- Force ramp of 0.05 N/min to 1 N.

Test temperature is higher than melt point (i.e. 220℃) of sample, so melting and accumulation of mass in lower clamp of machine is observed after test (see Figure 2.4 Right).

Figure 2.4 shows the specimen, before and after test at machine clamps.

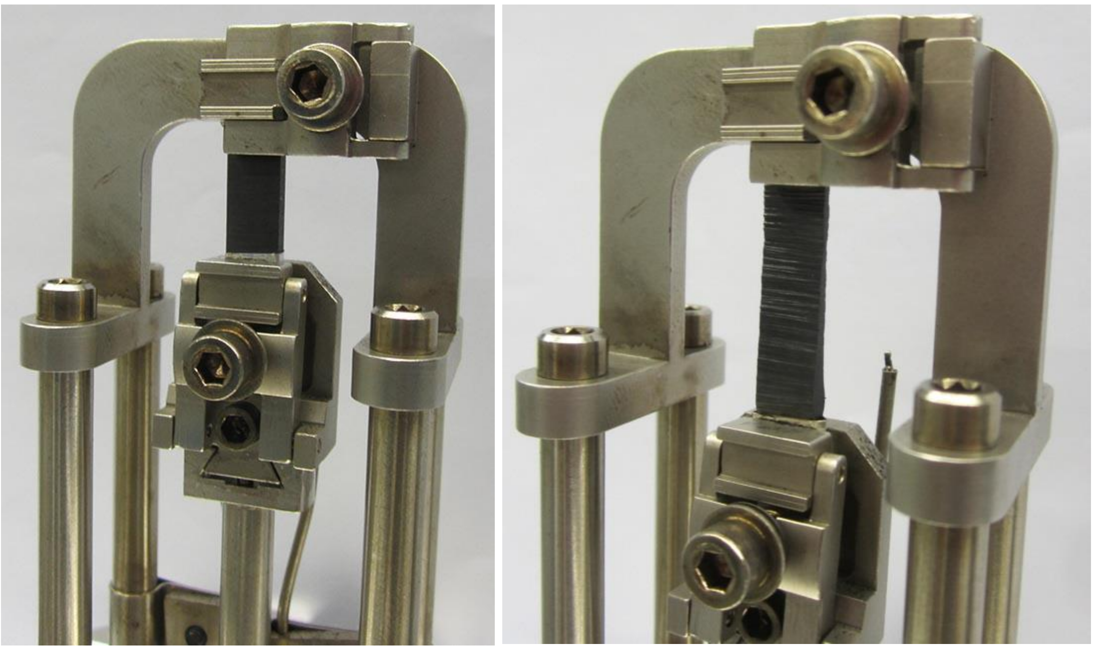

Figure 2.4 : Left: Sample before test, Right: Sample after test.

Test temperature is higher than melt point (i.e. 220°C) of sample, so melting and accumulation of mass in lower clamp of machine is observed after test (see Figure 2.4 Right).

2.4 Experimental Results

Test data are represented in Appendix B. Figures 2.5 and 2.6 shows diagrams of these results with respect to time.

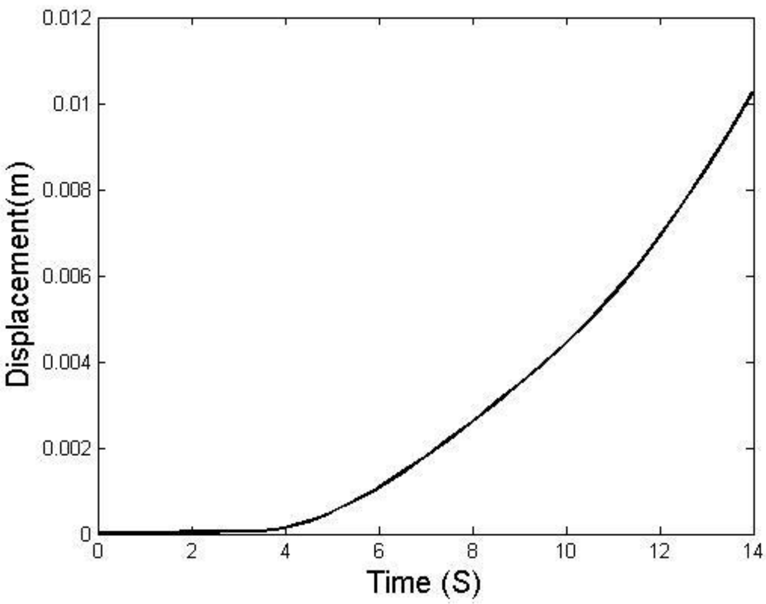

Figure 2.5 : Experimental results of test (displacement).

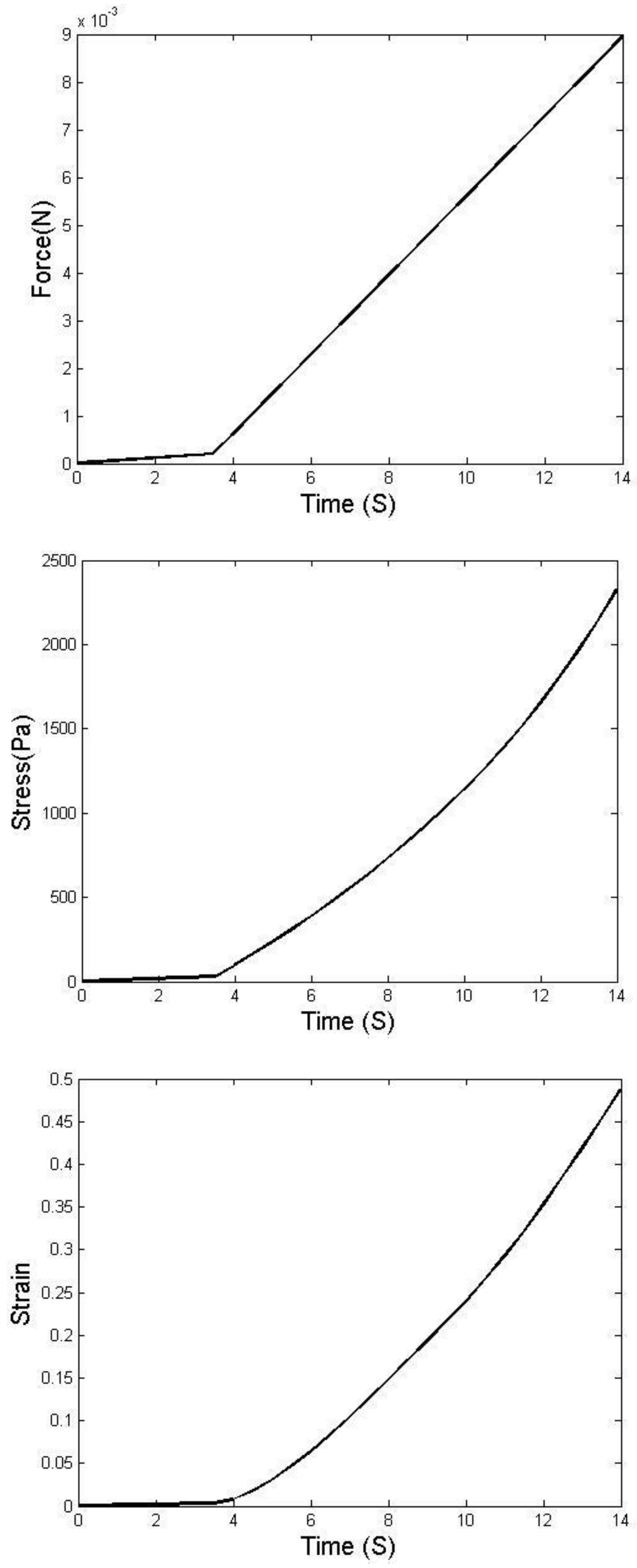

Figure 2.6 : Experimental results of test.

The increasing manner of all diagrams before and after 3.49 seconds is different. One probable reason can be error of machine. Machine does not measure changes accurately at beginning seconds of test or cannot apply accurate force at beginning. It is observed in this study, this fact causes large errors in calculations (especially Prony approximation-chapter 4.1). Thus 3.4902 seconds time shifting in results is performed. This increases the accuracy of calculations magnificently. Figure 2.6 represents test results after time shifting (also see Appendix B).

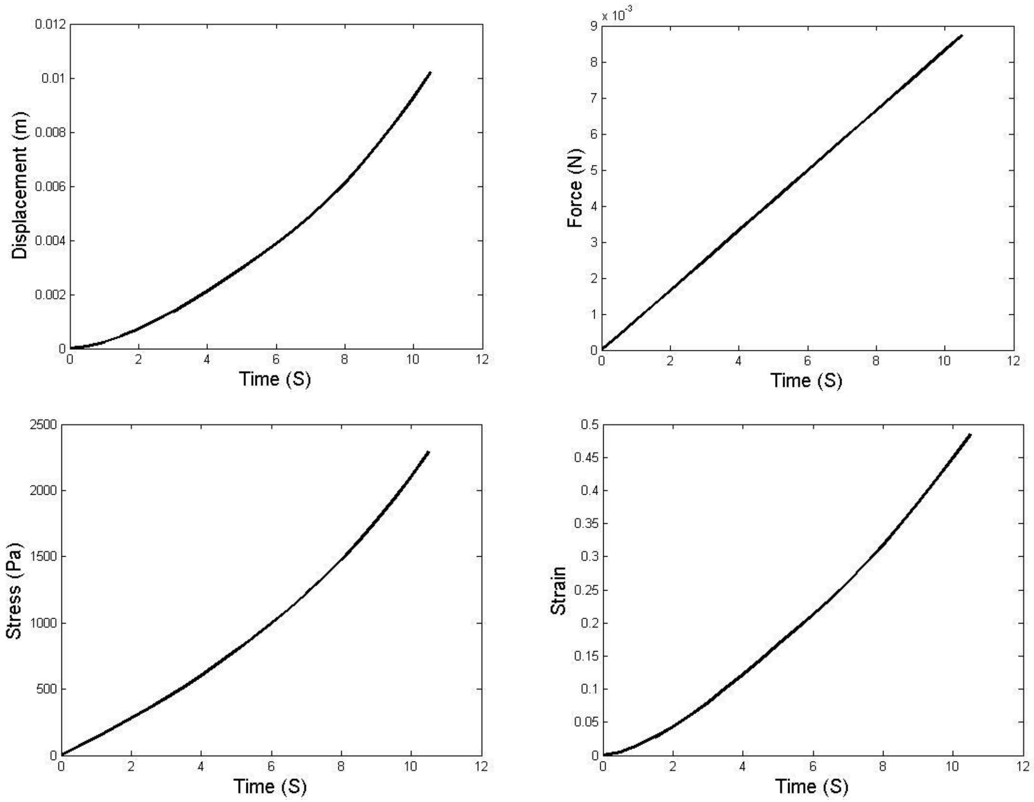

Figure 2.7 : Experimental results of test after time shifting.

In Figures, 2.6 and 2.7 stress and strain diagrams are based on DMA machine outputs. Detecting calculation method of these amounts is investigated in this section. Obviously, DMA machine can just measure displacement and force. Other outputs are results of calculation. In order to achieve this purpose, different stresses and strains should be defined and their amounts should be compared with test results.

L_0 (Initial length) = 10.3177 mm, A_0(Initial area) = 6.259675×10^{-6}m^2, i indicates ith time step, ν (Poisson's ratio) = 0.3468.

- Stress1 = Output of DMA machine
- Stress2 = $\frac{Force}{A_0}$
- Stress3 = $\frac{Force}{Mean\ final\ area}$, If we assume a linear reduction in cross sectional area, by equality of initial and final volumes of specimen, We can write:

$$A_0 L_0 = A_{final} L_{final} \Rightarrow Mean\ final\ area = \frac{A_0 L_0}{L_{final}} = 3.1484 \times 10^{-6} m^2$$

- Stress4 $=\frac{Force}{Instantaneous\ area}$, Cross sectional area in this approach is calculated at each time step, by assuming a linear reduction in area. Therefore, at nth time step, we have $A_n = \frac{A_{n-1}.L_{n-1}}{L_n}$.
- Stress5 = $\frac{Force}{Instantaneous\ area}$, Cross sectional area in this approach is calculated by using Poisson's ratio in reduction of dimensions of initial area. If we assume *l* and *w* as length and width of cross sectional area, We have
  $w_i = w_{i-1} - \nu.\left(\frac{w_{i-1}.Displacement_i}{L_{i-1}}\right)$
  $l_i = l_{i-1} - \nu.\left(\frac{l_{i-1}.Displacement_i}{L_{i-1}}\right)$
  $Instantaneous\ area_i = w_i l_i$
- Strain1 = Output of DMA machine
- Strain2 = $\frac{Displacement}{L_0}$
- Strain3 = $\frac{Displacement}{L_{final}}$
- Srtain4$_i = \frac{Displacement_i}{L_{i-1}}$
- Strain5$_i = ln\frac{L_i}{L_0}$

Fig. 2.8 shows the comparison of calculated amounts with test results.

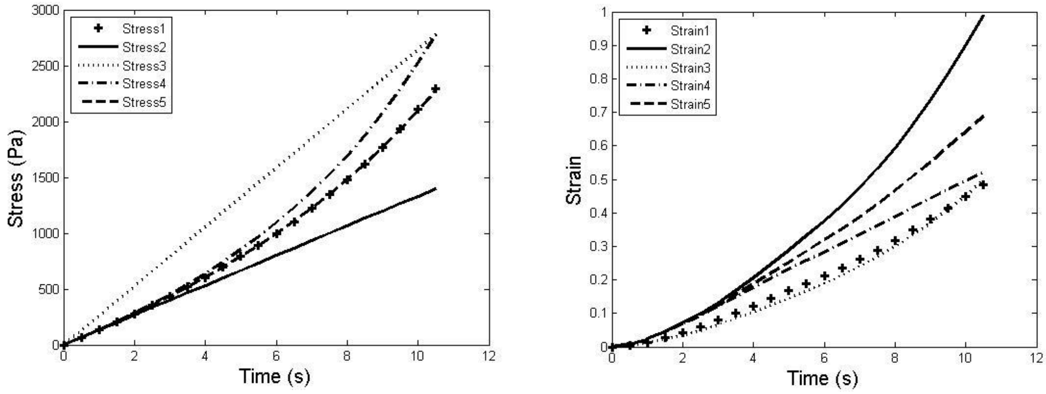

Figure 2.8 : Comparison of test results with calculated values.

As it is seen in Fig. 2.8, stress output of DMA machine is defined as force per real instantaneous area and strain output is defined as displacement per final length.

3. TENSILE TEST SIMULATION

The software used for modeling is ABAQUS 6.13. Linear or nonlinear analyze can be done in ABAQUS to deal with problems with time-dependent material response. Viscoelastic materials are a great portion of such materials. Mentioned analysis can be used when inertia effects are negligible like quasi-static tensile tests, which is our case [21].

3.1 Viscoelastic Modeling of Experimental Results

3.1.1 Stress-strain relations

First step for viscoelastic modeling of a tensile test is to investigate stress-strain relation of experiment. Which is necessary for Prony approximation of test result. In ABAQUS documentation, mentioned approximation is done by shear properties of material like τ and γ (see section 1.2.1.3). In literature, a similar procedure has been performed with tensile test results to determine Prony series coefficients [22]. I.e. σ is used instead of τ and ε instead of γ. By following a similar procedure we have:

$$G_R(t) = \frac{\sigma(t)}{\varepsilon} \tag{3.2}$$

And

$$g_R(t) = G_R(t)/G_0 \tag{3.2}$$

Figure 3.1 shows diagram of $G_R(t)$ with respect to time.

As a result of zero values for stress and strain at $t = 0$, G_R at this point is not a number. In order to find amount of $G_R(0)$ which is G_0, a two term exponential fitting to G_R diagram is performed by means of MATLAB. This leads to following equation:

$$G_R(t) = 9830\, e^{-1.325t} + 3426e^{-0.03831t} \quad \textbf{(3.3)}$$

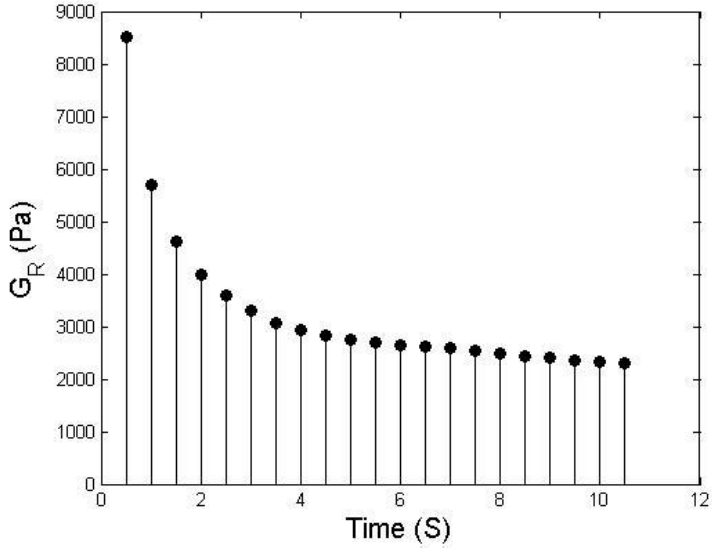

Figure 3.1 : Diagram of $G_R(t)$ with respect to time.

Figure 3.2 shows the diagram of Equation 3.3.

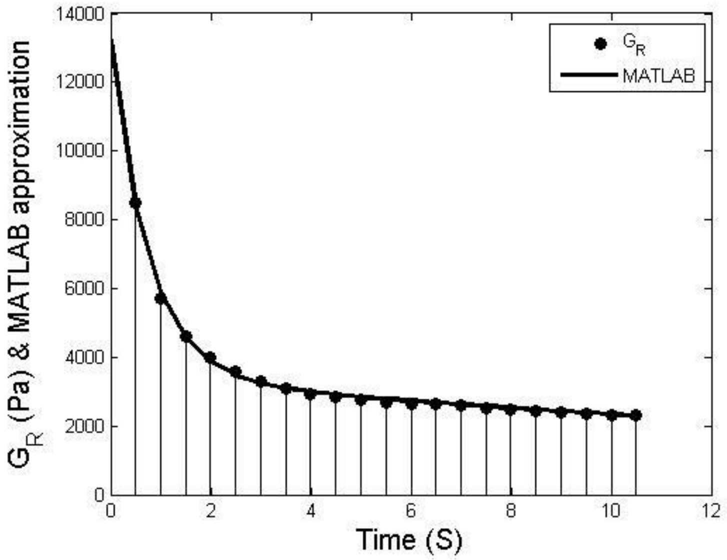

Figure 3.2 : G_R and MATLAB approximation of G_R.

According to Equation 3.3, $G_0 = G_R(0)$ =9830 + 3426 = 13256.

By means of Equation 3.2 diagram of $g_R(t)$ with respect to time can be plotted. Figure 3.4 depicts this diagram.

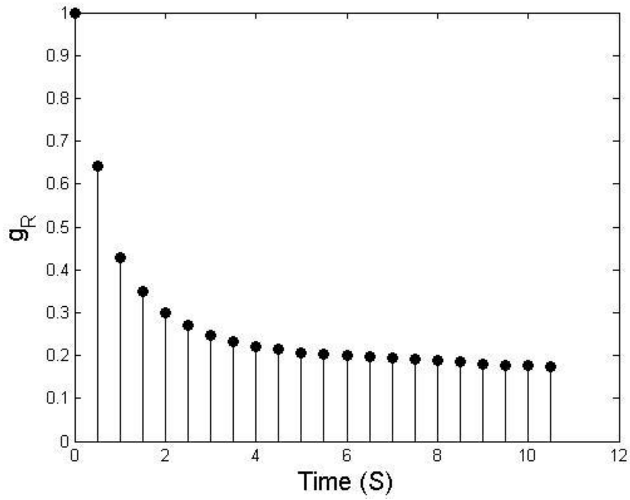

Figure 3.3 : Diagram of g_R with respect to time.

3.1.2 Prony series approximation

Prony series approximation of g_R is the next step for viscoelastic modeling of experimental results. To attain this purpose, MATLAB software is used again. Different Prony series with different numbers of terms are examined. Conclusion is that, following Prony series with 5 terms fits g_R the best. Figure 3.4 shows the diagram of this approximation.

$$g_R(t) = 1 - \left(0.4209 \times \left(1 - e^{-t/0.8836}\right) - 0.1613 \times \left(1 - e^{-t/0.01008}\right) + 0.1478 \times \left(1 - e^{-t/3.45}\right) + 0.98 \times \left(1 - e^{-t/0.2194}\right) - 0.561 \times \left(1 - e^{-t/0.03347}\right)\right) \tag{3.4}$$

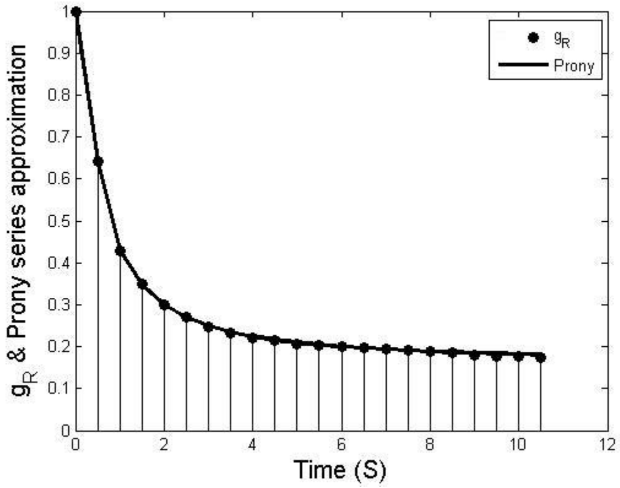

Figure 3.4 : Prony series approximation of g_R.

3.2 Simulation Models

Essential information to simulate tensile test with ABAQUS is achieved. After checking several simulation methods, Upcoming six models are ones that correlate best the experimental results.

Model1

In this model specimen is defined as three dimensional deformable shell. This definition is due to length to thickness ratio of sample. For material definition, a combination of elastic and viscoelastic properties is used. In elastic part 2100 Pa is considered as modulus of elasticity and 0.3468 is used as Poisson's ratio. For viscoelastic part, five term Prony series is used as calculated above. In section part, a composite shell is defined and Visco has been chosen in step part. In ABAQUS visco step is used in analysis with time-dependent material behavior (creep, swelling, and viscoelasticity). Time period of step is 10.5 seconds which is time of test. Nlgeom has been set to ON in order to let sample has large deformations. This option indicates that ABAQUS should deal with geometric nonlinearity during the step. For loading a force ramp is applied to model. Its amplitude is as Figure 3.5. These amounts are derived from division of force per width of sample (shell edge load-Appendix C). For boundary conditions top surface of model has been considered as cantilever (i.e. $\mathrm{U1} = \mathrm{U2} = \mathrm{U3} = 0$) and bottom surface can just move vertically ($\mathrm{U1} = \mathrm{U3} = 0$).

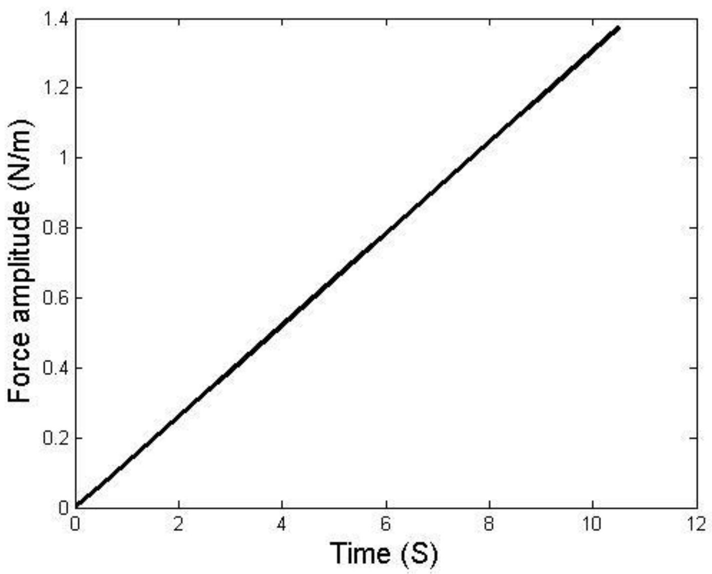

Figure 3.5 : Force amplitude for Model.

In this model standard, linear and non-reduced elements have been used.

Outputs of this model: Displacement and Stress.

Model2

This model is Model1 with *Quadratic* elements as geometric order.

Outputs: Displacement and Stress

Model3

This model is Model1 with displacement ramp instead of force ramp. i.e.:

Load:

$$\text{Boundary conditions:}\begin{cases} \text{Top: U1} = \text{U2} = \text{U3} = 0 \\ \text{Bottom: U1} = \text{U3} = 0 \\ \text{Bottom: U2} = -1, \text{Amplitude: Fig. 3.6 and Appendix C} \end{cases}$$

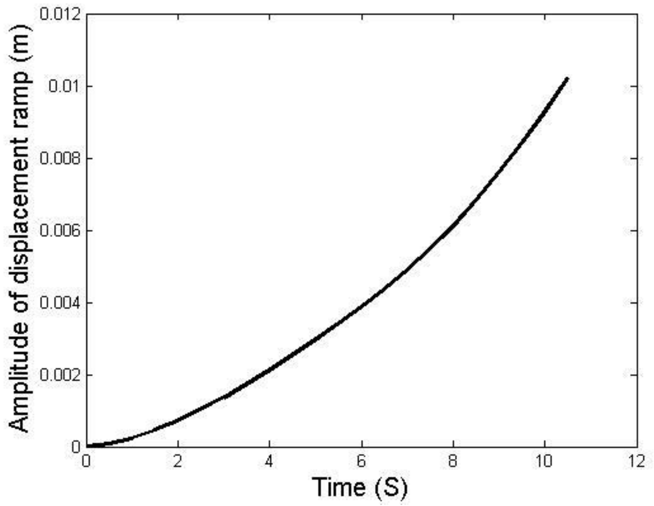

Figure 3.6 : Amplitude of displacement ramp.

Outputs: Reaction force and Stress.

Model4

This model is Model3 with *Quadratic* elements as geometric order.

Outputs: Reaction force and Stress.

Model5

This model is Model1 with linear elastic material modeling. Following properties have been used in this model:

$$\text{Material:}\begin{cases} \text{Elastic, E} = 450 \text{ Pa, which is an unreal value,} \\ \text{Density: } 1460 \ \text{kg/m}^3 \end{cases}$$

Step = Static, General.

Outputs: Displacement and Stress.

Model6

Model1 with E=1385 Pa. This amount for elasticity modulus is result of another experiment performed at LCC.

Outputs: Displacement and Stress.

4. RESULTS AND DISCUSSION

In this chapter, simulation results of six previously mentioned models are presented. First, convergence of these models is checked by increasing number of their elements from one to a final amount. For converged models, outputs of simulations and experimental results are compared. Finally, one model, which can predict tensile behavior of our composite well is introduced.

4.1 Model Convergence

Model1:

Here outputs of Model1 for different numbers of elements are compared. Figure 4.1 shows outputs for 1, 2, 8,72,648,3200 and 7140 elements. Dashed curves are outputs of one element, which are a bit different with others. As it is seen convergence for Model1 is achieved for 2 elements:

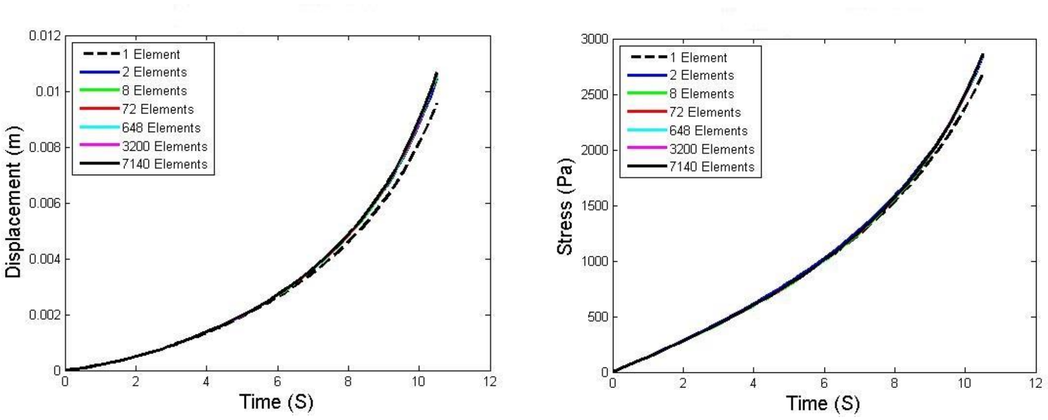

Figure 4.1 : Convergence of Model1.

Model2:

Results of Model2 for 1, 2, 8,72,648,3200 and 7140 elements are shown in Figure 4.2.

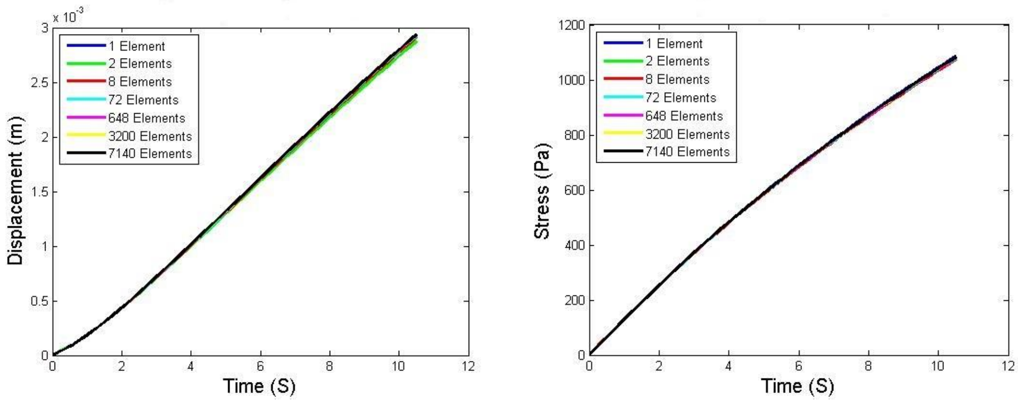

Figure 4.2 : Convergence of Model2.

As it is seen for this model, even with one element good convergence is achieved.

Model3:

Results of Model3 for 1, 2, 8,72,648,3200 and 7140 elements are shown in Figure 4.3. Like Model1, model with one element is a bit different with others and for two elements; a good convergence is achieved in this model.

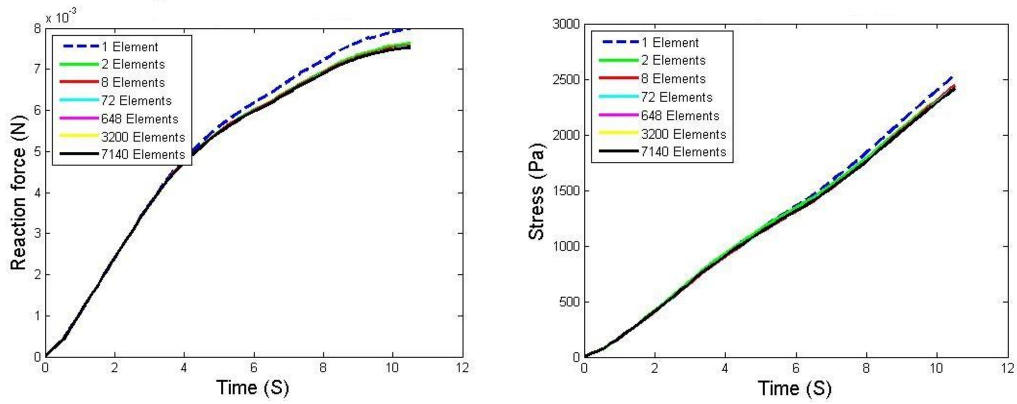

Figure 4.3 : Convergence of Model3.

Model4:

Results of Model4 for 1, 2, 8,72,648,3200 and 7140 elements are shown in Figure 4.4.

Like Model2, in this model with one element, good convergence is achieved.

Model5:

Results of Model5 for 1, 2, 72 and 800 elements are shown in Figure 4.5.

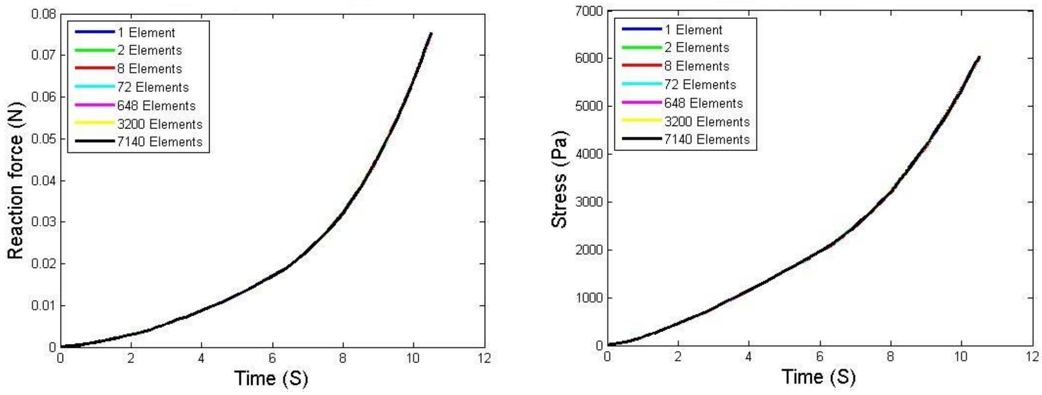

Figure 4.4 : Convergence of Model4.

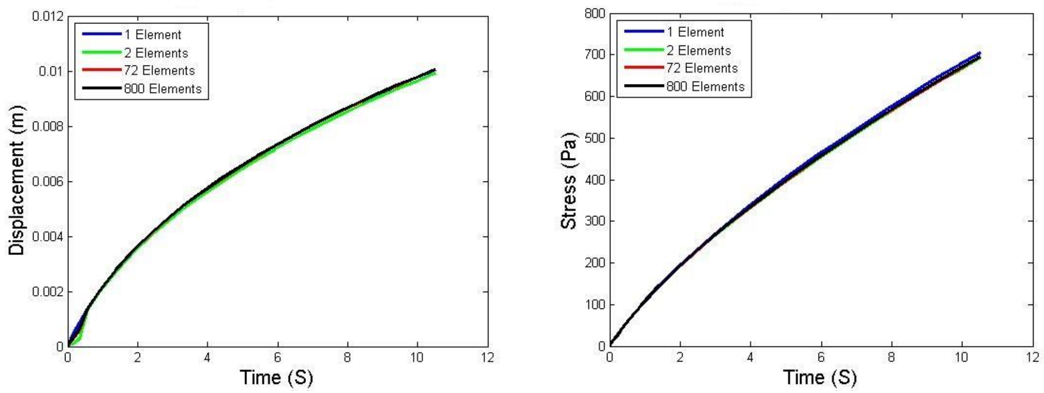

Figure 4.5 : Convergence of Model5.

In this model, convergence is achieved for one element.

Model6:

Results of Model6 for 1, 2, 8, 648 and 7140 elements are shown in Figure 4.6.

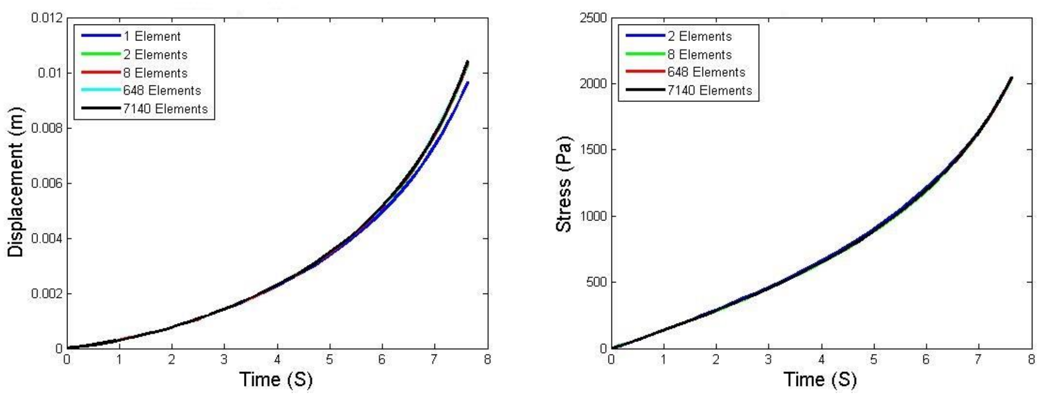

Figure 4.6 : Convergence of Model6.

As it is seen, convergence is achieved in this model for two elements. As a conclusion of convergence, it can be said, for all six models good convergence is achieved.

4.2 Final Results of Simulation

Model1:

Figure 4.7 shows comparison of experimental results with Model1. Star curve indicates experimental results

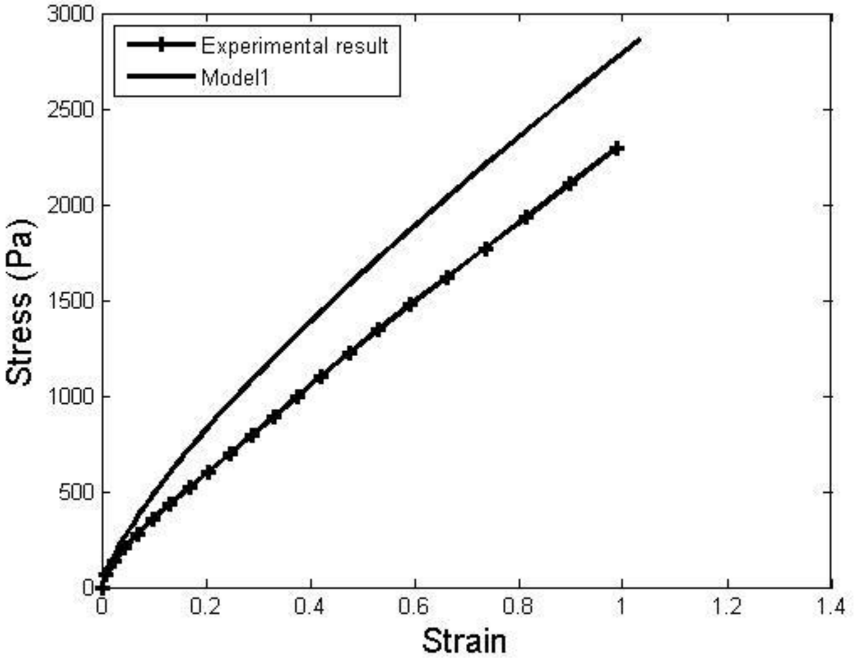

Figure 4.7 : Comparison of Model1 with experimental result.

Stress values for all models are mean amount of stress in midsection of model. In Figure 4.7, a maximum 20% deviation between experimental results and Model1 is observed.

In Figure 4.8, a uniform stress distribution is observed in whole model. Because of concentration of stress in top corners of sample, maximum stress is observed there. By receding from corners, stress reduces. In the vicinity of midsection, stress increases again due to reduction in cross sectional area. In this model there is good correlation of stress amount in 7 seconds of testing, between model and experimental result. Then a maximum deviation of 20% is observed at end.

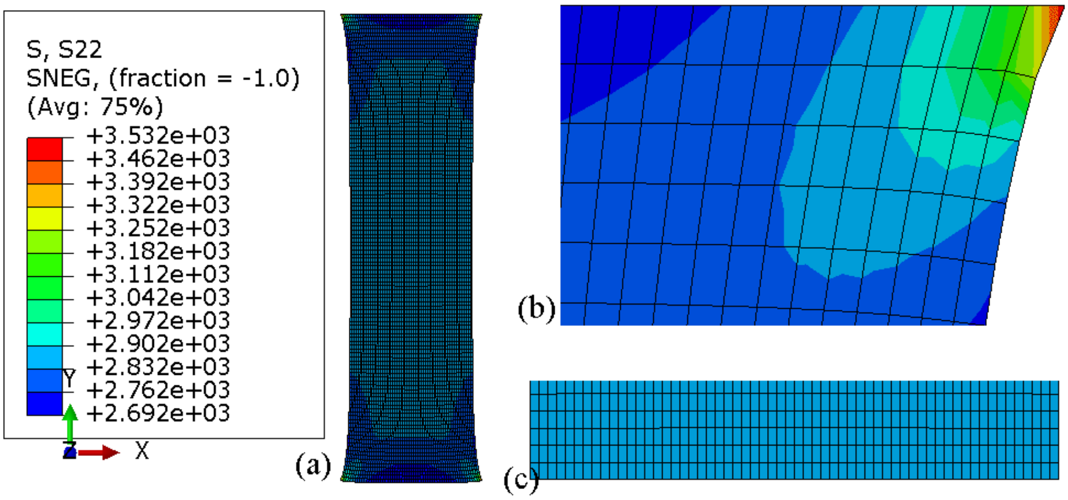

Figure 4.8 : Stress distribution of Model1(a: whole model, b: top right corner, c: midspan).

Figure 4.9 shows displacement of Model1. Although in this model at each time step elongation of model is less than experimental results, but at time = 10 seconds they reach to almost same length. This amount is 9.28 mm for specimen and 9.41 mm for model. Final elongation of specimen is 10.198 mm, while it is 10.658 mm for model.

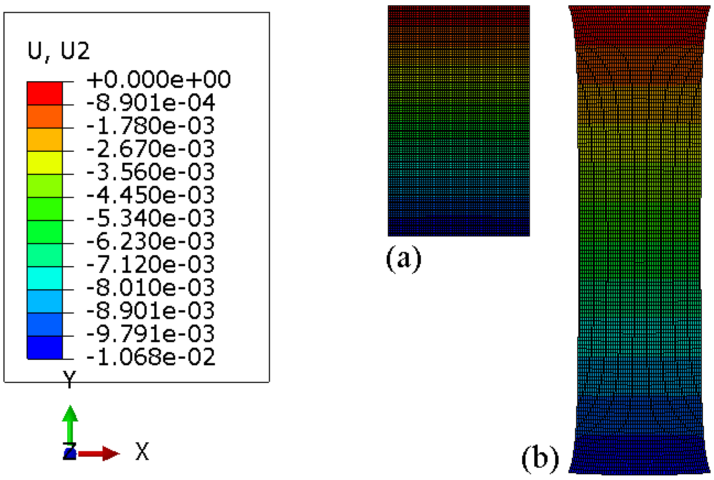

Figure 4.9 : Displacement of Model1 (a: undeformed,b: deformed shape sketch).

Model2:

Figure 4.10 shows results of Model2 and experiment. Deformation of this model is much less than real specimen and it does not show real elongation of sample. In simulation, nodes of the elements are used to determine displacements or other degrees of freedom. At other points of elements, or in whole model as final elongation, the displacements are obtained by interpolating from the nodal displacements. Generally number of nodes in the elements is used to determine the interpolation order. In quadratic elements of this model, 8 nodes exist in each element. These elements have midside nodes, and quadratic interpolation is used to calculate their deformation [23]. Result of Model2 indicates quadratic elements are not suitable for our case.

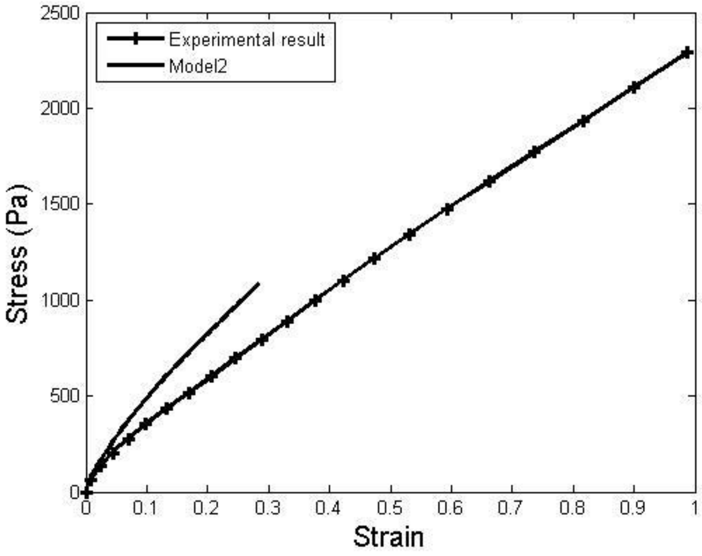

Figure 4.10 : Results of Model2 and experiment.

Figure 4.11 shows displacement of Model2. There is no correlation between model result and experiment in this model. Maximum elongation of model is 2.935 mm, while it is 10.198 mm for specimen.

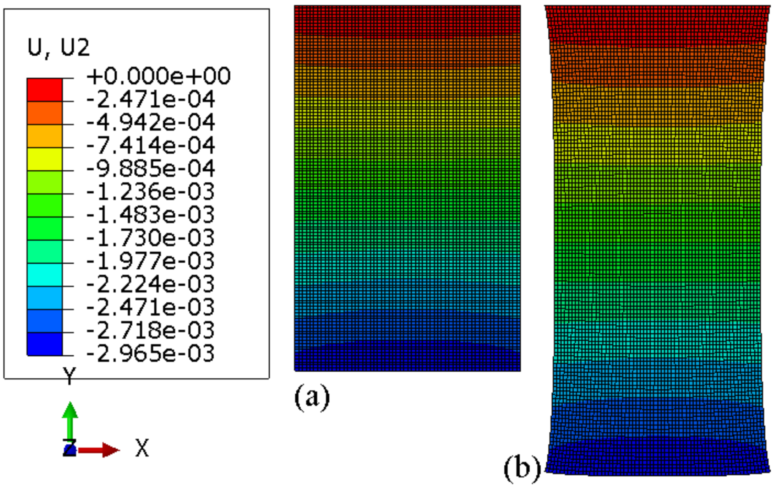

Figure 4.11 : Displacement of Model2(a:undeformed, b:deformed shape).

Fig. 4.12 depicts stress distribution of Model2. Amount of stress in this model correlates with specimen just in first two seconds of test. After that there is large deviation. Maximum amount of stress for specimen is 2.29 kPa, while it is 1.083 kPa for model.

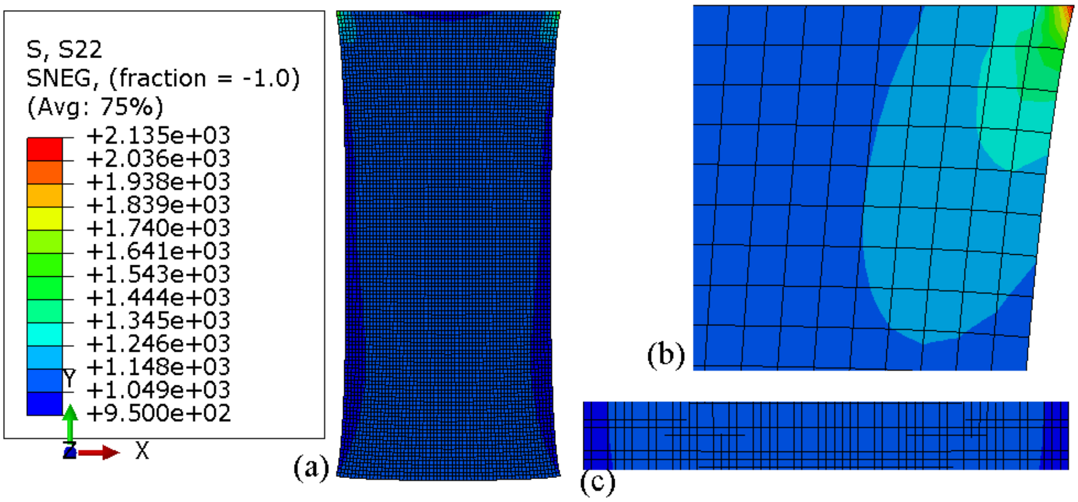

Figure 4.12 : Stress distribution of Model2(a:whole, b: top right corner,c: midspan).

Model3:

Figure 4.13 depicts comparison between experimental result and Model3. In this model displacement ramp is used instead of force ramp. Elongation of sample is input for this simulation. Therefore outputs of model will be reaction force and stress distribution.

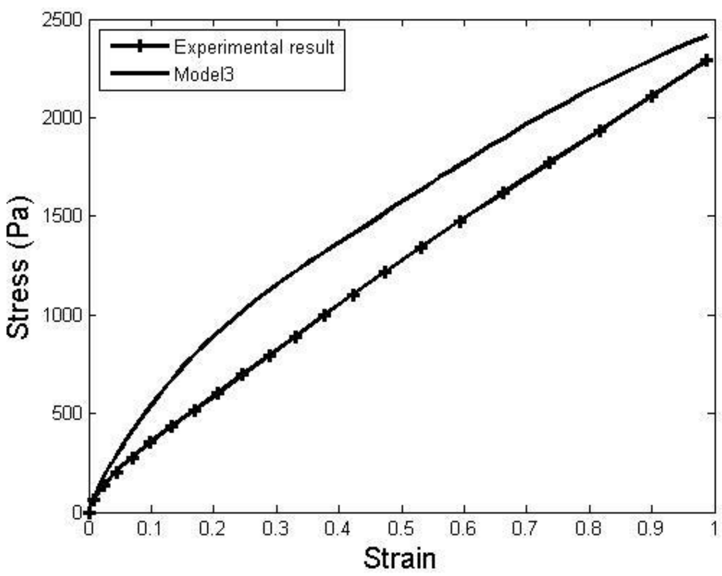

Figure 4.13 : Results of Model3 and experiment.

Figure 4.14 depicts reaction force of Model3. Reaction force in this model till time = 8.4 second is higher than experimental result. Maximum deviation occurs at time = 4 second, which is about 25%. Then two amounts reach to value of 7.067 mN at 8.4 second. After this point model shows lower reaction force than experiment. At the end of test (time = 10.5 sec) amount of reaction force of model is 7.525 mN, while it is 8.734 mN for specimen. This shows a deviation of 14% at end point.

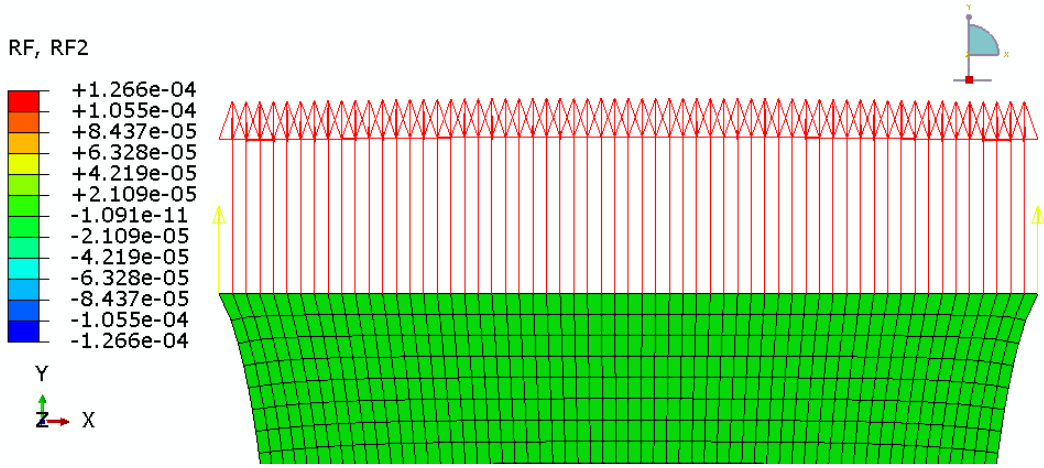

Figure 4.14 : Reaction force of Model3.

Figure 4.15 depicts stress distribution of Model3. In this model amount of mean stress in midspan, is always higher than test result. Maximum deviation of 28% at time = 5 second is observed.

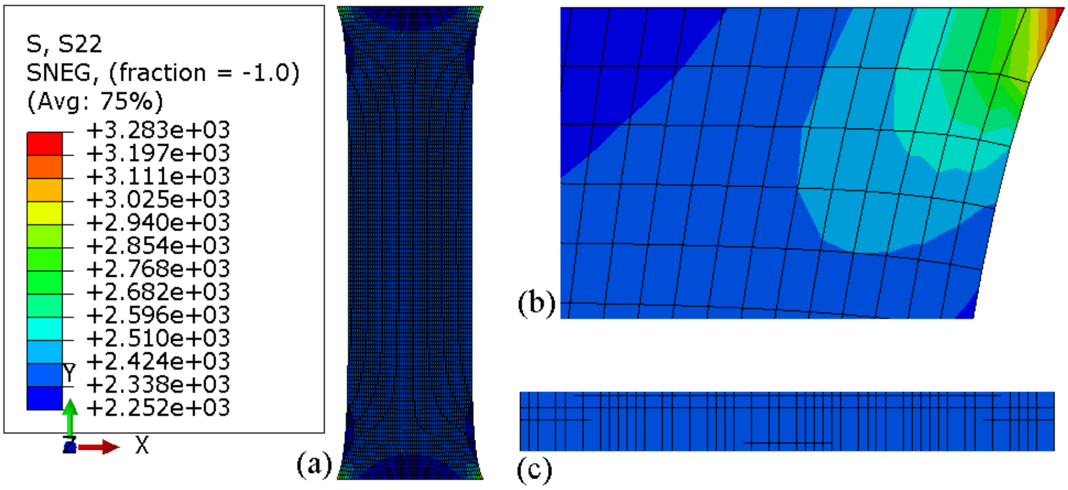

Figure 4.15 : Stress distribution of Model3 (a: whole, b: top right corner, c: midspan).

Ultimate amount of mean midspan stress at the end of test is 2.415 kPa model, while it is 2.29 kPa for specimen (deviation of 5%).

Model4:

Figure 4.16 shows stress-strain diagram of Model4 and specimen. As it is seen there is a large deviation between model results and test. Maximum stress of model is 6.024 kPa which occurs at end point, while it is 2.29 kPa for specimen.

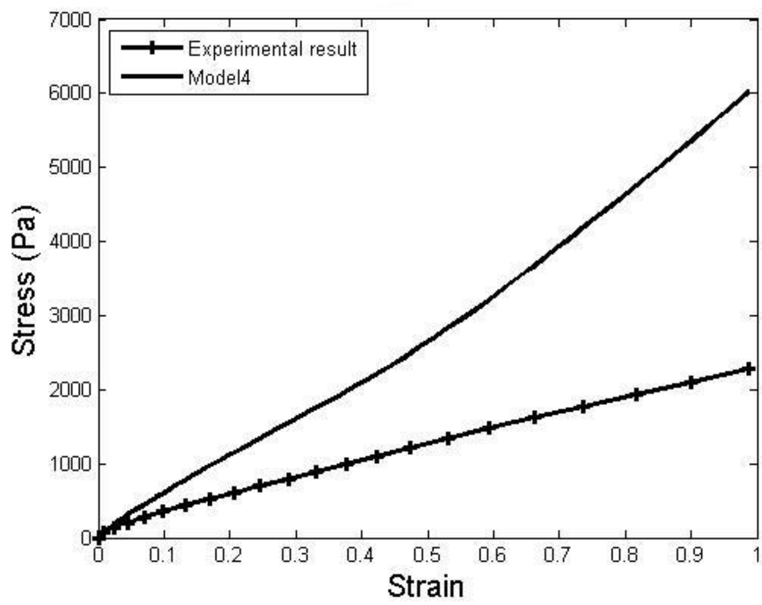

Figure 4.16 : Results of Model4 and experiment.

Figure 4.17 indicates reactional force of Model4. This amount is also much more than test result.

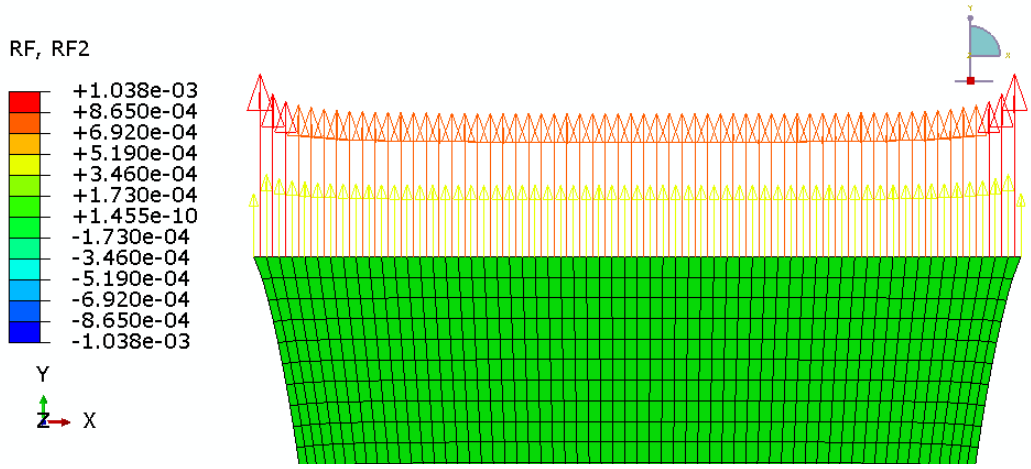

Figure 4.17 : Reaction force of Model4.

Amount of reaction force at end of test is 75.263 mN for this model, while it is 8.734 mN for real sample.

Stress distribution of Model4 is shown in Figure 4.18. Mean amount of midspan stress for this model is always more than experimental result. Reduction in cross sectional area of model in Figure 4.18 can not be considered as a true simulation for real sample (see Figure 2.4).

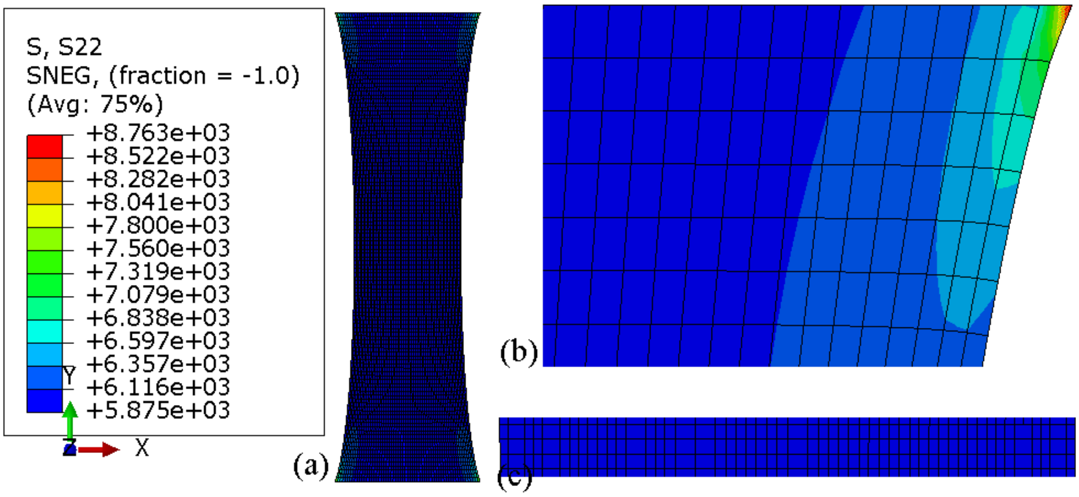

Figure 4.18 : Stress distribution of Model4 (a: whole, b: top right corner, c: midspan).

Model5:

Comparison of stress-strain diagrams of Model5 and specimen is performed in Figure 4.19. As it is seen in this figure, good correlation between these two amounts is not achieved. At end point of this diagram an approximate deviation of 70% is observed.

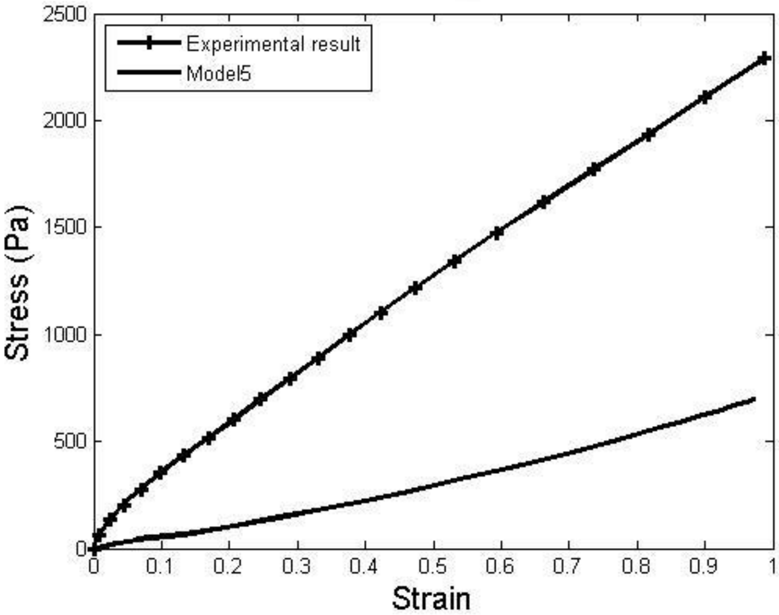

Figure 4.19 : Results of Model5 and experiment.

Deformation of Model5 is depicted in Figure 4.20. Although final elongation of this model correlates well with experimental result, but its elongation at each time step is higher than real sample. At time = 5 second, maximum deviation is observed. At this time elongation of model is 6.52 mm while it is 2.974 mm for specimen. This amount is 54% deviation. Final elongation of Model5 is 10.0388 mm, at the same time it is 10.198 mm for real sample.

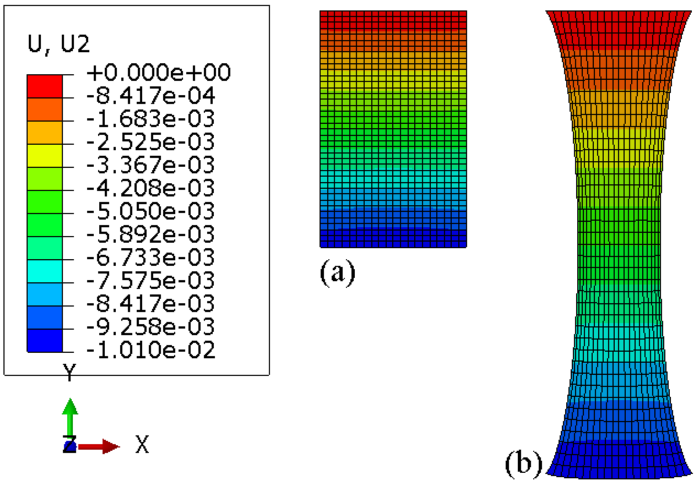

Figure 4.20 : Displacement of Model5 (a: undeformed, b: deformed shape).

Stress distribution of Model5 is shown in Figure 4.21. A good correlation between simulation result and experiment is not observed for this model.

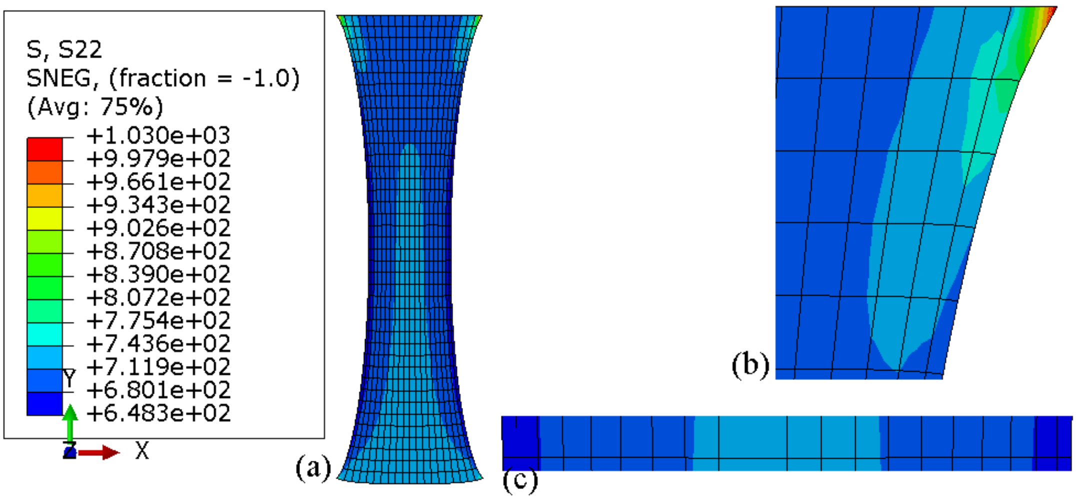

Figure 4.21 : Stress distribution of Model5 (a: whole, b: top right corner, c: midspan).

Mean value of midspan stress at end of test is 2290.85 Pa for test specimen, while it is 695.56 Pa for this model.

Model6:

Comparision of stress-strain diagrams for Model6 and experimental result is performed in Figure 4.22. This model has best correlation of stress-strain diagrams among all models.

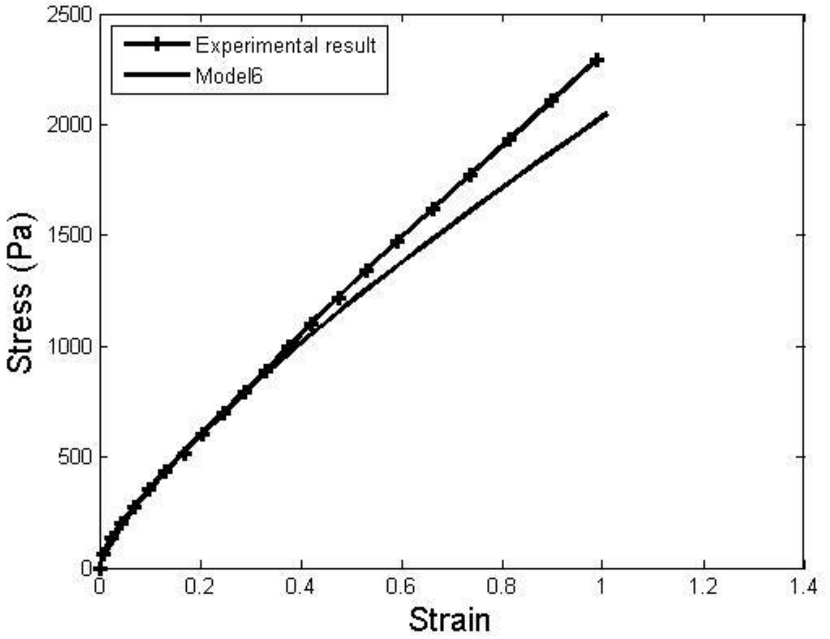

Figure 4.22 : Results of Model6 and experiment.

As it is observed in Figure 4.22, there is good correlation between model and experimental results for 40% of strain.

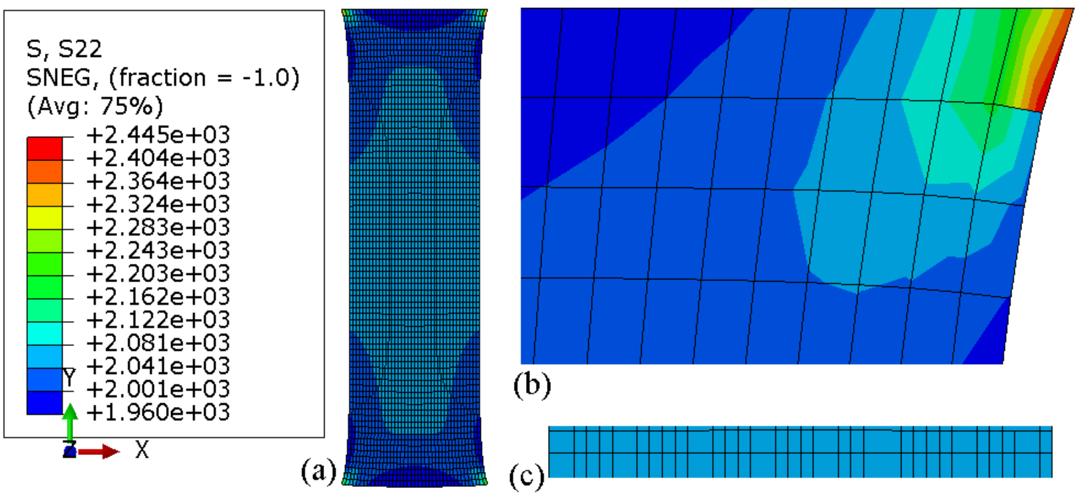

Figure 4.23 : Stress distribution of Model6 (a: whole, b: top right corner, c: midspan).

Stress distribution of Model6 is depicted in Figure 4.23. Maximum amount of mean stress value at midspan of Model6 is 2.047 kPa, while it is 2.291 kPa for specimen. This means 10% deviation between these two amounts

Deformation of Model6 is depicted in Figure 4.24. Final elongation for this model is 10.409 mm, while it is 10.198 mm for specimen.

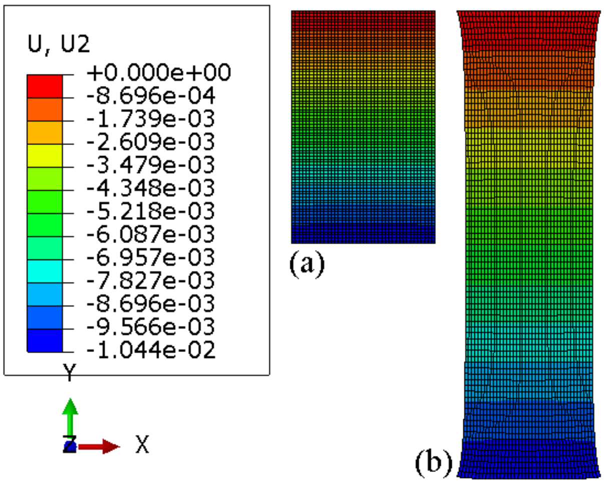

Figure 4.24 : Displacement of Model6.

4.3 Comparison of Different Models and Conclusion

Figure 4.25 depicts stress-strain diagrams for all models. As it can be seen Model6 has best correlation with experimental result.

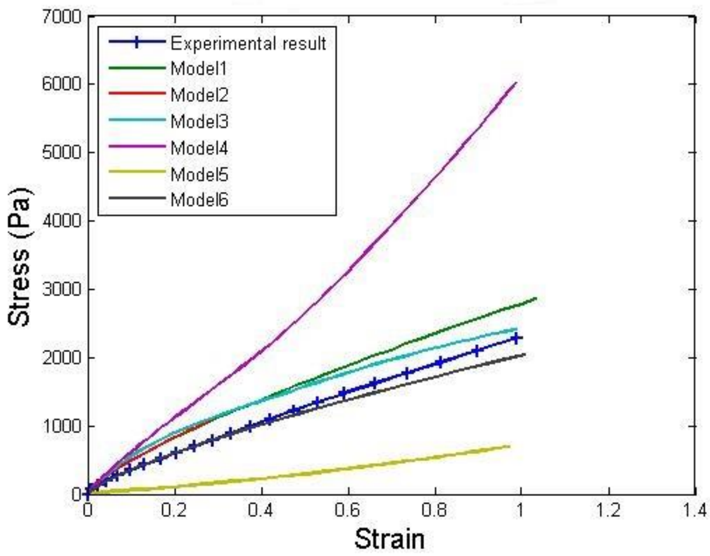

Figure 4.25 : Stress-strain diagrams of all models.

Figure 4.26 depicts reaction force with respect to time for three models. In this diagram Model3 has best correlation with experimental result.

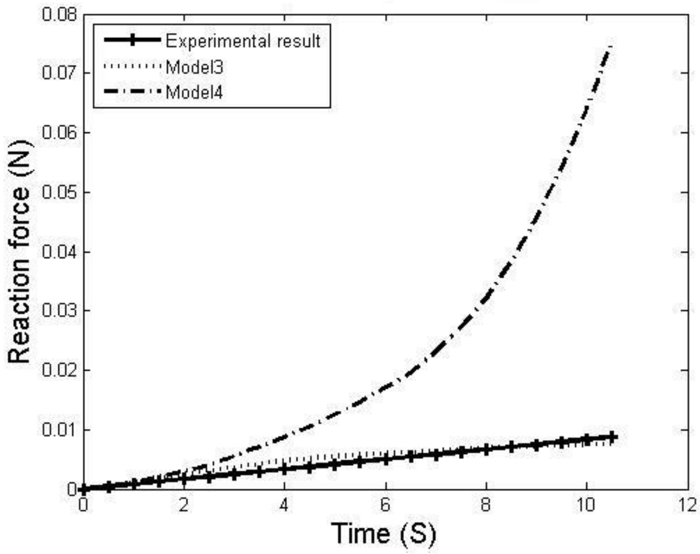

Figure 4.26 : Reaction force.

The only difference between Model3 and Model4 is element type. Model3 is meshed with linear elements, whereas Model4 is meshed with quadratic elements.

Figure 4.27 depics displacement with respect to time for all models. In first four seconds of test Model6 has best correlation with experimental result.

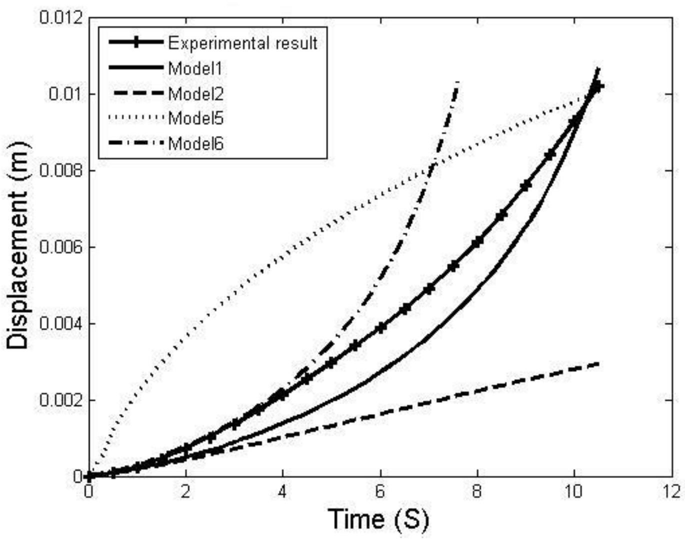

Figure 4.27 : Displacement of models.

From Figures 4.27 and 4.28, it can be concluded for describing studied prepreg's properties, Model1 and Model6 has best correlation with experimental results. The only difference between these two models is amount of elasticity modulus. Accurate measurement of this modulus can give better result for simulation.

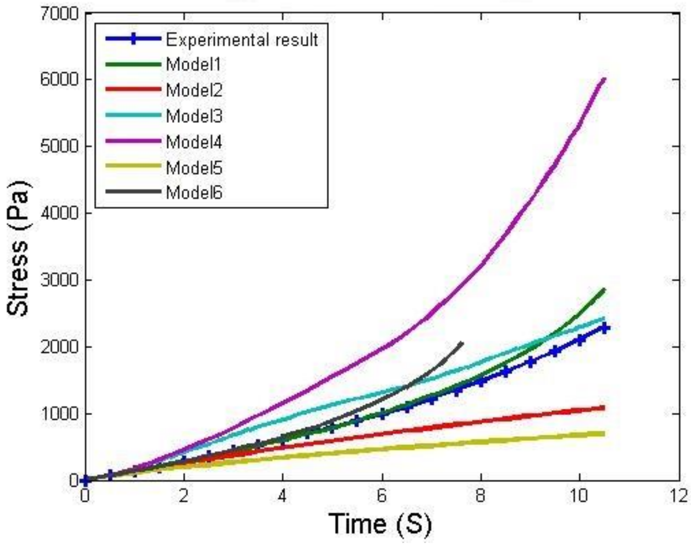

Figure 4.28 : Average midspan stress in different models.

As final conclusion it can be said linear and non-reduced elements give much better results than quadratic elements, (Models 1 and 3). It is decided in this research to fix linear elements as modeling elements. Moreover in calculation of stress among discussed models force ramp gives better results in comparison with displacement ramp. According to stress-strain diagram (Figure 4.25) Model6 is selected as final simulation model of this thesis.

Figure 4.29 shows test sample before and after test and Model6 as final model of this study. Slippage of sample while testing has been neglected. Good correlaton in elongation amount is observed between this model and sample. Final elongation of model is 0.211 mm more than specimen.

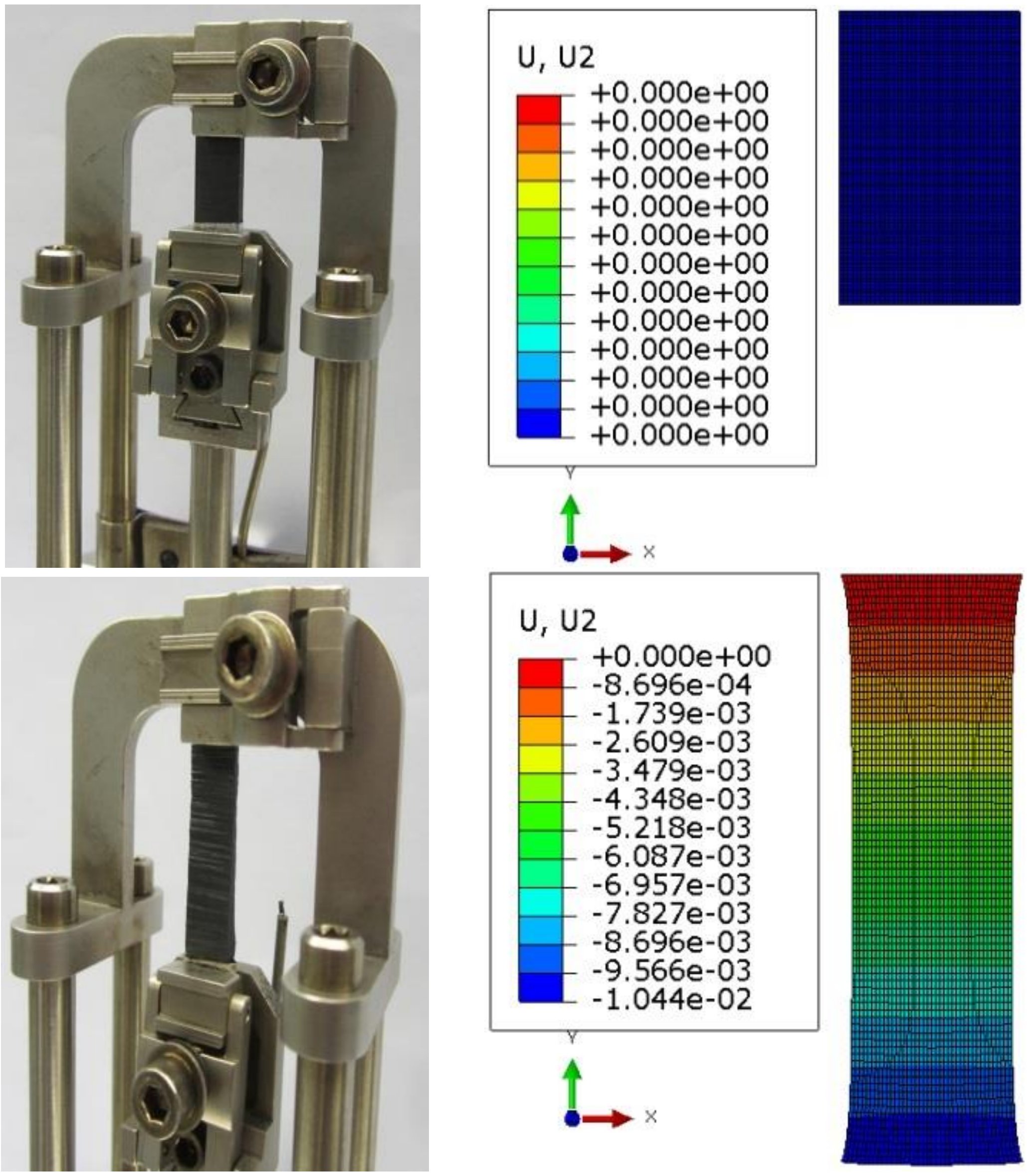

Figure 4.29 : Test specimen before (left) and after test (right), and Model6.

5. CONCLUSIONS AND RECOMMENDATIONS

5.1 Summary

After a literature research about static and dynamic tests of composites in general and fiber reinforced composites in detail, a quasi-static tensile test for Celstran®CFR-TP PA6 CF60-01 prepreg is performed in this study. Procedure and performance method of this test is developed in another research paralell to current thesis at LCC. Purpose of this study is to develop a material model for simulation of above mention prepreg using ABAQUS commercial software. For sample preparation tiger saw is used to cut prepreg sheets to thin strips with 1 cm width, then disc sander TSG 2501E is used for trimming. Final dimensions of test sample is 6.355×10.3177×0.985 mm.

Tensile test is performed with TA Instruments Q800 DMA machine. In test procedure, which is developed previously, sample is heated with a slow rate until reaching a uniform heat distribution in sample. Test temperature is higher than melting point of sample, so melting and accumulation of mass in lower clamp of machine is observed. Outputs of test consist essential information of simulation, which are deformation, tensile force and subsequently stress and strain with respect to time.

For simulation, Prony series coefficients are approximated from outputs of tensile test. MATLAB curve fitting is used for this approximation. Simulation models are generally a combination of elastic and viscoeladtic properties. MATLAB is used for numerical approximation, classifying, plotting and comparison of simulation results with experimental outputs. Finally it is concluded that introduced material model in this study gives realistic result and for tensile simulation of viscoelastic behavior, linear non-reduced elements give more pragmatic results than quadratic elements. Moreover force ramp for such simulations is better compared with displacement ramp.

5.2 Outlook

Performed calculations in this thesis are based on one data series of tensile test. As it is mentioned in literature, high data dispersibility is observed in experimental tests of prepregs [9]. For further investigations it would be useful if our method of simulation be repeated on more samples. And more results be compared with each other. In that case it may be possible to reach to a unique model which gives best correlation between experimental and simulation data. Also an algorithm can be found to relate modeling and empirical outputs.

In viscoelastic materials, loading rate has significant effect on test results. For further works developed material model in current thesis can be used for simulation of tests with different loading rates. And effects of this rate on modeling can be studied.

In this work literature research in dynamic testing of prepregs is performed. In viscoelastic modeling ABAQUS makes it possible to input Loss and Storage moduli with respect to angular velocity directly. As a future work dynamic testing and simulation of this kind of prepregs can be considered. Moreover amount of elasticity modulus which is an essential quantity for our introduced model, is obtainable from outputs of dynamic tests. In literature storage and loss moduli are used to attain this modulus [2]. This method of determination of elasticity modulus can also be investigated.

In future works any experiment which leads to more realistic amounts for elasticity modulus, will give more realistic results for introduced material model in this study.

REFERENCES

ABAQUS 6.13 Documentation, Abaqus Analysis User's Guide, 22.8.2 Parallel rheological framework.

ABAQUS 6.13 Documentation, Abaqus Analysis User's Guide, 22.7.1 Time domain viscoelasticity.

ABAQUS 6.13 Documentation, Abaqus Analysis User's Guide, 6.2.5 Quasi-static analysis.

ABAQUS 6.13 Documentation, Abaqus Analysis User's Guide, 27.1.1 Element library.

Bashaiwoldu, A. B., Podczeck, F., & Newton, J. M. (2004). Application of dynamic mechanical analysis (DMA) to determine the mechanical properties of pellets. *International journal of pharmaceutics*, *269*(2), 329-342.

Chang, S. H., & Wu, S. K. (2008). Isothermal effect on internal friction of Ti< sub> 50</sub> Ni< sub> 50</sub> alloy measured by step cooling method in dynamic mechanical analyzer. *Journal of Alloys and Compounds*, *459*(1), 155-159.

Deng, S., Hou, M., & Ye, L. (2007). Temperature-dependent elastic moduli of epoxies measured by DMA and their correlations to mechanical testing data. *Polymer testing*, *26*(6), 803-813.

Fritsch, J., Hiermaier, S., & Strobl, G. (2009). Characterizing and modeling the non-linear viscoelastic tensile deformation of a glass fiber reinforced polypropylene. *Composites Science and Technology*, *69*(14), 2460-2466.

Huang, H., & Talreja, R. (2005). Effects of void geometry on elastic properties of unidirectional fiber reinforced composites. *Composites Science and Technology*, *65*(13), 1964-1981.

Jiang, B., & Huang, Y. D. (2011). Investigation of the impregnation degree of the prepreg by near infrared spectroscopy. *Composites Part B: Engineering*, *42*(4), 946-948.

Karahan, M., Lomov, S. V., Bogdanovich, A. E., & Verpoest, I. (2011). Fatigue tensile behavior of carbon/epoxy composite reinforced with non-crimp 3D orthogonal woven fabric. *Composites Science and Technology, 71*(16), 1961-1972.

Kaw, A. K. (2005). *Mechanics of composite materials*. CRC press.

Larberg, Y., & Åkermo, M. (2014). In-plane deformation of multi-layered unidirectional thermoset prepreg–Modelling and experimental verification. *Composites Part A: Applied Science and Manufacturing*, *56*, 203-212.

Lee-Sullivan, P., & Dykeman, D. (2000). Guidelines for performing storage modulus measurements using the TA Instruments DMA 2980 three-point bend mode: I. Amplitude effects1Part of results in this paper was presented at the Canadian Society of Mechanical Engineering (CSME) Forum, Toronto, Canada, 19–22 May 1998.1. *Polymer testing*, *19*(2), 155-164.

Li, Q., Li, D., Wang, L. J., Özkan, N., & Mao, Z. H. (2010). Dynamic viscoelastic properties of sweet potato studied by dynamic mechanical analyzer. *Carbohydrate polymers*, *79*(3), 520-525.

McWilliams, B., Yu, J., Klier, E., & Yen, C. F. (2014). Mechanical response of discontinuous ceramic fiber reinforced metal matrix composites under quasi-static and dynamic loadings. *Materials Science and Engineering: A*, *590*, 21-29.

Menard, K. P. (2008). *Dynamic mechanical analysis: a practical introduction*. CRC press.

Meyers, M. A., & Chawla, K. K. (2009). *Mechanical behavior of materials* (Vol. 547). Cambridge: Cambridge University Press.

Paiva, J. M. F. D., Mayer, S., & Rezende, M. C. (2005). Evaluation of mechanical properties of four different carbon/epoxy composites used in aeronautical field. *Materials Research*, *8*(1), 91-97.

TA instruments (2007). DMA Dynamic Mechanical Analyzer, Q Series™ Getting Started Guide, *109 Lukens Drive, New Castle, DE 19720*.

Tzikang, C. (2000). Determining a Prony series for a viscoelastic material from time varying strain data

Wang, J., Laborie, M. P. G., & Wolcott, M. P. (2007). Application of beam mechanics to sensing the cure development of wood-phenolic joints by dynamic mechanical analysis. *Thermochimica Acta*, *465*(1), 18-24

[1] **Paiva, J. M. F. D., Mayer, S., & Rezende, M. C.** (2005). Evaluation of mechanical properties of four different carbon/epoxy composites used in aeronautical field. *Materials Research*, *8*(1), 91-97.

[2] **Meyers, M. A., & Chawla, K. K.** (2009). *Mechanical behavior of materials* (Vol. 547). Cambridge: Cambridge University Press.

[3] ABAQUS 6.13 Documentation, Abaqus Analysis User's Guide, 22.8.2 Parallel rheological framework.

[4] ABAQUS 6.13 Documentation, Abaqus Analysis User's Guide, 22.7.1 Time domain viscoelasticity.

[5] **Fritsch, J., Hiermaier, S., & Strobl, G.** (2009). Characterizing and modeling the non-linear viscoelastic tensile deformation of a glass fiber reinforced polypropylene. *Composites Science and Technology*, *69*(14), 2460-2466.

[6] **Karahan, M., Lomov, S. V., Bogdanovich, A. E., & Verpoest, I.** (2011). Fatigue tensile behavior of carbon/epoxy composite reinforced with non-crimp 3D orthogonal woven fabric. *Composites Science and Technology*, *71*(16), 1961-1972.

[7] **McWilliams, B., Yu, J., Klier, E., & Yen, C. F.** (2014). Mechanical response of discontinuous ceramic fiber reinforced metal matrix composites under quasi-static and dynamic loadings. *Materials Science and Engineering: A*, *590*, 21-29.

[8] **Deng, S., Hou, M., & Ye, L.** (2007). Temperature-dependent elastic moduli of epoxies measured by DMA and their correlations to mechanical testing data. *Polymer testing*, *26*(6), 803-813.

[9] **Xie, M., Zhang, Z., Gu, Y., Li, M., & Su, Y.** (2009). A new method to characterize the cure state of epoxy prepreg by dynamic mechanical analysis. *Thermochimica Acta*, *487*(1), 8-17.

[10] **Menard, K. P.** (2008). *Dynamic mechanical analysis: a practical introduction*. CRC press.

[11] **Lee-Sullivan, P., & Dykeman, D.** (2000). Guidelines for performing storage modulus measurements using the TA Instruments DMA 2980 three-point bend mode: I. Amplitude effects1Part of results in this paper was presented at the Canadian Society of Mechanical Engineering (CSME) Forum, Toronto, Canada, 19–22 May 1998.1. *Polymer testing*, *19*(2), 155-164.

[12] **Wang, J., Laborie, M. P. G., & Wolcott, M. P.** (2007). Application of beam mechanics to sensing the cure development of wood-phenolic joints by dynamic mechanical analysis. *Thermochimica Acta*, *465*(1), 18-24.

[13] **Li, Q., Li, D., Wang, L. J., Özkan, N., & Mao, Z. H.** (2010). Dynamic viscoelastic properties of sweet potato studied by dynamic mechanical analyzer. *Carbohydrate polymers*, *79*(3), 520-525.

[14] **Bashaiwoldu, A. B., Podczeck, F., & Newton, J. M.** (2004). Application of dynamic mechanical analysis (DMA) to determine the mechanical properties of pellets. *International journal of pharmaceutics*, *269*(2), 329-342.

[15] **Chang, S. H., & Wu, S. K.** (2008). Isothermal effect on internal friction of Ti< sub> 50</sub> Ni< sub> 50</sub> alloy measured by step cooling method in dynamic mechanical analyzer. *Journal of Alloys and Compounds*, *459*(1), 155-159.

[16] **Deng, S., Hou, M., & Ye, L.** (2007). Temperature-dependent elastic moduli of epoxies measured by DMA and their correlations to mechanical testing data. *Polymer testing*, *26*(6), 803-813.

[17] **Huang, H., & Talreja, R.** (2005). Effects of void geometry on elastic properties of unidirectional fiber reinforced composites. *Composites Science and Technology*, *65*(13), 1964-1981.

[18] **Kaw, A. K.** (2005). *Mechanics of composite materials*. CRC press.

[19] **Larberg, Y., & Åkermo, M.** (2014). In-plane deformation of multi-layered unidirectional thermoset prepreg–Modelling and experimental verification. *Composites Part A: Applied Science and Manufacturing*, *56*, 203-212.

[20] **Jiang, B., & Huang, Y. D.** (2011). Investigation of the impregnation degree of the prepreg by near infrared spectroscopy. *Composites Part B: Engineering*, *42*(4), 946-948.

[21] ABAQUS 6.13 Documentation, Abaqus Analysis User's Guide, 6.2.5 Quasi-static analysis.

[22] **Tzikang, C.** (2000). Determining a Prony series for a viscoelastic material from time varying strain data.

[23] ABAQUS 6.13 Documentation, Abaqus Analysis User's Guide, 27.1.1 Element library.

APPENDICES

APPENDIX A

PRELIMINARY DATA

Celstran® CFR-TP PA6 CF60-01

Ticona
Performance Driven Solutions™

General Description: Celstran® CFR-TP PA6 CF60-01 is a 60% carbon fiber by weight polyamide 6 (nylon 6) continuous fiber (uni-directional) reinforced thermoplastic composite tape. This material exhibits a high strength-to-weight ratio, excellent toughness and impact resistance. It is well suited for industrial, automotive and sporting goods applications where strength and toughness are critical as well as ease of processing.

	Property	Value	Unit	Value	Unit
MATERIAL	Polymer	PA6			
	Fiber Type	Carbon			
	Density	0.053	lb/in^3	1.46	g/cm^3
	Fiber Content	60	% by wt.		
	Fiber Volume	48	% by vol.		
	Tape Thickness**	0.0076	in	0.19	mm
	Tape Width (max.)*	10	in	254	mm
	Tape Areal Weight**	8.3	oz/yd^2	280	g/m^2
	Fiber Areal Weight**	5.0	oz/yd^2	170	g/m^2

*Custom tape widths may be available. Slit tapes are available down to 0.25 in (6mm).
**Nominal value shown, actual value may vary.

	Property[1]	Value	Unit	Value	Unit	Test Method
MECHANICAL	Tensile Strength	262	ksi	1800	MPa	D3039
	Tensile Modulus	15.6	Msi	107.7	GPa	D3039
	Elongation at Break	1.53	%	1.53	%	D3039
	Flexural Strength	116	ksi	800	MPa	D790
	Flexural Modulus	14.1	Msi	96.9	GPa	D790

[1]Orientation 0°

	Property	Value	Unit	Value	Unit
THERMAL	Melt Temperature	428	°F	220	°C
	Glass Transition Temperature	117	°F	47	°C

Contact Information

Americas
Ticona Engineering Polymers
Product Information Service
8040 Dixie Highway
Florence, KY 41042
USA
Tel.: +1-800-833-4882
Tel.: +1-859-372-3244
Customer Service
Tel.: +1-800-526-4960
Tel.: +1-859-372-3214
Fax: +1-859-372-3125
email: prodinfo@ticona.com

Europe
Ticona GmbH
Information Service
Am Unisyspark 1
65843 Sulzbach, Germany
Tel.: +49 (0)180-584 2662 (Germany)*
+49 (0)69-305 16299 (Europe)**
Fax: +49 (0)180-202 1202
See example below for rate information:
* 0.14 €/min + local landline rates
**0.06 €/call + local landline rates
email: infoservice@ticona.de
Ticona on the web: www.ticona.com

Asia
Celanese (China) Holding Co., Ltd.
4560 Jinke Road
Shanghai 201210
P.R. China
Customer Service
Tel.: +86-21-3861 9288
Fax: +86-21-3861 9588
email: infohelp@ticona.com

Celanese
Ticona – A Business of Celanese

APPENDIX B

Table B.1: Test results

Time (S)	Displacement(m)	Force (N)	Stress (Pa)	Strain
0	0	0	0	0
3.4902	5.31E-05	0.0002	32.2471	0.0032
3.99	0.00013113	0.0006	96.8426	0.008
4.4898	0.00029357	0.001	165.572	0.0178
4.9902	0.00050741	0.0014	236.253	0.0306
5.49	0.00076783	0.0019	309.487	0.046
5.9904	0.00106727	0.0023	385.77	0.0634
6.4902	0.00141057	0.0027	465.92	0.0829
6.99	0.00179115	0.0031	549.832	0.1042
7.4898	0.00218258	0.0035	636.899	0.1255
7.9902	0.00259381	0.0039	728.164	0.1475
8.49	0.00302676	0.0044	823.846	0.1702
8.9904	0.00347265	0.0048	923.326	0.1929
9.4902	0.00392885	0.0052	1027.221	0.2157
9.99	0.00440611	0.0056	1136.024	0.239
10.4904	0.0049469	0.006	1252.396	0.2648
10.9902	0.00553418	0.0064	1376.19	0.292
11.49	0.00617099	0.0069	1507.905	0.3208
11.9898	0.0068902	0.0073	1650.686	0.3522
12.4902	0.00765186	0.0077	1802.717	0.3845
12.99	0.00847001	0.0081	1965.32	0.4181
13.4904	0.00933151	0.0085	2138.119	0.4523
13.9902	0.01025113	0.0089	2323.102	0.4875

Table B.2: Test results after time shifting

Time (S)	Displacement(m)	Force (N)	Stress (Pa)	Strain
0	0	0	0	0
0.4998	0.000078	0.0004	64.5955	0.004755
0.9996	0.00024	0.000817	133.3249	0.014582
1.5	0.000454	0.001234	204.0059	0.027373
1.9998	0.000715	0.00165	277.2399	0.042733
2.5002	0.001014	0.002066	353.5229	0.060107
3	0.001357	0.002484	433.6729	0.079661
3.4998	0.001738	0.002902	517.5849	0.100902
3.9996	0.002129	0.003317	604.6519	0.122287
4.5	0.002541	0.003733	695.9169	0.144272
4.9998	0.002974	0.004151	791.5989	0.166907
5.5002	0.00342	0.004566	891.0789	0.189696
6	0.003876	0.004983	994.9739	0.212486
6.4998	0.004353	0.005401	1103.7769	0.235784
7.0002	0.004894	0.005817	1220.1489	0.261545
7.5	0.005481	0.006235	1343.9429	0.288788
7.9998	0.006118	0.006651	1475.6579	0.317514
8.4996	0.006837	0.007067	1618.4389	0.348994
9	0.007599	0.007484	1770.4699	0.381286
9.4998	0.008417	0.007901	1933.0729	0.41485
10.0002	0.009278	0.008317	2105.8719	0.449014
10.5	0.010198	0.008734	2290.8549	0.484241

APPENDIX C

Table C.1: Amplitude of force ramp for Model1

Time(S)	Amplitude(N/m)
0	0
0.4998	0.062999
0.9996	0.128606
1.5	0.194123
1.9998	0.259607
2.5002	0.325149
3	0.39094
3.4998	0.456571
3.9996	0.52192
4.5	0.587485
4.9998	0.653165
5.5002	0.718567
6	0.784179
6.4998	0.849816
7.0002	0.915399
7.5	0.981045
7.9998	1.046551
8.4996	1.112068
9	1.177717
9.4998	1.243284
10.0002	1.308796
10.5	1.374358

Table C.2: Amplitude of displacement ramp for Model3

Time (S)	Amplitude (m)
0	0
0.4998	7.80E-05
0.9996	0.00024
1.5	0.000454
1.9998	0.000715
2.5002	0.001014
3	0.001357
3.4998	0.001738
3.9996	0.002129
4.5	0.002541
4.9998	0.002974
5.5002	0.00342
6	0.003876
6.4998	0.004353
7.0002	0.004894
7.5	0.005481
7.9998	0.006118
8.4996	0.006837
9	0.007599
9.4998	0.008417
10.0002	0.009278
10.5	0.010198

APPENDIX D

This code reads outputs of DMA test and after time shifting returns Prony series coefficients. Then by reading outputs of simulation, it returns comparison figures of experimental and simulation results for our models.

```
clear
clc
format long
% Reading experimental data and time shifting
a = xlsread('Data_Tension_Test_Kaveh.xlsx','A11:E33');
time = a(:,1)*60;
time = time - 3.490199999999817;
time(1) = [];
displacement = a(:,2)*10^-6;
displacement = displacement - 0.000053099740000;
displacement(1) = [];
displacement(1) = 0;
force = a(:,3);
force = force - 0.000201296000000;
force(1) = [];
% Defining different Stresses and Strains to detect outputs of
DMA
stress1 = a(:,4)*10^6;
stress1 = stress1 - 32.247100000000;
stress1(1) = [];
stress1(1) = 0;
strain1 = a(:,5)/100;
strain1 = strain1 - 0.003248844000000;
strain1(1) = [];
L0 = 0.0103177;
initialarea = 0.000006259675;
A(1,1) = initialarea;
L(1,1) = L0;
for i=2:22
    L(i,1) = L0+displacement(i);
    A(i,1) = A(i-1,1)*L(i-1,1)/L(i,1); % Instantaneous area,
                                       % Assumption:linear
reduction of area
end
meanFinalArea = initialarea*L0/L(end);
stress2 = force / initialarea; % Average stress
stress3 = force / meanFinalArea;
stress4 = force./A; %Instantaneous area,Assumption:linear
reduction of area


% Instantaneous area, by using poisson's ratio
v = 0.3468;  % Poisson's ratio
width(1) = 6.355e-3;
thickness(1) = 0.985e-3;
A2(1) = width(1)*thickness(1);
for i=2:22
    width(i) = width(i-1) - v*(width(i-1)*(L(i)-L(i-1)))/L(i-
1);
```

```
    thickness(i) = thickness(i-1) -v*(thickness(i-1)*(L(i)-
L(i-1)))/L(i-1);
    A2(i) = width(i)*thickness(i);
end
stress5 = force./A2'; % true stress
% Comparison of stresses with DMA output
figure(1)
plot(time,stress1,'+k',time,stress2,'-k',time,stress3,':k'...
    ,time,stress4,'-.k'...
    ,time,stress5,'--k','LineWidth',2.35),xlabel('Time
(s)','FontSize',15),...
    ylabel('Stress (Pa)','color','k','FontSize',15)...

,legend('Stress1','Stress2','Stress3','Stress4','Stress5','Loc
ation','NorthWest')

strain2 = (displacement/L0);
strain3 = displacement/L(end);
strain4(1) = 0;
for i=2:22
    strain4(i) = (displacement(i)/L(i-1));
end
strain4 = strain4';
strain5 = log(L/L0); % true strain

% Comparison of strains with DMA output
figure(2)
plot(time,strain1,'+k',time,strain2,'-
k',time,strain3,':k',time,strain4,...
    '-.k',time,strain5,'--k','LineWidth',2.35),xlabel('Time
(s)','FontSize',15)...
    ,ylabel('Strain','FontSize',15)...

,legend('Strain1','Strain2','Strain3','Strain4','Strain5','Loc
ation','NorthWest')

% stress5 (true stress)
% strain2 (displacement/L0)
clc
clear GR;
clear gR;
% G0 = GR(1)

for i=1:22
    GR(i) = stress5(i)./strain2(i);
end
GR(1) = NaN;
% GR with respect to time
figure(3)
stem(time,GR,'filled','k'),xlabel('Time (S)','FontSize',15)...
    ,ylabel('G_R (Pa)','FontSize',15)


% Determination of GR formula by means of "cftool"
% GR = a*exp(b*x) + c*exp(d*x)
%        a =        9830  (9180, 1.048e+04)
```

```
%         b =      -1.325  (-1.453, -1.197)
%         c =        3426  (3233, 3618)
%         d =    -0.03831  (-0.04628, -0.03035)

% Experimental GR and "cftool" approximation
figure(4)
stem(time,GR,'filled','k')
hold on
plot(time,9830*exp(-1.325*time) + 3426*exp(-0.03831*time),...
    'k','LineWidth',2.3)...
    ,xlabel('Time (S)','FontSize',15)...
    ,ylabel('G_R (Pa) & MATLAB
approximation','FontSize',15)...
    ,legend('G_R','MATLAB')


% GR(1) == a+c == 13256
GR(1) = 13256;
gR = GR./GR(1);

% gR with respect to time
figure(5)
stem(time,gR,'filled','k'),xlabel('Time (S)','FontSize',15)...
    ,ylabel('g_R','FontSize',15)



% 5 terms Prony approximation by means of "cftool"
% gR = 1-a*(1-exp(-x/b))-c*(1-exp(-x/d))-e*(1-exp(-x/f))-g*(1-
exp(-x/h))
% -k*(1-exp(-x/l))-m*(1-exp(-x/n))
%         a =      0.4209
%         b =      0.8836
%         c =     -0.1613
%         d =     0.01008
%         e =      0.1478  (-0.1997, 0.4954)
%         f =        3.45  (-2.328, 9.228)
%         g =        0.98  (-389.6, 391.6)
%         h =      0.2194  (-20.74, 21.18)
%         k =      -0.561  (-9.782e+12, 9.782e+12)
%         l =     0.03347  (-3.826e+10, 3.826e+10)

gp = [0.4209 -0.1613 0.1478 0.98 -0.561];
TG = [0.8836 0.01008 3.45 0.2194 0.03347];
prony = 1;
for i=1:5
    prony = prony - gp(i)*(1-exp(-time/TG(i)));
end

% gR & Prony approximation
figure(6)
stem(time,gR,'filled','k')
hold on
plot(time,prony,'k','LineWidth',2.3)...
    ,xlabel('Time (S)','FontSize',15)...
```

```
    ,ylabel('g_R & Prony series
approximation','FontSize',15)...
    ,legend('g_R','Prony')


% Model1
timeModel1 = xlsread('U2Model1.xlsx','A4:A64');
U2Model1 = -xlsread('U2Model1.xlsx','BK4:BK64');
S22Model1 = xlsread('S22Model1.xlsx','DT4:DT64');

% Model1_1:6

% Model1 with 1 element
timeModel1_1 = xlsread('U2Model1_1.xlsx','A4:A62');
U2Model1_1 = -xlsread('U2Model1_1.xlsx','D4:D62');
S22Model1_1 = xlsread('S22Model1_1.xlsx','B5:B63');

% Model1 with 2 elements
timeModel1_2 = xlsread('U2Model1_2.xlsx','A4:A62');
U2Model1_2 = -xlsread('U2Model1_2.xlsx','D4:D62');
S22Model1_2 = xlsread('S22Model1_2.xlsx','F4:F62');

% Model1 with 8 elements
timeModel1_3 = xlsread('U2Model1_3.xlsx','A4:A63');
U2Model1_3 = -xlsread('U2Model1_3.xlsx','E4:E63');
S22Model1_3 = xlsread('S22Model1_3.xlsx','H5:H64');

% Model1 with 72 elements
timeModel1_4 = xlsread('U2Model1_4.xlsx','A4:A62');
U2Model1_4 = -xlsread('U2Model1_4.xlsx','I4:I62');
S22Model1_4 = xlsread('S22Model1_4.xlsx','P5:P63');

% Model1 with 648 elements
timeModel1_5 = xlsread('U2Model1_5.xlsx','A4:A63');
U2Model1_5 = -xlsread('U2Model1_5.xlsx','U4:U63');
S22Model1_5 = xlsread('S22Model1_5.xlsx','AN5:AN64');

% Model1 with 3200 elements
timeModel1_6 = xlsread('U2Model1_6.xlsx','A4:A63');
U2Model1_6 = -xlsread('U2Model1_6.xlsx','AQ4:AQ63');
S22Model1_6 = xlsread('S22Model1_6.xlsx','CF5:CF64');



% Model2
timeModel2 = xlsread('U2Model2.xlsx','A4:A62');
U2Model2 = -xlsread('U2Model2.xlsx','DS4:DS62');
S22Model2 = xlsread('S22Model2.xlsx','IJ5:IJ63');

% Model2_1:6

% Model2 with 1 element
timeModel2_1 = xlsread('U2Model2_1.xlsx','A4:A62');
U2Model2_1 = -xlsread('U2Model2_1.xlsx','E4:E62');
S22Model2_1 = xlsread('S22Model2_1.xlsx','B5:B63');
```

```
% Model2 with 2 elements
timeModel2_2 = xlsread('U2Model2_2.xlsx','A4:A62');
U2Model2_2 = -xlsread('U2Model2_2.xlsx','E4:E62');
S22Model2_2 = xlsread('S22Model2_2.xlsx','H5:H63');

% Model2 with 8 element
timeModel2_3 = xlsread('U2Model2_3.xlsx','A4:A62');
U2Model2_3 = -xlsread('U2Model2_3.xlsx','G4:G62');
S22Model2_3 = xlsread('S22Model2_3.xlsx','L5:L63');

% Model2 with 72 element
timeModel2_4 = xlsread('U2Model2_4.xlsx','A4:A62');
U2Model2_4 = -xlsread('U2Model2_4.xlsx','O4:O62');
S22Model2_4 = xlsread('S22Model2_4.xlsx','AB5:AB63');

% Model2 with 648 element
timeModel2_5 = xlsread('U2Model2_5.xlsx','A4:A62');
U2Model2_5 = -xlsread('U2Model2_5.xlsx','AM4:AM62');
S22Model2_5 = xlsread('S22Model2_5.xlsx','BX5:BX63');

% Model2 with 3200 element
timeModel2_6 = xlsread('U2Model2_6.xlsx','A4:A62');
U2Model2_6 = -xlsread('U2Model2_6.xlsx','CE4:CE62');
S22Model2_6 = xlsread('S22Model2_6.xlsx','FH5:FH63');


% Model3
timeModel3 = xlsread('RF2Model3.xlsx','A4:A62');
RF2Model3 = xlsread('RF2Model3.xlsx','BK4:BK62');
S22Model3 = xlsread('S22Model3.xlsx','DT5:DT63');
U2Model3 = -xlsread('U2Model3.xlsx','BK4:BK62');

% Model3_1:6

% Model3 with 1 element
timeModel3_1 = xlsread('RF2Model3_1.xlsx','A4:A62');
RF2Model3_1 = xlsread('RF2Model3_1.xlsx','D4:D62');
S22Model3_1 = xlsread('S22Model3_1.xlsx','B5:B63');

% Model3 with 2 elements
timeModel3_2 = xlsread('RF2Model3_2.xlsx','A4:A62');
RF2Model3_2 = xlsread('RF2Model3_2.xlsx','D4:D62');
S22Model3_2 = xlsread('S22Model3_2.xlsx','F5:F63');

% Model3 with 8 elements
timeModel3_3 = xlsread('RF2Model3_3.xlsx','A4:A62');
RF2Model3_3 = xlsread('RF2Model3_3.xlsx','E4:E62');
S22Model3_3 = xlsread('S22Model3_3.xlsx','H5:H63');

% Model3 with 72 elements
timeModel3_4 = xlsread('RF2Model3_4.xlsx','A4:A62');
RF2Model3_4 = xlsread('RF2Model3_4.xlsx','I4:I62');
S22Model3_4 = xlsread('S22Model3_4.xlsx','P5:P63');

% Model3 with 648 elements
timeModel3_5 = xlsread('RF2Model3_5.xlsx','A4:A62');
```

```
RF2Model3_5 = xlsread('RF2Model3_5.xlsx','U4:U62');
S22Model3_5 = xlsread('S22Model3_5.xlsx','AN5:AN63');

% Model3 with 3200 elements
timeModel3_6 = xlsread('RF2Model3_6.xlsx','A4:A62');
RF2Model3_6 = xlsread('RF2Model3_6.xlsx','AQ4:AQ62');
S22Model3_6 = xlsread('S22Model3_6.xlsx','CF5:CF63');

% Model4
timeModel4 = xlsread('RF2Model4.xlsx','A4:A74');
RF2Model4 = xlsread('RF2Model4.xlsx','DS4:DS74');
S22Model4 = xlsread('S22Model4.xlsx','IJ5:IJ75');
U2Model4 = -xlsread('U2Model4.xlsx','DR4:DR74');

% Model4_1:6

% Model4 with 1 element
timeModel4_1 = xlsread('RF2Model4_1.xlsx','A4:A70');
RF2Model4_1 = xlsread('RF2Model4_1.xlsx','E4:E70');
S22Model4_1 = xlsread('S22Model4_1.xlsx','B5:B71');


% Model4 with 2 elements
timeModel4_2 = xlsread('RF2Model4_2.xlsx','A4:A70');
RF2Model4_2 = xlsread('RF2Model4_2.xlsx','E4:E70');
S22Model4_2 = xlsread('S22Model4_2.xlsx','H5:H71');

% Model4 with 8 elements
timeModel4_3 = xlsread('RF2Model4_3.xlsx','A4:A72');
RF2Model4_3 = xlsread('RF2Model4_3.xlsx','G4:G72');
S22Model4_3 = xlsread('S22Model4_3.xlsx','L5:L73');

% Model4 with 72 elements
timeModel4_4 = xlsread('RF2Model4_4.xlsx','A4:A69');
RF2Model4_4 = xlsread('RF2Model4_4.xlsx','O4:O69');
S22Model4_4 = xlsread('S22Model4_4.xlsx','AB5:AB70');

% Model4 with 648 elements
timeModel4_5 = xlsread('RF2Model4_5.xlsx','A4:A74');
RF2Model4_5 = xlsread('RF2Model4_5.xlsx','AM4:AM74');
S22Model4_5 = xlsread('S22Model4_5.xlsx','BX5:BX75');

% Model4 with 3200 elements
timeModel4_6 = xlsread('RF2Model4_6.xlsx','A4:A75');
RF2Model4_6 = xlsread('RF2Model4_6.xlsx','CE4:CE75');
S22Model4_6 = xlsread('S22Model4_6.xlsx','FH5:FH76');

% Model5
timeModel5 = xlsread('U2Model5.xlsx','A4:A29');
U2Model5 = -xlsread('U2Model5.xlsx','AQ4:AQ29');
S22Model5 = xlsread('S22Model5.xlsx','CF5:CF30');

% Model5_1,2,4

% Model5 with 1 element
timeModel5_1 = xlsread('U2Model5_1.xlsx','A5:A30');
```

```
U2Model5_1 = -xlsread('U2Model5_1.xlsx','E5:E30');
S22Model5_1 = xlsread('S22Model5_1.xlsx','F6:F31');

% Model5 with 2 elements
timeModel5_2 = xlsread('U2Model5_2.xlsx','A4:A29');
U2Model5_2 = -xlsread('U2Model5_2.xlsx','E4:E29');
S22Model5_2 = xlsread('S22Model5_2.xlsx','H5:H30');

% Model5 with 72 elements
timeModel5_4 = xlsread('U2Model5_4.xlsx','A4:A29');
U2Model5_4 = -xlsread('U2Model5_4.xlsx','O4:O29');
S22Model5_4 = xlsread('S22Model5_4.xlsx','AB5:AB30');


% Model6
timeModel6 = xlsread('U2Model6.xlsx','A4:A50');
U2Model6 = -xlsread('U2Model6.xlsx','AQ4:AQ50');
S22Model6 = xlsread('S22Model6.xlsx','CF5:CF51');

timeModel6_1 = xlsread('U2Model6_1.xlsx','A4:A49');
U2Model6_1 = -xlsread('U2Model6_1.xlsx','D4:D49');

timeModel6_2 = xlsread('U2Model6_2.xlsx','A4:A49');
U2Model6_2 = -xlsread('U2Model6_2.xlsx','D4:D49');
S22Model6_2 = xlsread('S22Model6_2.xlsx','F5:F50');

timeModel6_3 = xlsread('U2Model6_3.xlsx','A4:A49');
U2Model6_3 = -xlsread('U2Model6_3.xlsx','E4:E49');
S22Model6_3 = xlsread('S22Model6_3.xlsx','H5:H50');

timeModel6_5 = xlsread('U2Model6_5.xlsx','A4:A50');
U2Model6_5 = -xlsread('U2Model6_5.xlsx','U4:U50');
S22Model6_5 = xlsread('S22Model6_5.xlsx','AN5:AN51');

% Convergence of Model1,Displacement
figure(7)
plot(timeModel1_1,U2Model1_1,'k--
',timeModel1_2,U2Model1_2,'b',...

timeModel1_3,U2Model1_3,'g',timeModel1_4,U2Model1_4,'r',...

timeModel1_5,U2Model1_5,'c',timeModel1_6,U2Model1_6,'m',timeMo
del1,U2Model1,'k'...
    ,'LineWidth',2.3)...
    ,title('Convergence of Model1','FontSize',15)...
    ,xlabel('Time (S)','FontSize',15)...
    ,ylabel('Displacement (m)','FontSize',15)...
    ,legend('1 Element','2 Elements','8 Elements','72
Elements',...
    '648 Elements','3200 Elements','7140
Elements','Location','NorthWest')

% Convergence of Model1,Stress
figure(8)
plot(timeModel1_1,S22Model1_1,'k--
',timeModel1_2,S22Model1_2,'b',...
```

```
timeModel1_3,S22Model1_3,'g',timeModel1_4,S22Model1_4,'r',...

timeModel1_5,S22Model1_5,'c',timeModel1_6,S22Model1_6,'m',time
Model1,S22Model1,'k',...
    'LineWidth',2.3),title('Convergence of
Model1','FontSize',15)...
    ,xlabel('Time (S)','FontSize',15)...
    ,ylabel('Stress (Pa)','FontSize',15)...
    ,legend('1 Element','2 Elements','8 Elements','72
Elements',...
    '648 Elements','3200 Elements','7140
Elements','Location','NorthWest')

% Comparison of Model1 with experimental data
figure(9)
plot(displacement/L0,stress1,'+-
k',U2Model1/L0,S22Model1,'k','LineWidth',2.3)...
    ,title('Model1','FontSize',15)...
    ,xlabel('Strain','FontSize',15)...
    ,ylabel('Stress (Pa)','FontSize',15)...
    ,legend('Experimental
result','Model1','Location','NorthWest')


% Convergence of Model2,Displacement
figure(10)
plot(timeModel2_1,U2Model2_1,'b',timeModel2_2,U2Model2_2,'g',.
..

timeModel2_3,U2Model2_3,'r',timeModel2_4,U2Model2_4,'c',...

timeModel2_5,U2Model2_5,'m',timeModel2_6,U2Model2_6,'y',...
    timeModel2,U2Model2,'k','LineWidth',2.3)...
    ,title('Convergence of Model2','FontSize',15)...
    ,xlabel('Time (S)','FontSize',15)...
    ,ylabel('Displacement (m)','FontSize',15)...
    ,legend('1 Element','2 Elements','8 Elements','72
Elements',...
    '648 Elements','3200 Elements','7140
Elements','Location','NorthWest')

% Convergence of Model2,Stress
figure(11)
plot(timeModel2_1,S22Model2_1,'b',timeModel2_2,...
    S22Model2_2,'g',timeModel2_3,S22Model2_3,'r',...

timeModel2_4,S22Model2_4,'c',timeModel2_5,S22Model2_5,'m',time
Model2_6,...

S22Model2_6,'y',timeModel2,S22Model2,'k','LineWidth',2.3)...
    ,title('Convergence of Model2','FontSize',15)...
    ,xlabel('Time (S)','FontSize',15)...
    ,ylabel('Stress (Pa)','FontSize',15)...
    ,legend('1 Element','2 Elements','8 Elements','72
Elements',...
```

```
    '648 Elements','3200 Elements','7140
Elements','Location','NorthWest')

% Comparison of Model2 with experimental data
figure(12)
plot(displacement/L0,stress1,'+-
k',U2Model2/L0,S22Model2,'k','LineWidth',2.3)...
    ,title('Model2','FontSize',15)...
    ,xlabel('Strain','FontSize',15)...
    ,ylabel('Stress (Pa)','FontSize',15)...
    ,legend('Experimental
result','Model2','Location','NorthWest')

% Convergence of Model3,Reaction force
figure(13)
plot(timeModel3_1,RF2Model3_1,'--b',timeModel3_2,...

RF2Model3_2,'g',timeModel3_3,RF2Model3_3,'r',timeModel3_4,RF2M
odel3_4,'c'...

,timeModel3_5,RF2Model3_5,'m',timeModel3_6,RF2Model3_6,'y',tim
eModel3,RF2Model3,'k',...
    'LineWidth',2.3)...
    ,title('Convergence of Model3','FontSize',15)...
    ,xlabel('Time (S)','FontSize',15)...
    ,ylabel('Reaction force (N)','FontSize',15)...
    ,legend('1 Element','2 Elements','8 Elements','72
Elements',...
    '648 Elements','3200 Elements','7140
Elements','Location','NorthWest')

% Convergence of Model3,Stress
figure(14)
plot(timeModel3_1,S22Model3_1,'--b',timeModel3_2,...
    S22Model3_2,'g',timeModel3_3,...

S22Model3_3,'r',timeModel3_4,S22Model3_4,'c',timeModel3_5,S22M
odel3_5,'m',...

timeModel3_6,S22Model3_6,'y',timeModel3,S22Model3,'k','LineWid
th',2.3)...
    ,title('Convergence of Model3','FontSize',15)...
    ,xlabel('Time (S)','FontSize',15)...
    ,ylabel('Stress (Pa)','FontSize',15)...
    ,legend('1 Element','2 Elements','8 Elements','72
Elements',...
    '648 Elements','3200 Elements','7140
Elements','Location','NorthWest')
% Comparison of Model3 with experimental data
figure(15)
plot(displacement/L0,stress1,'+-
k',U2Model3/L0,S22Model3,'k','LineWidth',2.3)...
    ,title('Model3','FontSize',15)...
    ,xlabel('Strain','FontSize',15)...
    ,ylabel('Stress (Pa)','FontSize',15)...
```

```
    ,legend('Experimental
result','Model3','Location','NorthWest')

% Convergence of Model4,Reaction force
figure(16)
plot(timeModel4_1,RF2Model4_1,'b',timeModel4_2,...
    RF2Model4_2,'g',...

timeModel4_3,RF2Model4_3,'r',timeModel4_4,RF2Model4_4,'c',time
Model4_5,...
    RF2Model4_5,'m',...

timeModel4_6,RF2Model4_6,'y',timeModel4,RF2Model4,'k','LineWid
th',2.3)...
    ,title('Convergence of Model4','FontSize',15)...
    ,xlabel('Time (S)','FontSize',15)...
    ,ylabel('Reaction force (N)','FontSize',15)...
    ,legend('1 Element','2 Elements','8 Elements','72
Elements',...
    '648 Elements','3200 Elements','7140
Elements','Location','NorthWest')

% Convergence of Model4,Stress
figure(17)
plot(timeModel4_1,S22Model4_1,'b',timeModel4_2,...
    S22Model4_2,'g',timeModel4_3,S22Model4_3,'r',...

timeModel4_4,S22Model4_4,'c',timeModel4_5,S22Model4_5,'m',time
Model4_6,...

S22Model4_6,'y',timeModel4,S22Model4,'k','LineWidth',2.3)...
    ,title('Convergence of Model4','FontSize',15)...
    ,xlabel('Time (S)','FontSize',15)...
    ,ylabel('Stress (Pa)','FontSize',15)...
    ,legend('1 Element','2 Elements','8 Elements','72
Elements',...
    '648 Elements','3200 Elements','7140
Elements','Location','NorthWest')
% Comparison of Model4 with experimental data
figure(18)
plot(displacement/L0,stress1,'+-
k',U2Model4/L0,S22Model4,'k','LineWidth',2.3)...
    ,title('Model4','FontSize',15)...
    ,xlabel('Strain','FontSize',15)...
    ,ylabel('Stress (Pa)','FontSize',15)...
    ,legend('Experimental
result','Model4','Location','NorthWest')
% Convergence of Model5,Displacement
figure(19)
plot(timeModel5_1,U2Model5_1,'b',timeModel5_2,U2Model5_2,'g',t
imeModel5_4,...
    U2Model5_4,'r',timeModel5,U2Model5,'k','LineWidth',2.3)...
    ,title('Convergence of Model5','FontSize',15)...
    ,xlabel('Time (S)','FontSize',15)...
    ,ylabel('Displacement (m)','FontSize',15)...
```

```
    ,legend('1 Element','2 Elements','72 Elements','800
Elements','Location','NorthWest')

% Convergence of Model5,Stress
figure(20)
plot(timeModel5_1,S22Model5_1,'b',timeModel5_2,S22Model5_2,'g'
,timeModel5_4,...

S22Model5_4,'r',timeModel5,S22Model5,'k','LineWidth',2.3),...
    ,title('Convergence of Model5','FontSize',15)...
    ,xlabel('Time (S)','FontSize',15)...
    ,ylabel('Stress (Pa)','FontSize',15)...
    ,legend('1 Element','2 Elements','72 Elements','800
Elements','Location','NorthWest')
% Comparison of Model5 with experimental data
figure(21)
plot(displacement/L0,stress1,'+-
k',U2Model5/L0,S22Model5,'k','LineWidth',2.3)...
    ,title('Model5','FontSize',15)...
    ,xlabel('Strain','FontSize',15)...
    ,ylabel('Stress (Pa)','FontSize',15)...
    ,legend('Experimental
result','Model5','Location','NorthWest')
% Convergence of Model6,Displacement
figure(22)
plot(timeModel6_1,U2Model6_1,'b',timeModel6_2,U2Model6_2,'g'..
.

,timeModel6_3,U2Model6_3,'r',timeModel6_5,U2Model6_5,'c'...
    ,timeModel6,U2Model6,'k','LineWidth',2.3)...
    ,title('Convergence of Model6','FontSize',15)...
    ,xlabel('Time (S)','FontSize',15)...
    ,ylabel('Displacement (m)','FontSize',15)...
    ,legend('1 Element','2 Elements','8 Elements','648
Elements'...
    ,'7140 Elements','Location','NorthWest')

% Convergence of Model6,Stress
figure(23)
plot(timeModel6_2,S22Model6_2,'b',timeModel6_3,S22Model6_3,'g'
...
    ,timeModel6_5,S22Model6_5,'r',timeModel6,S22Model6,'k'...
    ,'LineWidth',2.3)...
    ,title('Convergence of Model6','FontSize',15)...
    ,xlabel('Time (S)','FontSize',15)...
    ,ylabel('Stress (Pa)','FontSize',15)...
    ,legend('2 Elements','8 Elements','648 Elements','7140
Elements','Location','NorthWest')
% Comparison of Model6 with experimental data
figure(24)
plot(displacement/L0,stress1,'+-
k',U2Model6/L0,S22Model6,'k','LineWidth',2.3)...
    ,title('Model6','FontSize',15)...
    ,xlabel('Strain','FontSize',15)...
    ,ylabel('Stress (Pa)','FontSize',15)...
```

```
    ,legend('Experimental
result','Model6','Location','NorthWest')

%Comparision of all models (Stress-strain)
figure(25)
plot(displacement/L0,stress1,'+-
',U2Model1/L0,S22Model1,U2Model2/L0,S22Model2,...

U2Model3/L0,S22Model3,U2Model4/L0,S22Model4,U2Model5/L0,S22Mod
el5,...
    U2Model6/L0,S22Model6,'LineWidth',2.2)...
    ,title('Comparision of all models','FontSize',15)...
    ,xlabel('Strain','FontSize',15)...
    ,ylabel('Stress (Pa)','FontSize',15)...
    ,legend('Experimental
result','Model1','Model2','Model3','Model4',...
    'Model5','Model6','Location','NorthWest')
% Comparison of all Models, Reaction force
figure(26)
plot(time,force,'+-
',timeModel3,RF2Model3,':',timeModel4,RF2Model4,'-.',...
    'color','k','LineWidth',2.3)...
    ,title('Comparison of all models','FontSize',15)...
    ,xlabel('Time (S)','FontSize',15)...
    ,ylabel('Reaction force (N)','FontSize',15)...
    ,legend('Experimental
result','Model3','Model4','Location','NorthWest')

% Comparison of all Models, displacement
figure(27)
plot(time,displacement,'+-',timeModel1,U2Model1,'-
',timeModel2,U2Model2,'--'...
    ,timeModel5,U2Model5,':',timeModel6,U2Model6,'-
.','color','k','LineWidth',2.3)...
    ,title('Comparison of all models','FontSize',15)...
    ,xlabel('Time (S)','FontSize',15)...
    ,ylabel('Displacement (m)','FontSize',15)...
    ,legend('Experimental
result','Model1','Model2','Model5','Model6','Location','NorthW
est')
% Comparison of all Models, Stress
figure(28)
plot(time,stress1,'+-
',timeModel1,S22Model1,timeModel2,S22Model2...

,timeModel3,S22Model3,timeModel4,S22Model4,timeModel5,S22Model
5...
    ,timeModel6,S22Model6,'LineWidth',2.3)...
    ,title('Comparison of all
models','FontSize',15,'color','k')...
    ,xlabel('Time (S)','FontSize',15,'color','k')...
    ,ylabel('Stress (Pa)','FontSize',15,'color','k')...
    ,legend('Experimental
result','Model1','Model2','Model3',...
    'Model4','Model5','Model6','Location','NorthWest')
```

CURRICULUM VITAE

Name Surname: Kaveh Dargahi Noubary

Place and Date of Birth: Iran, Tabriz, 1986

E-Mail: Dargahikaveh@yahoo.com

EDUCATION:

B.Sc.: Mechanical Engineering, Mechanics in Heat and Fluids, Tabriz University, Iran, Tabriz.

M.Sc.: Mechanical Engineering, Solid Mechanics, Istanbul Technical University, Istanbul, Turkey.